Pergamon

Engineering Fracture Mechanics Vol. 57, No. 2/3, pp. 135–203, 1997
© 1997 Elsevier Science Ltd. All rights reserved
Printed in Great Britain

PII: S0013-7944(97)00007-6 0013-7944/97 $17.00 + 0.00

PHYSICS OF FRACTURE AND MECHANICS OF SELF-AFFINE CRACKS

ALEXANDER S. BALANKIN

SEPI-ESIME, Instituto Politecnico Nacional, Zacatenco, Mexico D.F., 07738, Mexico

Abstract—The physics associated with self-affine crack formation and propagation is discussed. Some novel concepts are suggested for the mechanics of self-affine cracks. These concepts are employed to model the crack face morphology and, in turn, to solve various problems with self-affine cracks. It is shown that linear elastic fracture mechanics (LEFM) is a special case of self-affine crack mechanics and should be used only in length scales larger than the self-affine correlation length. The theoretical results are confirmed by available experimental data. It is emphasized that the ASTM standards for test pieces for fracture toughness measurements must be completed by the specification of absolute specimen sizes which should be larger than the self-affine correlation length for the fracture surface roughness. © 1997 Elsevier Science Ltd

1. INTRODUCTION

THE FAILURE of complex engineering systems generally encompasses a set of scale levels that correlate with the scale lengths of separate elements and (or) groups of elements that made up the system. Predicting and evaluating the parameters and consequences of catastrophes, as well as developing measures to prevent them or reduce the level of danger from them, requires quantitative and qualitative descriptions of catastrophic failure in hierarchically organized complex engineering systems that take into account the nature and parameters of the interactions leading to a catastrophe and the properties of the materials in which they are located and (or) through which they come into contact with the complex system.

The fact that continuum approximation is often unsatisfactory for a real material is now beyond doubt [1–4]. In man-made structures, a variety of nano-, micro- and macro-defects appear at the production stage that may evolve during the structure's service life. Numerous fractographic and geophysical studies indicate the hierarchical non-Euclidean nature of the fracture patterns [3–5]. There are four fundamental scale levels of failure: (1) nanoscale, $1–10^3$ nm ($10^{-9}–10^{-6}$ m); (2) microscale, $1–10^3$ μm ($10^{-6}–10^{-3}$ m); (3) macroscale, $1–10^3$mm ($10^{-3}–1$ m); (4) global size-scale, $1–10^6$ m (1 m–1000 km).

The last is related to geophysical phenomena and failure of large engineering systems [3, 4]. The macroscale phenomena is common to experimental investigations in laboratories, whereas it is precise processes in micro- and nanoscale that govern macro behavior and fracture of deformed solids [5–15].

For this reason, a reliable prediction of the response of a solid to an external action should be based upon a clear understanding of the mechanics of processes in nano- and microscales. It is evident that only the description of failure processes within a single system, taking into account the interrelation of different processes in nano-, micro- and macroscale, would provide the development of an adequate theory of solid behavior and failure from first principles. It seems that this noble goal may be advantageously achieved, if one uses the experimental fact of statistical invariance of failure processes which leads to the fractal geometry of fracture patterns [1]. This gives a reason to use the powerful tools of fractal geometry and multifractal analysis for developing a statistical fracture mechanics within a framework of fractal solid mechanics [5, 16–60].

In this way one would wish to start with an atomic or molecular model of the material and then construct a completely general theory of behavior that transcends all length scales of possible behavior. To achieve this aim we should answer two fundamental questions: "What is the reason for fractal geometry of failure patterns?" and "How does the statistical scale invariance of crack faces affect crack mechanics?"

In this work the problems associated with these questions are discussed. The physics associated with self-affine crack formation and propagation is advanced. Some novel concepts are suggested to develop the mechanics of self-affine cracks. These concepts are employed to solve various problems with self-affine cracks.

In the next section we analyze failure pattern morphology. We try to give the list of references to this topic as completely as possible. A brief review of basic concepts of fractal mathematics with respect to their applications in solid mechanics is also given. Morphological aspects of brittle and ductile fracture are discussed. A nonstandard representation for crack faces in fractured solids is suggested. In Section 3 the physics of nano-, micro- and macrofracture is discussed. In Section 4 some problems with self-affine cracks are analyzed in detail. It is shown, that the self-affine roughness of real crack faces leads to changes in stress distribution near the crack and in this way affects the fracture toughness of brittle and ductile materials. The fractal representation of the real morphology of crack patterns provides a strict approach to derive relations between nano- and macrofracture parameters. Furthermore, some fracture phenomena can be adequately described only when the self-affine nature of crack faces is taken into account. Three examples of the dramatic role of fractality in crack mechanics are considered in the Section 4. Experimental methods of fractal measurement are briefly reviewed in Appendix A (the purpose of this review is to give a quite complete list of references, rather than to discuss experimental methods in detail).

2. STATISTICAL TOPOGRAPHY OF CRACKS

The propagation of cracks is a problem of both technological and scientific interest. This has motivated a large amount of research into how cracks form and how, once formed, they grow. It is well-known that real cracks in solid materials have little resemblance to ideal cracks with smooth edges which are usually considered in conventional fracture mechanics. For this reason, in recent years, the quantitative analysis of fractured surfaces has become an integral part of the study of deformation and rupture of materials [3, 61–64]. Such surface analysis often provides information about surface morphology which is complementary to that obtained by other metallurgical methods.

In the progress of science the ability to describe phenomena in precise quantitative terms frequently leads to important advances in understanding. This certainly seems to be true in the case of fracture surface formation. In the review [65], Nowicki has described 32 parameters and functions that have been used to characterize rough surfaces. Obviously, it is important to classify phenomena in such a way that the task of understanding and describing them can be reduced to a more reasonable magnitude. This noble goal can be achieved within a framework of statistical topography of cracks [66].

The term "statistical topography" was introduced by Ziman [67] for the theory of the shapes of random fields, with a special emphasis on the contour lines and surfaces of a random potential. A mathematical survey of the statistical topography of Gaussian random fields was given by Adler [68]. The most compelling example of statistical topography is presented by the diverse and whimsical patterns of natural coastlines and islands. The geographical considerations apparently inspired Mandelbrot [69] to introduce the concept of fractals.

Starting from the pioneer work of Mandelbrot *et al.* [70], there have been numerous investigations focusing on crack face morphology characterization within a framework of fractal geometry, that is believed to give promising parameters with which to establish structure–property relationships (see, for review [1–5, 16, 71–120] and references therein). Many different materials have been investigated with different fracture behavior, from ductile to brittle, at very different scales, from nanometer scale using atomic force or scanning tunneling microscopy, to the micrometer to centimeter scale using profilometry measurements and image analysis techniques, up to the meter to kilometer scale for geological faults and up to 1000 km scale for geophysical phenomena [3, 4].

It is now clearly established that, at first view, random fracture patterns can be treated as fractal objects. Fractal geometry, developed by Mandelbrot [69], allows the description of such irregular forms which are more complex than Euclidean, shapes.

A feature having fractal properties is not differentiable and is characterized by the fractional metric (fractal) dimension D_H, which exceeds its topological (Euclidean) dimension. The fractal dimension is a generalization of the Euclidean topological dimension in the metric sense (mass to length ratio) as well as in the topological sense (how many independent coordinates are necessary to identify a point in the structure). Furthermore, the shape of a rupture is commonly anisotropic. This anisotropy also manifests itself in the scaling properties of the fracture patterns. Although anisotropy is very often present, most of the efforts to understand the morphology of fractal fracture has been concentrated so far on the concept of self-similarity (see, for review, refs[2, 5] and references therein). It has been pointed out only quite recently that in many cases self-affinity should be the adequate framework for the interpretation of the scaling properties of the occurring structures[3].

First of all, we should be specific and determine what exactly is invariant in a selected pattern and what is not. It was found that in the case of failure patterns the phenomenon of "fractality" most strikingly manifested itself in the following aspects: (1) hierarchical nature and statistical scale invariance of the defect (pores, cracks, etc.) fields in a wide range of spatial scales $\ell_D < L < \xi_D$, where ℓ_D and ξ_D are, respectively, the lower and upper limits of length interval within of which the defect fields possess statistical scale invariance, and (2) statistical self-affinity of crack-faces within a wide, but bounded interval $\ell_0 < L < \xi_C$, where ℓ_0 is the self-affine cutoff and ξ_C is the self-affine correlation length. Generally, ℓ_0 and ξ_C differs from ℓ_D and ξ_D[3]. Moreover, the fractal properties of failure patterns generally differs within different ranges of length scales[3,4,113,121]. Hence, when we speak about the specified failure patterns fractality we should specify the scale interval under consideration.

Unfortunately, we cannot model real failure patterns using only the simple and well-accepted concept of statistical self-similarity and self-affinity. The shapes of real failure patterns require the introduction of the concepts of multi-fractality and multi-affinity (see refs[1,64,116–118,122–130] and references therein). The neglect of these factors was responsible for the strong contradictions between the results of experimental studies of the fractal properties of failure patterns and their relations with strength parameters[3,60,70,78–81,94,97,98,102–105,111,112]. In fact, in these studies, different definitions for the fractal dimension and different experimental techniques for its estimation were used (see Appendix A and refs[130–137]). These different techniques are associated with different definitions for the fractal dimension should give the same value of fractal dimension only for self-similar or statistically self-similar monofractals and may give dramatically different results for self-affine fractals, multi-fractals and multi-affine patterns [130,137].

Nevertheless, the aforementioned contradictions as well as some confusions in the theoretical analysis in this problem ([138–143]; see also the discussion in refs[41,144] and Sections 2.4, 2.6 and 4.1 of the present work) seem to give support to the arguments of traditional mechanists concerning the non-utility of fractal concepts for describing failure phenomena. To avoid confusion, we start with the definition of basic concepts used in fractal mathematics.

2.1. *The concept of fractals and intuitive definitions of the fractal dimension*

Before we tackle what a fractal is, let us ponder on what a fractal is not. For this purpose, let us take a geometric shape and examine it in increasing detail. That is, take smaller and smaller portions near a given point and allow each to be dilated, that is, enlarged to some prescribed overall size. If our shape belongs to standard geometry, it is well-known that the enlargements become increasingly smooth. Ultimately, nearly every connected shape is locally linear. One can say, for example, that a generic curve is attracted under dilatations to a straight line; a generic surface is attracted by dilatation to a plane, etc.

We all have a feeling for what is meant by a line or circle being one-dimensional, a plane or sphere being two-dimensional, a ball or space being three-dimensional and so on. Roughly speaking, we mean that the position of a point on a line can be specified by one coordinate; on a plane, by two; and in space, by three. That quantity of the number of coordinates is commonly an integer. Thus, to look for a way of introducing fractional dimension, two steps are necessary: (1) we have to find some relationship that characterizes dimension, but does not rely on integers; (2) we need to pin down the weak point in our naive ideas about dimensions, eliminating it so that we can ascribe, to certain objects, a fractional dimension.

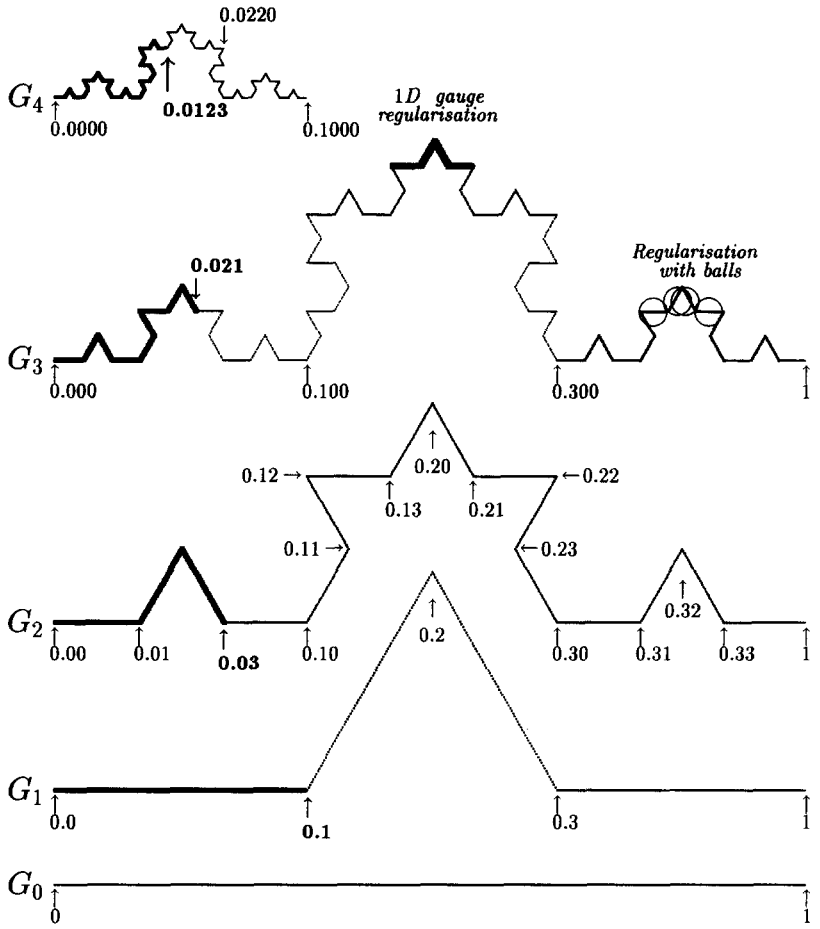

Fig. 1. Invariant construction of the triadic Koch curve and its fractal parametrization. A sequence of points on G_j with constant curvilinear distance $c^* = 0.1$ to the origin is shown by bold lines. Note, that the fractal geometry is obtained for an infinite number of iterations, G_j, i.e. $F = G_\infty$; the fractal curve is, therefore, nowhere differentiable. We can approximate this curve in two ways, with $1D$ gauge, or with uncertainty balls that give it a thickness.

In mathematics the place of ordinary (topological) dimensions is taken by the metric dimension, first introduced by Felix Hausdorff early in this century [145]. However, Hausdorff relied essentially on the ideas that had been expressed by Euclid.† Underlying his approach is the recognition that one- and two-dimensional structures are, in effect, three-dimensional portions of space, two or one of their characteristic scales being very small, so that the notations of length, ℓ, surface, ℓ^2, and volume, ℓ^3, have only a hypothetical meaning. By replacing these notions, by the concept of "fractal content", Mandelbrot [69] deliberately contributed to the review of traditional physics, in particular by writing the fundamental equation of fractal geometry.

$$N(\ell) \times \ell^D = \text{constant}, \tag{1}$$

where D is the fractal dimension. In this equation, the resolution scale ℓ of the analysis of an object is related by a power-law to the number of congruent segments ("modes") $N(\ell)$, necessary to describe the entire object as shown in Fig. 1.

†In fact, even in antiquity people realized how limited the concept of dimension is when it is restricted to an integer. "The line is inconceivable" said the skeptic philosopher Sextus Empiricus [146], "for the geometers state that the line is length without breadth, but we, in our inquiry, are unable to perceive length without breadth either in sensible or in intelligible; for whatever sensible length we perceive, we perceive as including a certain breadth". The end of the second century!

It reveals the existence of a constant that is the generalization of a Euclidean length (area, volume) obtained for the integer value $D = 1$ ($D = 2$ and $D = 3$ for the area and volume, respectively). The relevance of eq. (1) can be illustrated by the continuous, but nowhere differentiable triadic Koch curve shown in Fig. 1(a) and characterized by $D = 1 - \ln N(\ell)/\ln \ell = \ln 4/\ln 3 = 1.2618595$.

Now, let us build the sequence of curvilinear coordinates, r_j, of a given sequence of points A_j on the curves G_j (see Fig. 1(a)). It is readily seen that r_j can be defined as a distance along G_j

$$r_j = x_j \left(\frac{4}{3}\right)^j = 4^{j(D-1)} x_j = c^*,$$

where c^* is a constant. For example, in Fig. 1(b) the sequence of parameters 0.1, 0.03, 0.021, 0.0123,... defines points at a constant distance $c^* = 0.1$ from the origin on the respective curves G_1, G_2, G_3, G_4,... It is easy to understand, that in the limit $j \to \infty$ parameter $x_j \to 0$ and

$$\lim_{j \to 0} x_j = 0,$$

i.e. the point A_∞ in a fractal curve $F = G_\infty$ coincides with the origin **O** of F, while the curvilinear distance between **O** and A_∞ on F is equal $c^* = 0.1 > 0$. From this "paradox", it follows that the real coordinate, x, is insufficient to thoroughly describe the fractal curve F: the distance along F between two points parametrized by two different Xs is infinite, while points separated by a finite distance along F correspond to the same values of x.

While the number of conventional coordinates cannot be fractional, and to determine the position of a point on the triadic Koch curve, we need same number of coordinates, $n_1 = [D] + 1 = d = 2$ ([..] denotes the integer part of the number), that is necessary to determine the point position in a plane. It is easy to understand that a situation changes dramatically, when the positions of two or more points are analyzed. In fact, the positions of 1000 points on a smooth (differentiable) curve can be completely determined by $n_{1000} = 1 \times 1000 = 1000$ numbers (distances of each point from the origin). To determine the positions of 1000 points on a smooth surface or plane we need to use $n_{1000} = 2 \times 1000 = 2000$ numbers (coordinates), whereas the positions of 1000 points on the triadic Koch curve can be completely determined by $n_{1000} = [1.2618 \times 1000] + 1 = 1262$ numbers. In this sense, we can speak about a fractional number of coordinates, since $n_1^* = n_{1000}/1000 = 1.262$.

Another approach can be formulated, equally natural, but more comfortable to mechanists. With one-dimensional objects we associate the concept of length, ℓ; with two-dimensional objects, area, ℓ^2; and with three-dimensional ones, volume, ℓ^3. Characterizing these concepts is a construct which, similarly, is called dimensionality: [m], [m^2] and [m^3]. From other branches of mechanics and physics we know that these dimensions can also be fractional. For example, stress intensity factor and fracture toughness have the dimension of [Pa $\times$ m$^{1/2}$] = [kg/s^{2}m$^{1/2}$]; the constant C in the Paris power-law [147] for fatigue crack propagation has the dimension [Pa$^{-1/k} \times$ m$^{1-k/2}$], where k = constant, etc.

However, in order to put this fractional dimension into fractal geometry, we have to look at the concept of coordinates somewhat more broadly. To any preassigned accuracy we can specify a point inside a square, not just by a pair of coordinates, but also by only one, provided we use a coordinate line that fills the square more and more densely (for example, Peano curve in Fig. 2). In fact a coordinate of that kind is by no means exotic. For instance, a person's address in a city could, in principle, be specified by giving the geographic coordinates of his apartment, but we use a different method, first naming the street, then the building and the apartament numbers (like a coordinate with integer and fractional parts). Indeed, one could actually number all the citys' dwellings in a single sequence (the American nine digit ZIP code comes closest).

In natural sciences, the fractal concept was originally put forward to cope with a single salient example: measuring the length of the coast of Great Britain by Lewis Fry Richardson (see ref. [69]).

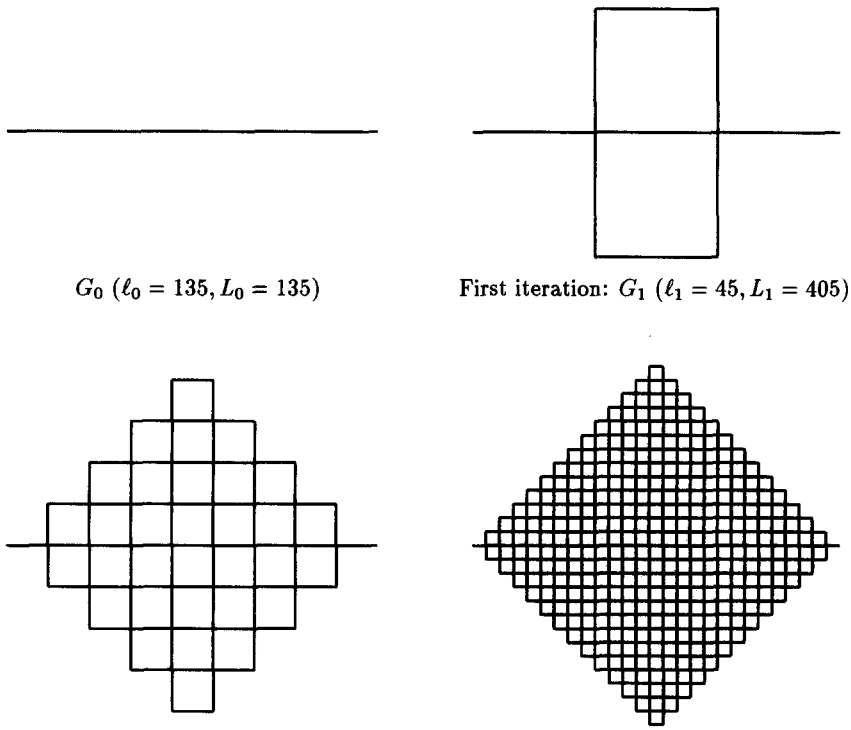

Fig. 2. Three first iterations in the construction of plane-filling self-similar Peano curve. In the limit of infinite number of iterations, the Peano curve densely fills the plane, so that the metric (fractal) dimension, D, of the Peano curve coincides with the topological dimension of the plane, i.e. $D = 2$.

Viewing a curve on a plane (Figs 1 and 2) at a given scale and the definition of its length are two intimately connected notions. There are many different ways to represent a curve at a given scale. For example, scaled curves can be derived from the actual curve by subdividing them with dividers set to intervals of length equal to one-forth, one-sixteenth, etc. of the length unit, starting at the beginning of the curve. Each new point is obtained by setting the compass point on the previous point and marking the intersection of the arc of the compass and the curve. The marked points are then connected with line segments. The relative length of the curve, $L(\ell)$, at scale ℓ is then defined by the relationship $L(\ell) = \ell \times N(\ell)$, where $N(\ell)$ is the number of segments of length ℓ that span the curve. The true length, L_t, of the actual curve is then defined as the limiting value that $L(\ell)$ approaches, as ℓ approaches zero or mathematically

$$L_t = \lim_{\ell \to 0} L(\ell) = \lim_{\ell \to 0} \ell \times N(\ell). \tag{2}$$

It is easy to verify that if we apply this method to each differentiable curve we obtain its true length. For example, for a circle, this method gives $L_t = 2\pi R$, where R is the circle radius.

However, when Richardson applied this method to determine the coastline length of Great Britain and some other countries, taking more and more detail maps, he discovered that for each of them the number of segments at scale ℓ satisfied the power-law (1), where the values of constant and D are constants for a given coastline. These constants are different for coastlines of different islands [69] and, as we shall see below, D is associated with the fractal dimension of coastline. Inserting eq. (1) in the conventional definition of length $L = \ell \times N(\ell)$ Mandelbrot suggested the relation

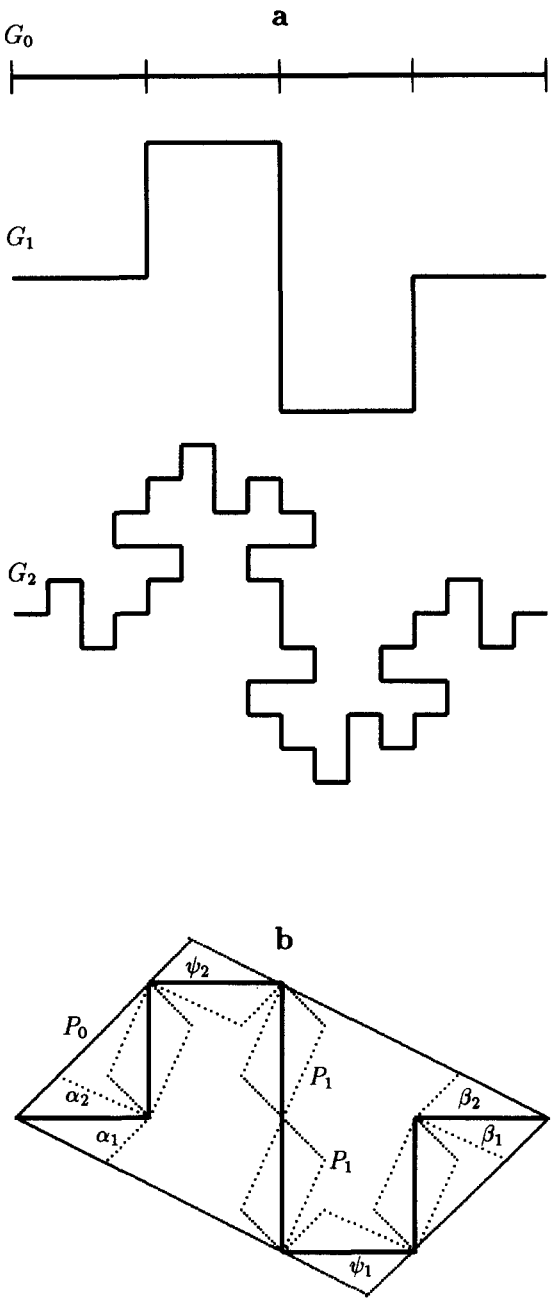

Fig. 3. (a) The iterative construction of Koch curve with $D = \ln 8/\ln 4 = 1.5$, and (b) building of this curve by deleting surface.

$$L(\ell) = C\ell^{1-D}, \tag{3}$$

which yields straight lines when $L(\ell)$ is plotted against ℓ on log–log graph paper.

By nature, eq. (3) diverges every time the geometrical approach is traditional, i.e. Euclidean. For example, a length is naturally expressed by $L = N \times \ell$, but for $D > 1$ fractal geometry imposes $L = N \times \ell \propto \ell^{1-D} \to \infty$, when $\ell \to 0$, thus length diverges. A surface area is expressed by $S = N \times \ell^2 \propto \ell^{2-D}$, when $\ell \to 0$ the surface area diverges if $D > 2$, or the surface density $1/S$ diverges if $D < 2$. As a result, such physical notions as extensive and intensive properties acquire diverging characteristics on the boundaries. However, as it was noted above, real failure patterns obey fractal (scaling) properties only within a bounded range of length scales

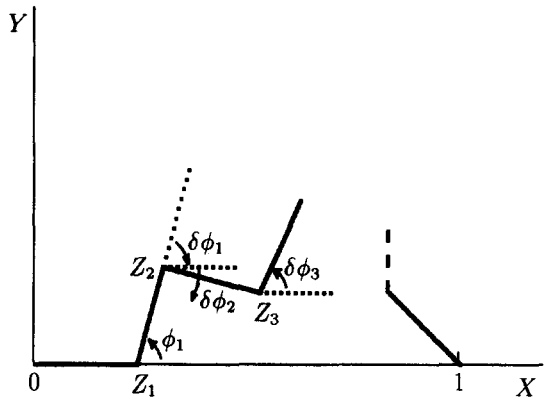

Fig. 4. Building of the basic structure of a fractal curve[149].

and, thus, have a finite length (area, volume). Hence, explicitly speaking, from a mathematical viewpoint, the metric dimension of a real failure pattern always coincides with its topological dimension. However, we can speak about fractal properties of failure patterns (as well as coastlines and many other natural fractals) in a sense of the concept of "intermediate asymptotic" (see ref. [148]).

A fractal curve with fractal dimension lying between 1 and 2 is intermediate between a line and a surface. Indeed, while it may be built by adding segments (Fig. 3(a)) it may also be obtained by deleting surfaces [149]. This construction allows one to deal with the problem of multiple points. Given an initial curve, G_1, consider a polygon, P_0, of surface, S_0, with one of its diagonals being the segment [0,1] and in which G_1 is included. Then building around each segment of G_1 an n-reduced scale version, P_0, we obtain a figure P_1, as it is shown in Fig. 3(b). Now, if we denote the angle between two segments in G_1 as $\delta\phi_j = \phi_j - \phi_{j-1}$ (Fig. 4) then an obvious condition for the absence of multiple points (all polygons of P_1, as well as all polygons of P_2, P_3,..., P_j,..., should be disjointed) implies

$$-\psi_1 = (\alpha_1 + \beta_1) - \pi < \delta\phi_j < \psi_2 = \pi - (\alpha_2 + \beta_2),$$

where all angles are defined in Fig. 3(b).

Another fundamental property of fractals, which distinguishes them in a basic manner from homogeneous euclidean objects, is the scaling invariance (self-similarity) of fractal patterns. Many fractals are made up of parts which are, in some way, similar to the whole, such as classic fractals that are shown in Figs 1–3. Structures are called self-similar if they appear the same at every scale.† In other words, if we look at the fractal structure from afar, it appears the same as it does in a close-up view, in terms of its details. Broadly speaking, mathematical and natural fractals are shapes whose roughness and fragmentation neither tend to vanish, nor fluctuate up and down, but remain essentially unchanged as one zooms in continually and examination is refined. Hence, the structure of every piece holds the key to the whole structure.

One may classify fractals in two broad categories, namely the regular and random fractals fractals[69]. Although all real failure patterns are random, the regular fractals, such as shown in Figs 1–3, may be used as models, because the fractal dimension, D, does not change after a linear transformation of regular fractal structure. So, two curves in Fig. 5 are characterized by the same value of D. In this way, for random fractals, the concept of similarity must be replaced by the concept of "statistical self-similarity"[150].

To understand how self-similar curves relate to the Richardson power-law eq. (3), it is sufficient to set $C = 1$ and rewrite eq. (3) as

†Self-similarity is not only the key property of a fractal, it may actually be used to define them—an approach which is often extremely useful [69].

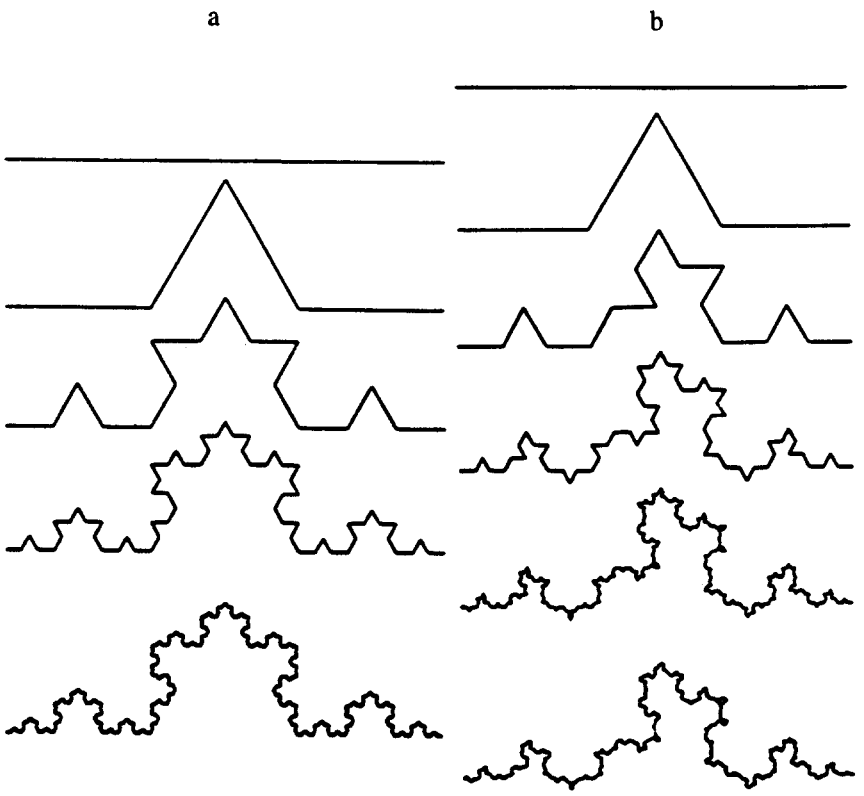

Fig. 5. (a) Regular self-similar, and (b) random statistically self-similar versions of the triadic Koch curve (see also Fig. 1). Notice that these curves are homeomorphic and characterized by the same fractal dimension $D = \ln 4/\ln 3 = D_S$[150].

$$L(\ell) = \ell\left(\frac{1}{\ell}\right)^D.$$

Now, let us consider a trivial example of self-similar triadic Koch curve shown in Fig. 1. This curve is generated iteratively by replacing each segment of one stage with four identical segments, one-third the original in length in the next stage. Thus, whereas for stage 1, $L(1) = 1$, for stage 2, $L(1/3) = 1/3 \times 4$, or $L(1/3) = (1/3)\times\frac{1}{1/3^D}$ etc. From this, it follows that the fractal dimension of the triadic Koch curve is $D = \ln 4/\ln 3$. For each successive stage in the development of the curve we have the same value of D. Mandelbrot[69] has shown that, as for the triadic Koch curve, any geometrically self-similar curve may be characterized by the dimension of self-similarity, D_S, also called the similarity dimension,

$$D_S = \frac{\ln N(\epsilon)}{\ln(1/\epsilon)}, \tag{4}$$

where $N(\epsilon)$ is the number of congruent segments of length $\epsilon\ell$ and ϵ is the contraction ratio that replaces the unit interval in the initial stage of the iteration. For a regular self-similar fractal we always have $D_S = D$ [69, 150]. Thus, for the Peano curve (Fig. 2): $N = 9$, $\epsilon = 1/3$ and $D = D_S = 2$; for the Koch curve in Fig. 3(a) we have $N = 9$, $\epsilon = 1/4$ and $D = D_S = 1.5$.

Notice that eq. (4) is also valid for statistically self-similar patterns, since any random, but statistically self-similar fractal can be transformed in the regular fractal with the same fractal dimension $D = D_S$ by a homeomorphic, one-to-one and onto transformation[130]. In this way the aforementioned Richardson's data indicate that the configuration of coastlines is derived from a general law of nature and Mandelbrot's analysis of Richardson's data led to the follow-

ing expression of that law: each segment of a coastline is statistically similar to the whole, i.e. the coastline is statistically self-similar[69].

When we speak of the fractality of coastline, non-smooth, broken-line trajectory of Brownian particle or its infinitely high velocity, the real situation is idealized. On very tiny scales the finite mass of a Brownian particle and the finite intercollision time will manifest themselves and the trajectory will become smooth. When we speak of a fractal surface (for example, fracture surface), we should think of a rough surface whose scale of irregularity gradually becomes smaller, as the projected area of the irregularities diminishes. The irregularities should, however, still be much coarser than the interatomic distance scale, otherwise the concept of a boundary for the body would not apply at all. When we say that a lengthy polymer molecule fills up a region of space, we mean that (in a different way to a Peano curve) from some filling factor onward we have to allow not only for the molecule's extension along a line, but also for its thickness and we can no longer describe the situation in terms of tangled lines. That is why in the natural sciences the fractal concept ties in with intermediate asymptotic: although the scale of roughness is small, it remains much larger than something still smaller[148].

Some useful relationships for the similarity dimension of regular fractals are given in Table 1. Prominent examples of the application of regular fractals to model real fractal patterns formed in deformed solids are given in Figs 6–11. Figure 6 demonstrated how the complex shape of grain boundaries in polycrystals can be modeled by the Koch curve. Figure 7 illustrated the Lüders–Chernov band formation in the deformed material and the fractal representation for final microstructure on the basis of Cantor set with fractal dimension $D_S = \ln 2/\ln 3$; in Fig. 8 given the schematic representation of defectless channels in the crystal deformed after irradiation or quenching; the dimple sizes distribution are shown in Fig. 9 together with corresponding homeomorphic regular fractal. Two examples of tree-like fractals are shown in Fig. 10(a,b). In ref. [108] these fractals were used as models of dendritic particles in iron alloys. Experimental results obtained in the electron microscope study [108] are reproduced in Table 2. Figure 11(a) illustrates the construction of a circle fractal the similarity dimension of which strongly depends on the geometrical characteristics of structure (Fig. 11(b)). The circle fractal was used as the model of dimples formed in ductile fracture surface[3].

The models considered, by virtue of their self-similarity are very useful for analysis of the problems associated with formation and evolution of the corresponding real patterns. Some useful variations of eq. (4), which may be directly applied for estimation of the fractal dimension of real (random) fractals, are listed in Table 3. The results of computer simulations [152] of diffusion-limited aggregation (DLA) and viscous fingering (VF) are reproduced in Table 4. Notice that DLA and VF clusters are random statistically self-similar fractals.

There are also non-fractal objects, called "scales", which are associated with this simple scaling rule and are useful for more adequate description of natural objects, such as porous media [5]. Scales are characterized by the integer metric dimension and are not fractals even through the scale length itself, while its boundary (i.e. the surface of the pore space) can be a fractal. Thus, in constructing such object we remain the important property of self-similarity, but abandon the fractional dimensionality, requiring instead that the scale be characterized by

Table 1. Relations between similarity dimension and parameters of structure for different regular fractal structures

NN	Type of regular fractal structure	Expression for similarity dimension	Comments
1	Cantor set, Peano curves, Koch curves	$D_S = \ln N/\ln(1/\epsilon)$	N—number of self-similar parts, ϵ—concern length of each part (Figs 1–3, 5, 7(c), 9(c), 10(c))
2	"Fir-trees"	$D_S = \ln P/\ln K$	P—number of branch with length L_{n+1} on the branch with length L_n $K = L_n/L_{n+1}$ (Fig. 10(a,b))
3	Sierpinski gaskets (carpets)	$D_S = \ln(b^d - R)/\ln b$	b—the base of lattice, R—number of ejection parts d—topological dimension (Fig. 12(a))
4	Round fractal lattice	$N\varphi^{D_S}\sum_{k=1}^{M}(1-2\varphi)^{D_S(k-1)} = 1$, $\varphi = \tan(\pi/N)\cdot\tan[(\pi/4)(1-2/N)]$	N—number of sectors M—number of possible scale transformations (Fig. 11).

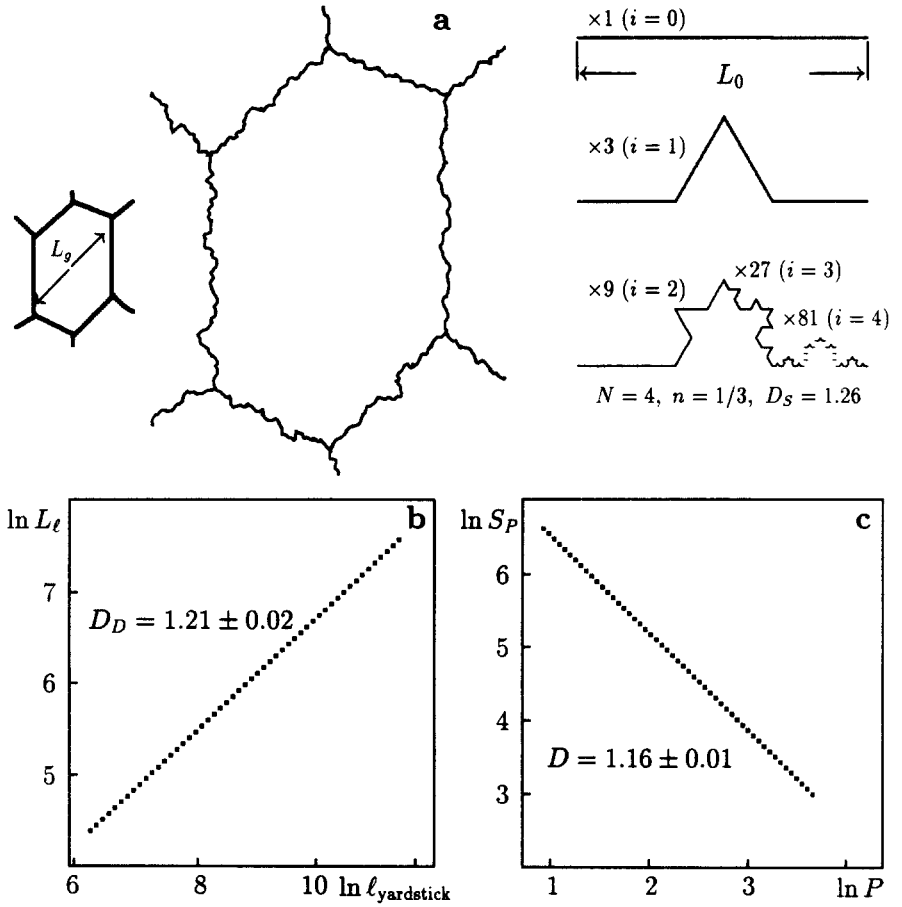

Fig. 6. (a) Grain boundary approximation by regular fractal curve; and the results of experimental evaluation of the fractal dimension D of grain boundaries in deformed zinc [151], by means of the (b) yardstick (divider) method and (c) by using the perimeter–area relation for the grain ensemble.

specified porosity p and a power-law distribution of the number of particles (pores) $N_p(L_n)$ over sizes, L_n:

$$\langle N_p(L_n)\rangle \propto L_n^{-\alpha} \tag{5}$$

as it is shown in Fig. 9(d). Since scales and fractals are similar in many respects, let us begin our construction of a regular scale by starting from the properties of a regular geometric fractal, namely Sierpinski gasket shown in Fig. 12(a). The procedure for constructing this object involves an iterative sequence of cutting out the central triangle. The fractal is obtained in the limit as the number of steps $n \to \infty$. In Fig. 12(b) do the cutting out, not at every step, but only at every other step, i.e. only at the odd-numbered steps, while keeping the rest of the procedure of constructing the fractal unchanged [5]. We see that in the resulting object, which is an example of a regular scale, there are black and white triangles of different sizes, both large and small. We call the black triangles particles and the white ones pores. Clearly, neither the set of particles nor the set of pores forms a fractal (for both $D = d = 2$), but both of these sets are self-similar, with the coefficient 1/4. The distribution of particles and pores for scale $F = G_\infty$ in Fig. 12(b) is described by the power-law eq. (5) with $\alpha = \ln 3/\ln 2$ and the porosity $p = 3/7$, whereas the porosity of Sierpinski gasket $F = G_\infty$ in Fig. 12(a) is one (100%). Random (stochastic) scales are defined by analogy with random fractals and, unlike the case of regular scales, the self-similarity, constancy of p and power-law distribution of particles and pores hold only in a statistical sense.

In the surge of interest in applications of the concepts of fractal geometry to problems in natural sciences following the publication of "*The Fractal Geometry of Nature*" [69], attention was focused primarily on simple self-similar fractals that can be characterized by a single fractal

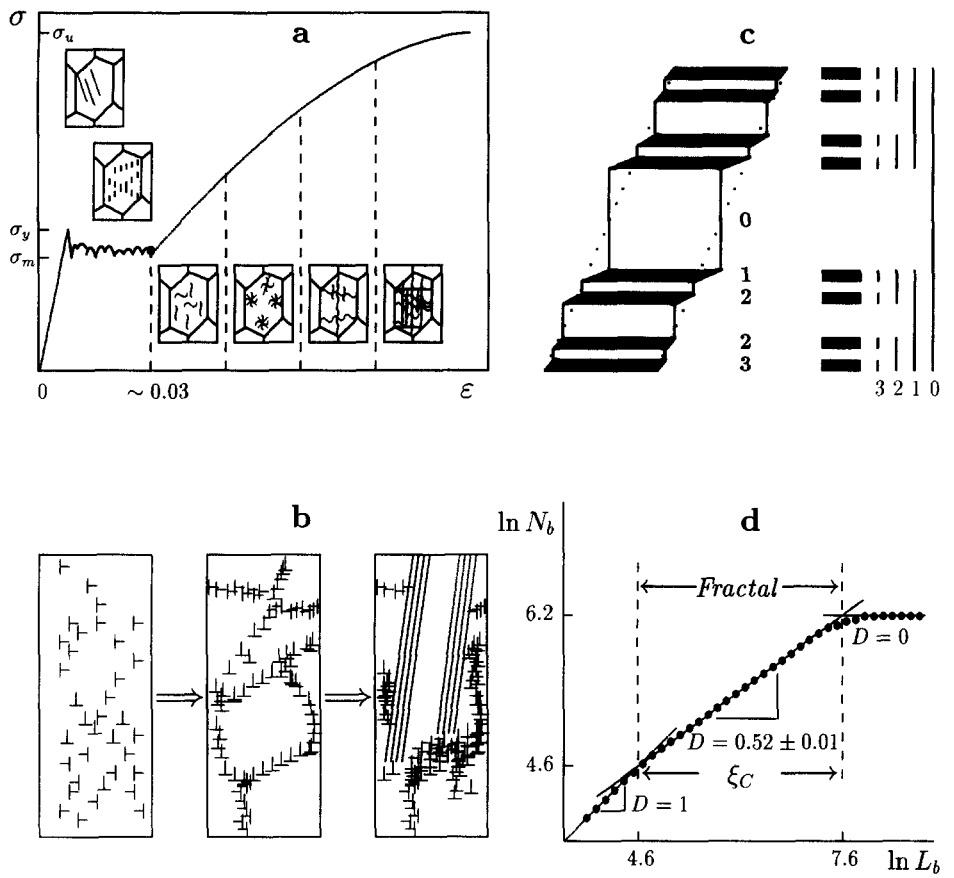

Fig. 7. (a) The stress–strain behavior with heterogeneous deformation region associated with the Lüders–Chernov bands formation; (b) the corresponding changes in the material microstructure[3]; (c) the scheme of the fractal spatial distribution of dislocation bands[56] and the corresponding nonstandard Cantor set; and (d) the results of experimental investigations of the fractal properties of dislocation bands system in the single crystals of copper[87]. N_b is the number of sliding planes in the band within the length interval L_b ($\ell_0 \sim 70$ nm, $\xi_C \simeq 2000$ nm).

dimension. For such structures almost any reasonable procedure for measuring the fractal dimension will lead to essentially the same results if the fractal sealing regime extends over a sufficiently wide range of length scales[137]. However, in some cases the higher chance of growing into a given direction leads to clusters whose linear size diverges with a smaller exponent in the direction perpendicular to that of the preferred growth. As a result the clusters become self-

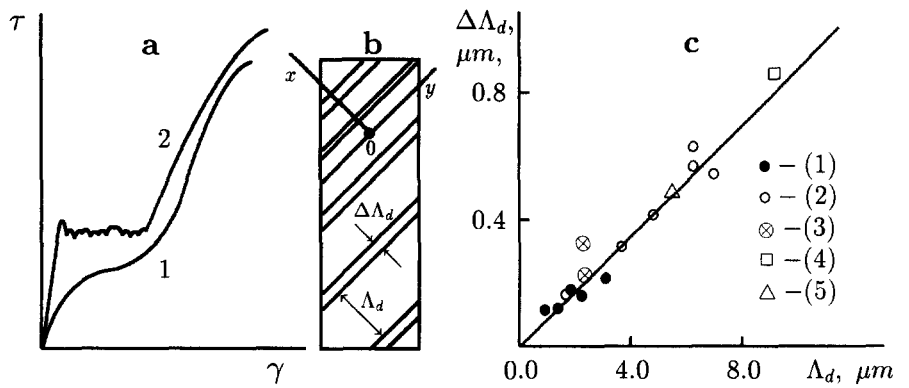

Fig. 8. Curves of strengthening $\tau(\gamma)$ for (1) annealed, and (2) irradiated or quenched (a) metal crystals [8]; and (b) schematic representation of defect channels in crystals deformed after irradiation or quenching; (c) the width of defectless channels $\Delta\Lambda_d$ as a function of the separation between them Λ, in irradiated: (1) Cu, (2) Nb, (3) Ni, and quenched: (4) Al, (5) Au crystals (the data are taken from [119] where the data collected by various authors were summarized).

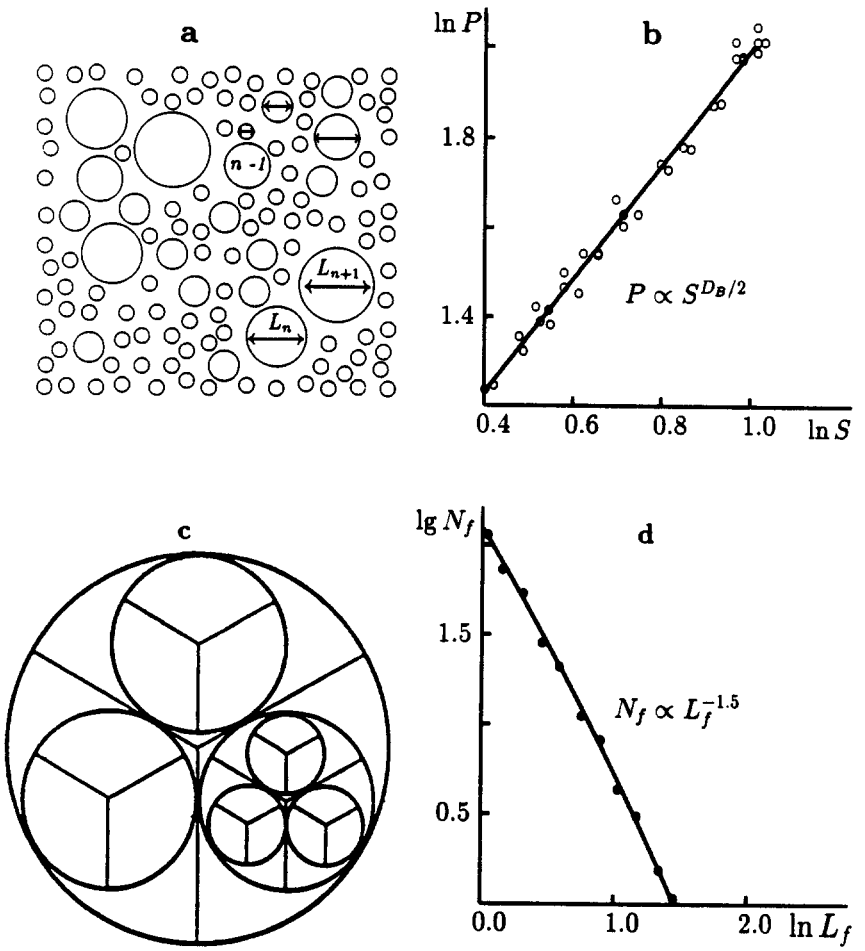

Fig. 9. (a) Schematic representation for ductile fracture surface of nickel alloy; (b) the perimeter – area relation for dimple ensemble; (d) the dimple size distribution; and (c) the corresponding homeomorphic (regular) fractal. Figure reproduced from[3], see also Table 1.

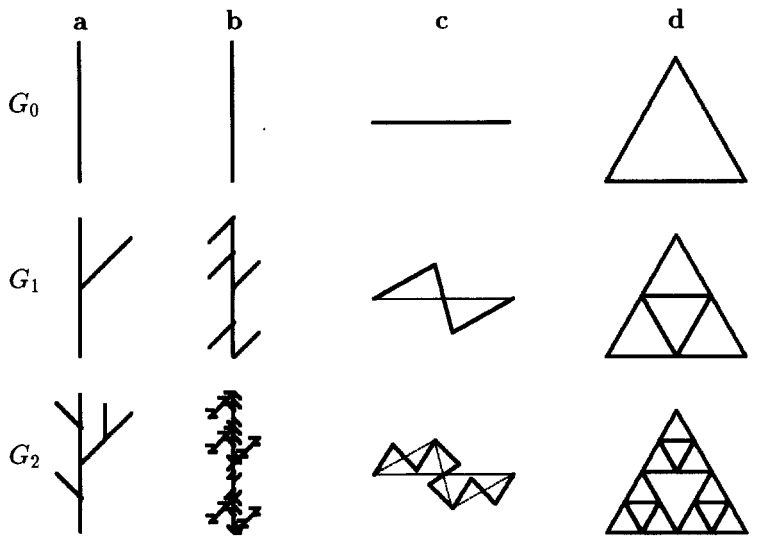

Fig. 10. Four homeomorphic fractals: (a, b) two examples of the tree-like fractals; (c) the Koch curve; and (d) the triangular Sierpinski gasket. Notice that all these fractals are characterized by the same fractal dimension D = ln 3/ln 2 while their connectivity properties are different.

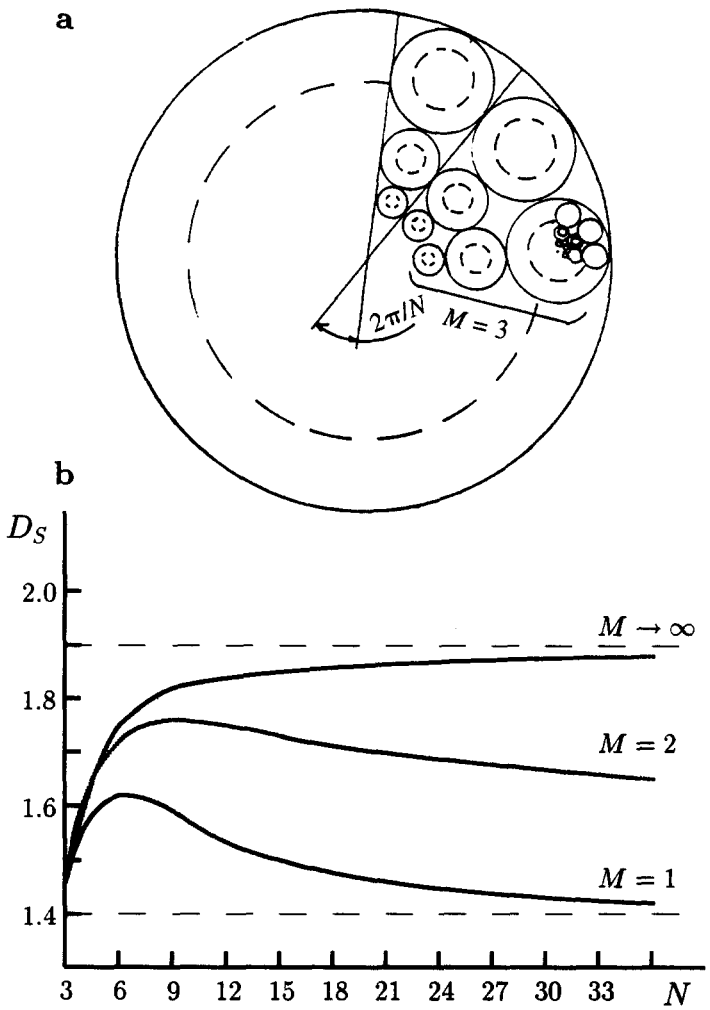

Fig. 11. (a) The circle fractal and (b) the graphs of its similarity dimension as a function of number of sections N plotted for different number of possible scale transformations, M (see Table. 1).

Table 2. The parameters of distribution histogram (ℓ_0, σ_D, $\bar{K}$, and $\bar{P}$) for zero-order of center axis of high disperse dendritic particles of iron and iron alloys formed by the two-layer electrolytic bath method (electrolysis parameters j, ω, M) and the comparison of experimental and theoretical values of the fractal (similarity) dimension of particles (results of electron microscope study from[108])

Material	Fe	Fe	Fe	F–Co–Ni	Fe–Co
Cathode current density j, A/m^2	1000	1000	2000	2000	2000
The disc cathode rotation rate ω, s^{-1}	0.30	2.00	1.05	1.03	1.05
The particle surface chemical modifier (M)	Myristic acid	Myristic acid	Oleic acid	Oleic acid	Oleic acid
Mean length ℓ_0, nm	180	130	260	480	430
Standard deviation, σ_D	1.82	2.14	1.52	1.47	1.40
$\bar{P}$[1]	27	28	23	26	25
$\bar{K} = L_{n+1}/L_n$[2]	16	10	12	8	9
$D_F = \ln\bar{P}/\ln\bar{K}$[3]	1.20	1.45	1.26	1.57	1.48
D_F^{exp}[4]	1.25	1.44	1.28	1.50	1.49

[1] Mean number of high-order branches on a branch of given order.
[2] Mean ratio of branch lengths.
[3] Theoretical values.
[4] Experimental values of fractal dimensions.

Table 3. Some definitions of fractal dimension (see ref.[130])

NN	Dimension	Expression for fractal dimension	Comments
1	Mandelbrot, Schirelman–Kolmogorov	$D_F = \lim_{\epsilon \to 0}\{\sup[\ln N_x(\epsilon)/\ln(1/\epsilon)]\} = \inf\{d \geq 0, \lim_{\epsilon \to 0}[\sup \epsilon^d \times N_x(\epsilon) = 0]\}$	$N_x(\epsilon)$ is the least number of balls of radius less than ϵ which are needed to cover fractal
2	Kolmogorov, Schirelman–Potjrajin	$D_K = \lim_{\epsilon \to 0}\{\sup \lg N(\epsilon)/\lg(1/\epsilon)\}$	$N(\epsilon)$ is the smallest number of balls of diameter less or equal to ϵ which are needed to cover fractal
3	Similarity	$D_S = \ln M/\ln R$	If set made up of M copies of itself scaled by factor R
4	Internal similarity	$\sum_{i=1}^{d} R_i^{d_{IS}} = 1$	d—topological dimension, R_i—similarity ratios
5	Cluster (or mass) dimension	$D_M \ln N/\ln(R/R_0)$	N is the number of monomers of length R_0 into monomers of dimension R

Table 4. Results of computer simulations of diffusion-limited aggregation (DLA) and viscous fingering (VF) clusters modeled by tree-like fractals[152]

Parameter and relationship	Comments	DLA	VF
$r_N = N_n/N_{n-1}$	N_n is the number of n-order branches	5.2 ± 0.2	4.8 ± 0.5
$r_L = L_n/L_{n-1}$	L_n is the length of n-order branch	0.35 ± 0.01	0.34 ± 0.04
$D_S = \log r_N/\log(1/r_L)$	D_S is the similarity dimension	1.6 ± 0.02	1.5 ± 0.1
D_B, $N(\delta) \sim \delta^{-D_B}$	D_B is the box dimension(δ is the size of boxes)	1.62 ± 0.02[1] 1.67 ± 0.03[2]	1.51 ± 0.06
D_g, $M(R_g) \sim R_g^{D_g}$	R_g is the radius of gyration and M is the mass	1.710 ± 0.005	–
D_{Cl}, $M(r) \sim r^{D_{Cl}}$	D_{Cl} is the cluster dimension $M(r)$ is the mass of cluster	1.69 ± 0.01[1)]	1.62 ± 0.05[1)]

[1] Estimated by scaling different cluster sizes on to the same curve.
[2] Box counting only points with $R < R_g$.

affine instead of self-similar, which means that the clusters of very different sizes can be scaled onto each other only by using direction dependent scaling factors. Self-affinity, i.e. a more general scaling transformation which takes anisotropy into account, has been found to appear naturally in quite a number of different areas. This scaling is fully characterized by $d-1$ exponents ν_i in d-dimensional Euclidean space. As pointed out by Mandelbrot[153–155], self-affine fractals play an important role in a large variety of physical and chemical phenomena. Many fractal

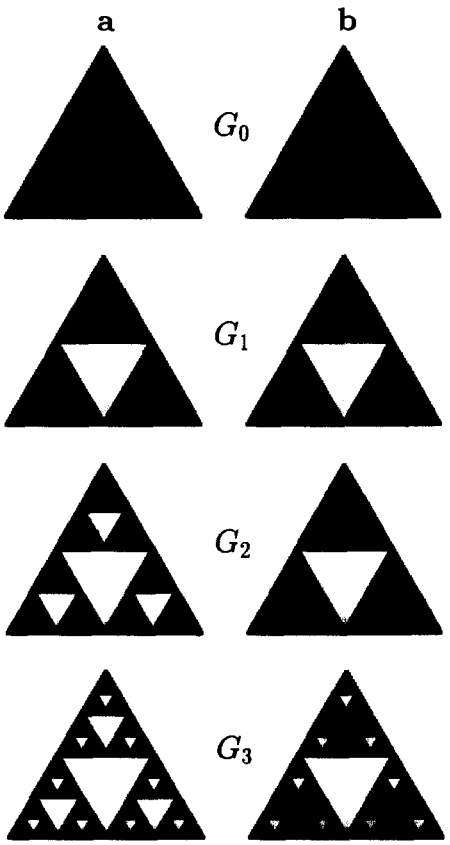

Fig. 12. (a) The Sierpinski gasket and (b) the corresponding "scale". Notice that while both patterns are self-similar, the first one is fractal (D_S = ln 3/ln 2 = 1.58...), whereas the second one is not (the metric dimension of the "scale" coincides with its topological dimension, i.e. $D = 2$)[5].

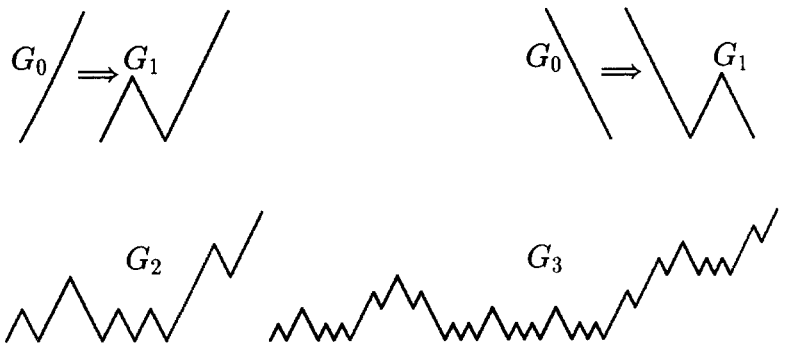

Fig. 13. Invariant construction of self-affine fractal by means of affine transformations[156].

structures found in nature, for example erosion and fracture surfaces, exhibit a self-affine geometry. A variety of different processes including corrosion, erosion, wear, growth, fracture, deposition and dissolution lead to the formation of rough surfaces that appear to be self-affine [64]. For some processes the self-affine geometry has been established as a result of experimental studies and/or computer simulations. Examples of this may be found in popular growth models such as the boundary of Eden clusters, or ballistic-deposition models [64, 156]. An entire pattern grown from an appropriate substrate such as a line (or a fiber) and a plane can often be subdivided into individual clusters (or trees) grown from the substrate. The individual clusters in the case of Scheidegger's river network, Eden and ballistic deposition models have self-affine structures [64]: the root-mean-square height from the substrate P_N of a cluster of size N (N is the number of particles or constituent units forming the cluster) and root-mean-square width, L_N, both scale as

$$P_N \sim N^{\nu_P} \text{ and } L_N \sim N^{\nu_L},$$

but the exponent ν_P and ν_L are, generally, different. Self-similar fractals such as individual clusters of diffusion-limited deposition models, on the other hand, can be characterized by only one exponent $\nu_P = \nu_L = \nu = D_F^{-1}$ [130], where D_F is the fractal dimension (Table 3).

A simple model for a self-affine fractal is shown in Fig. 13. The structure is invariant under the anisotropic magnification $x \to 4x$ and $y \to 2y$. If we cut a small piece out of the original picture (in the limit of $n \to \infty$ iterations) and re-scaled the x-axis by a factor 4 and the y axis by a factor 2, we will obtain the exact original structure. In other words, if we describe the form of the curve in Fig. 13 by the function $Y(x)$, this function satisfies the equation[156]

$$Y(4x) = 2Y(x) = 4^H Y(x), \text{ where } H = \frac{1}{2}.$$

In general, if a self-affine curve is scale invariant under the transformation $x \to \lambda_x x$ and $y \to \lambda_y y$, we have

$$Y(\lambda_x x) = \lambda_y Y(x) \equiv \lambda_x^H Y(x), \tag{6}$$

where the roughness exponent

$$H = \frac{\ln \lambda_y}{\ln \lambda_x} \tag{7}$$

is called the Hurst exponent[64,69]. In the example of Fig. 13, $H = 1/2$.

Considerable difficulties and confusions were encountered when attempts were made to measure the fractal dimensions of self-affine structures using the approaches that worked well for self-similar fractals.† Fortunately, confusion of self-affine and self-similar fractals is now

†Imagine that on the fracture surface is a whole hierarchy of mounds having a common base area but differing in height, so that the higher mounds occur much more rarely than the low ones. Clearly you can't describe a roughness of this kind by any single number, as a fractional dimension. Hence the fractal concept must build upon a premise which excludes such complication upon the postulate that the corresponding power–spectrum expansions contain random phases.

much less common as a result of the much broader dissemination of the principles of fractal geometry and the efforts that have been made by Mandelbrot [153–155], Falconer [150], Matsushita and Ouchi [157], Voss [158], Matsushita, Ouchi and Honda [159], Moreira *et al.* [160], Schmittbuhl and Vilotte [161] and other authors (see refs [64, 130]) to clarify the basic nature of self-affine fractals.

In general, fractal analysis provides a description of how space is occupied by a particular curve or shape. The fractal dimension measures the relative amounts of detail or "roughness" occurring over a range of measurement intervals. The more tortuous, convoluted and richer in detail the curve, the higher fractal dimension. However, roughness and fractal dimension are not synonymous. Roughness is generally measured as the average variation about the mean value and is not related to the scale or changes in scale of measurement. Fractal dimension is used to quantify the variation of the length or area with changes in the scale of measurement interval. Hence, the fractal dimension is an intensive property, while roughness is not.

Nowadays the concept of fractals is increasingly considered in the natural sciences for several reasons:

1. The unifying concept underlying fractals, power-law and chaos is self-similarity (or self-affinity). Self-similarity, or invariance against changes in scale or size, is an attribute of many laws of nature and innumerable phenomena in the world around us. Self-similarity is, in fact, one of the decisive symmetries that shape our universe and our efforts to comprehend it [1, 130, 148, 156].
2. The length of a fractal curve (as well as the area of fractal surface) is dependent on the resolution with which it is measured and diverges when the resolution tends to be infinite. The analog of this phenomenon was discovered in the fractographic investigations of fracture surfaces [3, 61–64].
3. Fractal curves are functions which are continuous, but nowhere differentiable. This property has already been observed for some natural phenomena, such as trajectory of Brownian particle and particle trajectories in quantum mechanics, [130, 156], crack paths [2], etc. Some of the most fertile fields for fractals are fluctuating phenomena [1]. The nondifferentiability of fractals and their infinite length forbid a complete description based on usual real numbers. It was shown that, using nonstandard analysis, it is possible to solve problem of the nondifferentiability of fractals: a class of nonstandard curves (whose standard part is the usual fractal) was defined so that a curvilinear coordinate along the fractal can be built [149].
4. A fractal dimension can be any real number.† So this concept may apply to various fields of physics, such as theory of critical phenomena, where non-integer dimension has become a necessity [1, 156, 162, 163].
5. The concept of fractals is closely related to the concepts of renormalization group, self-similar solution and intermediate asymptotic. Actually, all these concepts are the most fruitful applications of self-similarity [1–5, 130, 148, 162].

These properties are mainly concerned with the static or kinetic aspects of the systems under consideration. Physics, however, is primarily interested in dynamics, whose laws have been formulated in terms of calculus since the Newtonian revolution three centuries ago. There is a reasonable question: How are fractal structures generated in the framework of our conventional physics formulated in the language of differential or partial differential equations?

The answer to this question was given only in the mid eighties, when it has been recognized that differential equations genetically and inescapably produce fractals which are, in fact, responsible for the complex time–space behavior (chaos) exhibited by these systems. Dynamic systems are the foundation of the most of physical models (for example, the hydrogen and the helium in quantum mechanics and the Solar system in astrophysics). Although elementary and deterministic, their motions look almost random over long time intervals and cannot be explained by the traditional approaches. The fact that deterministic processes are able to generate seemingly random output has philosophical, as well as practical, implications. Deterministic chaos was brought to the fore of our scientific awareness by happenstance in the early 1960 s by

†Notice, however, that there are concepts of negative and even complex fractal dimension (see for review ref. [130] and references therein.

the meteorologist Edward Lorenz[164], when he was attempting to model convection in the atmosphere by computer calculations. As a natural consequence, there is widespread interest in this subject[165]. Many thousands of scientific and technical articles have been written on the subject and some of the language and ideas of fractal theory are regularly referred to in popular magazines, in daily newspapers, in novels and on television shows.

Roughly speaking, the aforementioned concepts form the basis of the application of fractal theory in fracture mechanics. Actually, in many experimental works, as well as in some theoretical models, the relations eqs (1)–(5) are directly used to characterize or model real patterns observed in experiments. In practice, however, this leads to some confusion associated with, for example, the notable Schwarz area paradox,[127], or its fractal analog,[153]. Furthermore, the fact that real failure patterns are often multifractal or self-affine may also lead to some confusion when eqs (1)–(5) applied, so that we need a more rigorous definition for the fractal dimension of real patterns.

2.2. *The concept of metric dimension and mathematical foundations of fractal geometry*

Nature presents to us a great multiplicity of forms. The shapes of plants, animals, forest, mountains, seas, clouds and universe know no bounds. Yet something in the human mind has sought to tame this great diversity and reduce its orders of complexity to a few general principles. All mythologies and religions begin by creating a world of order from the surrounding chaos. The words of Blake express a yearning to see through the diversity of nature to the underlying connectedness of all things. Natural sciences have introduced ways of naming, classifying and finally understanding our observations of the natural world in order to gain mastery over it for better or worse. The usefulness of mathematics as a tool for understanding the world results from the process of abstraction involved in mathematical description, which focuses on the general, rather than the particular[69].

Until very recently, scientists have been accustomed to describing the world in terms of what can be called "smooth" mathematics. "Smooth mathematics" is the mathematics of continuous and unjagged structures: unbroken lines, curves, surfaces, volumes. It includes major portions of arithmetic, algebra, geometry and calculus. Its roots are in ancient human history. Galileo, the first more or less modern scientist, expressed a deep belief that the geometry of Euclid is the language in which the secrets of the cosmos are written. Newton invented calculus, in part to relate Euclidean geometry formally to the description of continuously evolving processes. The objects of classical geometry, associated with Newtonian mechanics, straight lines, circles, spheres, cones and so on are "simple". That is, each can be represented (modeled) by simple equations that describe the shape and extent of the object. At the same time, as far as we can tell, the universe is an intrinsically nonlinear place. Linear behavior, wherever it seems to surface, only approximates more general phenomena. Nonlinearity is the source of the diversity and apparent complexity surrounding us[156]. Schooled in the Newtonian paradigm of linearization, we are constantly challenged to recall that the real, nonlinear world is filled with nonlinear peculiarities. Striking to a linear path in a nonlinear terrain can inflict painful lessons. Due to this, our physical world is no longer symbolized by the stable and periodic planetary motions that are at the heart of classical mechanics. It is a world of instabilities and fluctuations, which are ultimately responsible for the amazing variety and richness of the forms and structures we see in nature around us. New concepts and new tools are clearly necessary to describe nature, in which evolution and pluralism become the key words. Chaos, self-organization, fractals, emergent properties the stuff of the study of complexity have begun to appear as potentially useful tools and guiding principles in many areas of human intellectual endeavor[1,127,130,145,150,156,162].

Fortunately, the mathematical foundations for these tools were developed in the latter half of past century and the beginning of this century. Namely, as early as the latter half of the past century, mathematicians of the school who criticized the foundations of analysis, above all Karl Weierstrass (1815–1897), David Hilbert (1862–1943) and Giuseppe Peano (1858–1932) devised functions that were continuous, but none had derivatives (such as shown in Fig. 1), as well as curves that densely filled a square (see Fig. 2). Later, the analytic apparatus capable of describing such uneven objects was developed. Taking the place of ordinary dimensions in the fractional metric dimensionality first introduced by Felix Hausdorff[145] earlier this century, while the derivative is replaced by the so-called Hölder index or fractional derivative, a concept put

forward by a number of mathematicians. It was shown, that the strange properties of nondifferentiable patterns reflect their having been thought of as one-dimensional, whereas it would be more natural to regard them as objects of higher, including fractional, metric dimension, or in present nomenclature, fractals. Hence, Weierstrass, in effect, was in possession of the fractal concept without suspecting it!†

The topics associated with fractal theory have a long and interesting history in mathematics, involving many mathematicians from many parts of the world over the last few centuries, including Augustin Louis Cauchy (1789–1857), Carl Friedric Gauss (1777–1855), Henry Smith (1826–1883), Karl Weierstrass, Vito Volterra (1860–1940), Georg Cantor (1845–1918), Alexander Lyapunov (1857–1918), Jules-Henri Poincare (1854–1912), Hermann Minkowski (1864–1890), Giuseppe Peano (1858–1932), David Hilbert (1862–1943), Pierre Fatou (1878–1927), Georges Bouligand (1889–1979), Helge von Koch, Waclaw Sierpinski (1882–1968), Felix Hausdorff (1868–1942), Andrei Andreevich Markov (1856–1922), Abram Besicovitch (1891–1970), Jacques Hadamard (1865–1963), Norbert Wiener, Arnaud Denjoy (1884–1974), Gaston Julia (1893–1978), Andrei Nikolaevich Kolmogorov (1903–1987), A. Rényi and many others. However, the systematic study of fractal geometry began with Mandelbrot's research at IBM in the 1970 s, culminating in his books *Les Objets Fractals*, followed in 1982 by *The Fractal Geometry of Nature*[69].

Mandelbrot first realized that the bizarre, seemingly contrived geometric constructions and mathematical ideas engineered by these mathematicians were not at all pathological, as they at first regarded. Rather, he showed that many everyday objects such as coastlines, snowflakes, leaves, ferns, clouds, mountain ranges, fracture surfaces and many others were naturally described by fractals. Mandelbrot's book[69] is the most popular reference and contains both the elementary concepts and an unusually broad range of new and rather advanced ideas, such as multifractals, currently under active study. This book can be regarded as an excellent example of scientific advertising or popularization, in this case of naturally new concepts and models.‡ Thus, was born a new branch of mathematics, fractal geometry and fractal analysis that are powerful mathematical tools for dealing with complex systems that obeyed scale-invariance and are usually characterized by non-integer metric (fractal) dimensions. The development of fractal theory represents the revolution in geometry. Like non-Euclidean geometries before it, fractal geometry provides a new view of the world. The interest, in the mathematics and in the anomalies of fractal sets, encompasses the foundations of quantum mechanics [162],§ the possibility of defining classical and relativistic quantum mechanics on fractal support and the implication of fractal geometry in particle physics, in cosmology and solid mechanics (see ref.[130] and references therein).

Fractal mathematics considerably extends the potentialities of natural science and makes it possible to unravel new facets of unity of natural phenomena. This, in particular, leads to a sophisticated understanding of the important and, sometimes decisive, influence of morphology on the physical properties and the nature of the behavior of various objects. However, the potentialities of fractal mathematics are not used in full measure. This is easy to understand, because Mandelbrot's works were published in english as recently as 15 years ago. One might expect that the progress in fractal analysis will have an impact on the modern natural science which is comparable with the progress that was achieved by applying calculus!¶

†There is a profound historical irony in the fact that these old characters of the new geometry had been among the "monsters" for a long time.

‡A book that preceded by more than half a century Mandelbrot's classic book[69] and was known by every scientist at that time is *On Growth and Form* by W. D'Arcy Thompson (1917). This book first called attention to the fact that on microscopic level are completely random, despite the fact that on the macroscopic level we can perceive patterns and structures.

§The observation that quantum paths exhibit fractal properties was first made by Feynman[166].

¶Skeptics, overemphasizing a generally correct observation, that most physically significant results which were achieved by application of fractal analysis in physics, can be obtained within a framework of conventional methods of theoretical physics without use of the concept of metric dimension and without the notion of fractals, can be reminded that Newton's "*Philosophic Naturalis*"[167] was written without the use of the concept of derivative (this was somewhat forgotten, even though Newton was one of the founders of calculus). Now, let us imagine modern exposition of classical mechanics without calculus! At the same time, most of the known results, in principle, can be obtained without using the concepts of derivative and integrals. Moreover, computer modeling inevitably substitutes continuum of physical theory by discrete set of numerical models and differential equations are substituted by equations in finite differences which in essence brings us back to the original Newton's formulation in "*Philosophle Naturalis*". However, who will take risks today talk about uselessness of calculus?!

Table 5. The properties which must be hold for any reasonable definition of dimension (see ref.[150])

NN	Property	Relation for dimension	Conditions
1	Monotonicity	$\dim_H E \leq \dim_H F$	If E F
2	Stability	$\dim_H F = \max\{\dim_H E, \dim_H A\}$	If F: $E \cup A$
3	Countable stability	$\dim_H\{\cup_{i=1}^{\infty} F_i\} = \sup_{1\leq i\leq\infty}\{\dim_H F_i\}$	If F_i is a (countable) sequence of sets
4	Geometric invariance	$\dim_H f(F) = \dim_H F$	If $f(F)$ is a transformation of $\mathscr{R}^n$ such as a translation, rotation, similarity, affinity
5	Lipschitz invariance	$\dim_H f(F) = \dim_H F$	If $f(F)$ is bi-Lipschitz transformation (i.e. $C_1\cdot\|x-y\| \leq \|f(x)-f(y)\| \leq C_2\cdot\|x-y\|$, for $(x, y \in F)$ and $0 < C_1 \leq C_2 < \infty$

Talking about fractals, we usually think of the fractal dimension concept of which was discussed in a previous section, but the original concepts of fractal mathematics reside in the early development of topology. The last deals with questions of form and shape from a qualitative point of view. Two of its basic postulates are dimension and homeomorphism. All the objects of Nature can be treated as the sets of points in a d-dimensional Euclidean space. A topological dimension can be introduced for any such set. This quantity is introduced as follows. The dimension of any finite or denumerable set of points is $d_T = 0$. The dimension of any connected set is $d_T^+ = d_T + 1$, if it can be cut into two unconnected parts by excluding at least a d_T-dimensional set of points (by a d_T-dimensional cut). From the very definition of the topological dimension it follows that it can be only an integer. The topological dimension of a line is $d_T = 1$, that of a plane or spherical surface is 2, for a sphere it is $d_T = 3$, etc. The invention of space filling curves (such as Peano curve which is shown in Fig. 2) was a major event in the development of the concept of dimension. They questioned the intuitive perception of curves as one-dimensional objects, because they filled the plane, i.e. an object which is intuitively perceived as two-dimensional.

In mathematics, fractal and its fractal (or metric) dimension D both are defined in terms of an embedding metric space.† Obviously, any reasonable definition of the dimension, specifically the metric dimension, should satisfy the basic properties listed in the Table 5.

Intuitively one can interpret metric (fractal) dimension $\dim_M F$ as the smallest non-negative real number for which one can define a volume form on $\mathscr{R}^n$ space which is not identically zero; such a volume form being entirely described by the metric dimension or capacity. Underlining this approach is the recognition that one- and two-dimensional structures are in effect three-dimensional portions of space, two or one of their characteristic scales being very small. While the first definition of the metric dimension was given by Hausdorff, here, we first consider the definition of the Kolmogorov capacity of a set of points (F) in a d-dimensional Euclidean space.

Let $N(r)$ be the smallest number of spheres of radius r needed to cover this set. The Kolmogorov's capacity is the number D_K for which the following limit differs from zero:

$$\lim_{r\to 0} N(r)\Gamma(D_K + 1/2)r^{D_K}/\Gamma^{D_K}(1/2). \tag{8}$$

In this definition we simply multiply $N(r)$ by a quantity which is the generalization of the formula for the volume of a d-dimensional sphere to the case of fractional value D_K. The limit discussed here is simply an upper bound for the D_K-dimensional volume of our set. Notice that spheres are used to deal with the coverage only in order to avoid the problem of orientation. We can equally use d-dimensional cubes; the term with the Γ-functions in eq. (8) should then be omitted. In the experimental determination of D_K it is preferable to use the latter method.

By this means one can define the metric dimension in the following way: the real number $\dim_M F$ is the smallest positive real number for which one can construct non-zero measure on the system F, or equally, it is the greatest real number for which one can construct finite measure on the system F. The original Hausdorff definition of the "dimensional number" D_H of

†On the other hand, Schmutz [168] has pointed out that D can be interpreted as an intrinsic metric property of the object.

Table 6. Hausdorff–Besicovitch dimension of some objects (see ref. [150])

NN	Object	Conditions	Dimension
1	Open sets	F is open subset of $\mathscr{R}^n$	$\dim_H F = n$
2	Countable set	F is finite of countable set	$\dim_H F = 0$
3	Smooth manifolds	F is a smooth (i.e. continuously differentiable) m-dimensional submanifold of $\mathscr{R}^n$	$\dim_H F = m$
		Smooth curves	$\dim_H C_{sm} = 1$
		Smooth surfaces	$\dim_H S_{sm} = 2$
4	Hölder function of exponent α	$\lvert f(x) - f(y)\rvert \le C\cdot\lvert x - y\rvert^{\alpha}$, $(x,y \in F)$ for some constant C $F\mathscr{R}^n$, f: $F \to \mathscr{R}^m$	$\dim_H f(F) \le (1/\alpha)\dim_H F$
5	Lipschitz function	$F \in \mathscr{R}^n$, f: $F \to \mathscr{R}^m$, $\lvert f(x) - f(y)\rvert \le C\cdot\lvert x - y\rvert$, $C < \infty$	$\dim_H f(F) \le \dim_H F$
6	Jordan curve on the plane	C is the image of an interval $[a,b]$ under a continuous bijection f: $[a,b] \to \mathscr{R}^2$	$1 \le \dim_H C \le 2$

a set of points F embedded in d-dimensional space is as follows. Let F be covered by the "boxes" U_1, U_2,... (meaning $F\ U_1 \cup U_2 \cup ...$) having the diameters (maximum linear size measured in the d space) r_1, r_2,..., respectively. Denote by $U(F,r)$ the set of all possible coverings of F with $r_i \le r$. Then the "exterior s-dimensional measure" $M_S(F)$ is defined as

$$M_S(F) = \lim_{r \to +0} \inf_{U(F,r)} \sum_i r_i^S, \tag{9}$$

where the sum is taken over all the "boxes" of radius $r_i \le r$. Finally, if $M_S(F) = 0$ for $s > D_H$ and $M_S = \infty$ for $s < D_H$, then D_H is the "dimensional number", or the Hausdorff dimension, also called the Hausdorff–Besicovitch dimension, of F is

$$D_H = \inf\{s : M_S(F) = 0\} = \sup\{s : M_S = \infty\}. \tag{10}$$

This definition becomes more physically intuitive if the mass (M) of the object is taken to depend on the linear extent L by the power-law $M \propto L^{D_H}$.

The Hausdorff–Besicovitch as well as the Kolmogorov notations of metric dimension capture properties which are not all topologically invariant. For "well-behaved" sets, both the metric (Hausdorff–Besicovitch) dimension D_H and the capacity D_K are equal to the topological dimension d_T, which is an integer. For example, for the straight line $D_K = D_H = 1$, for the smooth plane $D_K = D_H = 2$, while for the triadic Koch curve (Fig. 1) they are equal to $D_S = \ln 4/\ln 3$. In other words, the metric dimension has changed, through from a topological point of view the Koch curve is just a straight line (the topological dimension of the Koch curve is $d_T = 1$). The Hausdorff–Besicovitch dimensions of some classical objects are listed in Table 6.

The Kolmogorov capacity and the Hausdorff–Besicovitch dimension are often equal $D_K = D_H$, specifically for regular fractals, such as Cantor set, Peano, Hilbert and Koch curves, Sierpinski carpets and gaskets, etc. (see [69, 130]). At the same time the Hausdorff–Besicovitch dimension and the Kolmogorov capacity may differ even for very simple patterns. For example, for a set of points on a straight line with the coordinates $X_N = 1/N$ the former is 0 and the latter is $D_K = 1/2$ [150]. Another interesting example of an object with different metric dimension and Kolmogorov capacity is presented by the algebraic spiral $R(\Phi) = \Phi^{-\alpha}$, $\alpha > 0$, where R and Φ are the polar radius and angle, respectively, [169]. Being clearly different from conventional fractals, such a spiral still has the nontrivial Kolmogorov capacity,

$$D_K = \max\left\{1, \frac{2}{1+\alpha}\right\},$$

associated with a single accumulation point at the origin [169]. However, for any $\epsilon > 0$, a variable-size covering (with the box sizes r, depending algebraically on Φ) can be found such that the sum of $r_i^{1+\epsilon}$ tends to zero as $r \to 0$. That is the Hausdorff–Besicovitch dimension of the spiral is unity: $D_H = d_T = 1$. Such objects (which is not fractals in Mandelbrot's sense) were called "K-fractals" [170]. The algebraic spiral is an example of local self-similarity with respect to only its center. Notice that the Hausdorff–Besicovitch dimension is generally not greater than

Table 7. Some different definitions of metric dimension (see refs[130,150])

NN	Dimension	Measure	Definition of dimension
1	Hausdorff- Besicovitch dimension	$\{U_i\}$ is a δ-cover of F, i.e. $F \subset \cup_{i=1}^{\infty}$ with $0 < \lvert U_i\rvert \le \delta$, where U is any non-empty subset of n-dimensional Euclidean space, $\mathscr{R}^n$. Hausdorff measure is $H^S(F) = \lim_{\delta\to 0} H_\delta^S(F)$, where $H_\delta^S(F) = inf\left\{\sum_{i=0}^{\infty}\lvert U_i\rvert^S : \{U_i\}\right\}$ and diameter of U is $\lvert U\rvert = \sup\{\lvert x-y\rvert: x,y \in U\}$	$\dim_H F = = \inf\{S: H^S(F) = 0\} = = \sup\{S: H^S(F)\} = \infty$
2	Mincowski– Bouligand dimension (logarithmic density)	Let $N_\delta(F)$ denotes the least number of balls in a covering of F by balls of radius ϵ. It is follows from the definition of H_δ^S that $H_\delta^S(F) \le (2\delta)^S \times N_\delta(F)$	$\Delta(F) = \bar{\lim}_{\delta\to 0}\{\lg N_\delta(F)/\lg(1/\delta)\}$, $\Delta(F) \ge \dim_H F$
3	Divider dimension (of Jordan curves)	$M_\delta(C)$-maximum number of points $x_0, x_1,\ldots,x_m$, on the curve C, in that order, such that $\lvert x_k - x_{k-1}\rvert = \delta$, $k = 1,2,\ldots,m$	$D_D = \lim_{\delta\to 0}\{\lg M_\delta(C)/\lg(1/\delta)\}$
4	Packing dimension	$\{B_i\}$ is a collection of disjoint balls of radius at most δ with centers in F. Packing measure is $P^s(F) = inf\{\sum P_0^S(F_i) : : F \subset \cup_{i=1}^{\infty i} F_i\}$,where $P_0^S = \lim_{\delta\to 0} P_\delta^S(F), P_\delta^S = \{\lvert B_i\rvert^S : \{B_i\}\}$	$\dim_P F = = \inf\{S: P^S(F) = 0\} = = \sup\{S: P^S(F) = \infty\}$ $\dim_H F \le \dim_P F \le \Delta(F)$

Table 8. Some definition of box-counting (or box) dimensions (see refs[145,150])

Dimension	Definition	Comments
Lower box-counting (or lower box)	$\underline{\dim}_B F = \underline{\lim}_{\delta\to 0}\{\log N_\delta(F)/\log\delta\}$	F is non-empty subset of $\mathscr{R}^n$ $N_\delta(F)$ is any of the following: **A**. The smallest number of
Upper box-counting (or upper box)	$\overline{\dim}_B F = \overline{\lim}_{\delta\to 0}\{\log N_\delta(F)/\log\delta\}$	(1) closed balls of radius δ,(2) cubes of side δ,(3) sets of diameter at most δ, that cover F;
Box-counting (or box)	$\dim_B F = \lim_{\delta\to 0}\{\log N_\delta(F)/\log\delta\}$	**B**. The largest number of disjoint balls of radius δ with center in F; **C**. The number of δ-mesh cubes that interset of F.
Minkowski	$\dim_B^M(F) = n - \lim_{\delta\to 0}\{\log vol^n(F_\delta)/\log\delta\}$	F_δ is the δ-parallel body to F: $F_\delta = \{x \in \mathscr{R}^n : \lvert x-y\rvert \le \delta$, for some $y \in F\}$; n—topological dimension
Lower modified box-counting	$\underline{\dim}_{MB} F = = inf\{\sup_i \underline{\dim}_B F_i : F \subset \cup_{i=1}^{\infty} F_i\}$	If F can be decomposed into a countable number of pieces F_i in such a way that the largest piece has a small a dimension as possible.
Upper modified box-counting	$\overline{\dim}_{MB} F = = inf\{\sup_i \overline{\dim}_B F_i : F \subset \cup_{i=1}^{\infty} F_i\}$	

$$\dim_H F \le \underline{\dim}_B F \le \overline{\dim}_B F$$

$$0 \le \dim_H F \le \underline{\dim}_{MB} F \le \overline{\dim}_{MB} F = \dim_P F \le \overline{\dim} F \le n$$

the Kolmogorov's capacity, i.e. $D_H \leq D_K$. In contrast to the dimensions, particularly in the case of the Hausdorff–Besicovitch dimension, the capacities do not remain invariant in the case of piecewise-smooth (but with possible singularities) transformation of the coordinates: in the case of the quantities that lay claim to being dimensions such an invariance is an essential feature.

Of the wide variety of fractal dimension in use, the definition of Hausdorff, based on a construction of Carathéodory, is the oldest and probably the most important. Hausdorff dimension has the advantage of being defined for any set and is mathematically convenient, as is based on measures, which are relatively easy to manipulate. A major disadvantage is that in many cases it is hard to calculate or to estimate by computational methods. However, for an understanding of the mathematics of fractals, familiarity with Hausdorff measure and dimension is essential. At the same time, for practical applications a wide variety of other definitions of metric dimension have been introduced, many of them only of limited applicability, but nonetheless useful in their context. Some of the most important definitions of metric dimension are listed in Table 7.

In practice, the characterization of natural random (stochastic) fractals usually use the box-counting (or box) dimensions. Various definitions for box dimensions are listed in Table 8. The special forms of some types of fractals give rise to the different definitions of some other dimensions. However, some of the confusion and ambiguity in quantifying a fractal dimension could be related to differences in the procedures (thus definitions) among different dimensions. Some of them are listed in Tables 9 and 10. We have listed these definitions because, as a rule, different studies of the fractal geometry of nature use different definitions of fractional dimensions. For example, the comparison of various experimental measurements of the fractal dimension of fracture surfaces is given in Table 11 (experimental techniques are discussed in details in ref. [137]). Notice that the difference can be very large (see refs[130, 133, 137]). Thus, more attention needs to be given to the problem of linking the mathematical definitions with the practical applications.

Table 9. Definitions of some other fractional dimensions (see refs[145, 150])

Dimension	Definition	Comments
Capacity dimension	$\dim_C F =$ $\begin{cases} 0, \text{ if } C_\alpha(F) = 0, & \forall \alpha > 0 \\ d_C > 0, \text{ if } C_\alpha(F) = 0, & \forall \alpha > d_C \\ \text{and } C_\alpha(F) > 0, & \forall 0 < \alpha < d_C \end{cases}$	Capacity is $C_\alpha(F) =$ $\begin{cases} [W_\alpha(F)]^{-1/\alpha}, \text{ if } W(E) < \infty, \\ 0, \text{ otherwise} \end{cases}$ where $W_\alpha(F) = \inf\{I_{\alpha,m}(F)\}, I_{\alpha,m}(F) = \int_F \int_F \|x - y\|^{\alpha - n} dm(x) dm(y)$, for each $0 < \alpha < n$, where n is a topological dimension of F and $\|...\|$ is the euclidean norm.
One-sided dimension (of boundary F of set A in $\mathscr{R}^n$)	$\dim_{OS} F = n - \lim_{\delta \to 0} \{\log vol^n(F \cap A)/\log \delta\}$	F is the boundary of a set A; F_δ is the δ-parallel body of F: $F_\delta = \{x \in \mathscr{R}^n : \|x - y\| \leq \delta, \text{ for some } y \in F\}$, n is a topological dimension.
Fourier dimension	$\dim_F = \max\{t : \|\hat{\mu}(U)\| \leq B\|U\|^{-t/2}\}$, for some constant B where the mass distribution $\hat{\mu}(U)$ on $\mathscr{R}^n$ is $\hat{\mu}(U) = \int_{\mathscr{R}^n} \exp(ix \cdot U) d\mu$ where $U \in \mathscr{R}^n$ and $x \cdot U$ represents usual scalar product.	If $\|\hat{\mu}(U)\| \leq B\|U\|^{-t/2}$ for some constant B, $\|\hat{\mu}(U)\| \leq \mu(\mathscr{R}^n)$ for all U, we have $I_k(\mu) = (2\pi)^n C \int \|U\|^{k-n} \|\hat{\mu}(U)\|^2 dU \leq$ $\leq C^1 \int_{\|U\| \leq 1} \|U\|^{k-n} dU +$ $+ C_2 \int_{\|U\| > 1} \|U\|^{k-n} \|U\|^{-1} dU$ which converges if $k < t$.

Table 10. Definitions of Menger–Urysohn dimension and dimension print (see ref.[150])

Dimension	Definition	Comments
Menger–Urysohn	The $\dim_{(M-U)}F$ is defined inductively as follows: (1) The empty set F has $\dim_{(M-U)}F = -1$, (2) A topological space F has $\dim_{(M-U)}F = n$ if n is the largest natural number such that each point of F has arbitrarily small neighborhoods with frontiers of dimension less than n.	A. If every point p of space F has arbitrarily small neighborhoods with empty frontier (i.e. for every neighborhood U of p there exists a neighborhood V of p that $V \subset U$, $\mathrm{fr}(V) = \varnothing$) then $\dim_{(M-U)}F = 0$. B. The set of irrational numbers, the Cantor set and any countable space are of dimension 0 is itself zero dimensional. C. If X is a separable metric space, then $\dim_{(M-U)} X = \inf\{\dim_H X'\}$, where the minimum is taken over the set of spaces X' homotropic to X. D. If $\dim_{(M-U)} X - \dim_{(M-U)} Y = K > 0$, then there exist point of Y whose inverse image under F has $\dim_{(M-U)} \geq K$.
Dimension print	print F of subset F is defined to be the set of non-negative pairs (k, p) for which $H^{k,p}(F) > 0$	U is a rectangle (the sides need not be parallel to the coordinate axes). Let $a(U) \geq b(U)$ is the length of sides of U; k and p are non-negative numbers. For F a subset of $\mathscr{R}^2$, $H^{k,p}(F) = \lim_{\delta \to 0} H^{k,p}_\delta(F)$. $H^{k,p}_\delta(F) = \inf\{\sum_i a(U_i)^k b(U_i)^p :$ $\{U_i\}$ is a δ-cover of F by rectangles$\}$ $H^{k,0}$ is just the k-dimensional Hausdorff measure

Table 11. Comparison of fractal measurements of the fractal dimensions of fracture surfaces by means of different techniques (data are taken from ref.[133] where the data collected by various authors were summarized)

Material	D_B	D_D (Vertical sections)	D_F (Slit-island)	D (Power spectrum)
Titanium	–	2.099 ÷ 2.126	2.320	–
Copper	2.21	2.47	2.31	2.54
Steel	2.330 ÷ 2.395	2.180 ÷ 2.310	2.280	2.450
Rock	2.041 ÷ 2.159	2.058 ÷ 2.261	–	2.124 ÷ 2.383
Rock	–	2.410 ÷ 2.500	–	2.51

Clearly the knowledge of the fractal dimension does not tell everything about the morphology of the system.† For example, two systems with the same fractal dimension may actually look very different and have very different connectivity properties (see for example four different fractals with the same fractal dimension in Fig. 10). So for a more complete determination of the morphological properties of the structure, it is quite reasonable to complete the study of its dimensionality with other types of studies, particularly, correlation analysis and the analysis of connectivity using percolation theory concepts [40, 170–174]. A new topological measure for quantitative analysis of fragmentation for brittle materials was suggested in ref. [175]. It seems that the generalized statistical mechanics developed by Tsallis [176, 177] offers new possibilities for the quantitative analysis of the statistical topography of multifractal failure patterns[66]. We expect that a certain combination of various approaches and models can give an adequate representation of failure topography within a framework of fractal geometry.

2.3. *Non-standard representation of fractal patterns*

The nondifferentiability of fractals and their infinite length (area, volume, hyper-volume) forbid a complete description based on usual real numbers. Nottale and Schneider [149] have proposed to deal with the infinities appearing on fractals and then to work effectively on the actual fractal F instead of on its approximations $G_n(\lim_{n \to \infty} G_n = F)$ by using non-standard analysis (NSA).

It has been shown by Robinson[178] that proper extensions $^*\mathscr{R}$ of the field of real numbers $\mathscr{R}$ could be built, which contain infinitely small and infinitely large numbers. The theory, first evolved by using free ultrafilters and equivalence classes of sequences of real, was latter formal-

†The morphology of a system has two major aspects: the topology, the interconnectiveness of individual microscopic elements of the system and geometry, the shape and size of this individual elements and their distribution.

ized by Nelson [179] as an axiomatic extension of the Zermelo set theory. Let us briefly recall some results of NSA which is the most relevant for application to fractals[149,180].†

The set $^*\mathscr{R}$ of hyper-real numbers is a totally ordered and non-Archimedean field, of which the set $\mathscr{R}$ of standard numbers is a subset. $^*\mathscr{R}$ contains infinite elements, i.e. numbers such that $\forall n \in \mathrm{N}$, $|A| > n$ (where N refers to the set of integers). It also contains infinitesimal elements, i.e. numbers B such that $\forall n \neq 0 \in \mathrm{N}$, $|B| < n^{-1}$. A finite element C is defined as $\exists n \in N$, $|C| < n$. Now all hyper-real numbers may be added, subtracted, multiplied and divided; subsets like hyper-integers $^*\mathrm{N}$ (of which N and the set of infinite hyper-integers $^*\mathrm{N}_\infty$ are subsets), hyper-rational $^*Q$, positive or negative numbers, odd or even hyper-integers, etc. may be defined and, more generally, most standard methods and definitions may be applied in the same way as in the standard set $\mathscr{R}$, but the different set of properties are classified as being either internal or external.

An important result is that any finite number α can be split up in a single way as the sum of a standard real number $r \in \mathscr{R}$ and an infinitesimal number

$$\varepsilon \in \Im : \alpha = r + \epsilon.$$

In other words the set of finite hyper-real contains the ordinary real plus new numbers (α) clustered infinitesimally closely around each ordinary real r. The set of these additional numbers $\{\alpha\}$ is called the monad of r. More generally, one may demonstrate that any hyper-real number A may be decomposed in a single way as $A = N + r + \epsilon$, where $N \in {}^*\mathrm{N}$, $r \in \mathscr{R} \cap [0,1[$ and $\epsilon \in \Im$.

The real r is said to be the "*standard part*" of the finite hyper-real α, this function‡ being denoted by $r = St(\alpha)$. Indeed, apart from the usual strict equality, one introduced equivalence relation "$\simeq$", meaning "infinitely close to" and defined as $\alpha \simeq \beta \Leftrightarrow St(\alpha - \beta) = 0$. Hence, two numbers of the same monad are infinitely close one to the other, but are not strictly equal.

The practical consequence is that a very large domain of mathematics may be reformulated in terms of NSA and, in particular, concerning physics, the integro-differential calculus. The method consists of replacing the Cauchy–Weierstrass limit formulation by effective sums, products and ratios involving infinitesimal and infinite numbers and then taking the standard part of the result. Hence, the derivative of a function, $f(x)$ will be defined as a ratio

$$\frac{d}{dx} f(x) = St\left\{\frac{f(x+\varepsilon) - f(x)}{\varepsilon}\right\} \tag{11}$$

with $\epsilon \in \Im$, provided this expression is finite and independent of ϵ.

The integral of a function is defined from an infinitesimal portion of the interval $[a,b]$ in an infinite number ζ of bins, as a sum:

$$\int_a^b f(x)dx = St\left\{\sum_{i=1}^{s} f(x_i)\delta x_i\right\} \tag{12}$$

provided it is finite and independent of the portion. The number of bins, s, infinite from the standard point of view, is assumed to be given integer of $^*\mathrm{N}_\infty$. It is said to be *-finite.§

By its ability to deal properly with infinite and infinitesimal, NSA proved to be particularly well-adapted to the description of fractals. Nottale and Scheider[149] have proposed to continue the fractalization process G_0, G_1,... G_n,..., (see Figs 1 and 2) up to an *-finite number of stages s. This yields a curve G_s, from which the fractal F is defined as

$$F = St\{F_s\}. \tag{13}$$

Now, let us come back to Koch curve in a plane shown in Fig. 3. This curve may be generalized in the complex plane by first given ourselves a generator G_1 made of k segments of equal

†We do not intend to give here a detailed account of this branch of mathematics, ref.[179].

‡This operation, "take the standard part of", plays a crucial role in the NSA, since it allows one to solve the contradictions which prevented previous attempts, such as Leibniz's to be developed (see Ref.[180]).

§A summation from 0 to ∞ may be replaced by summation over an *-finite number of terms ranging from 0 to $s \in {}^*\mathrm{N}_\infty$. The sum will be said to converge if for different s's its standard part remains equal to the same finite number.

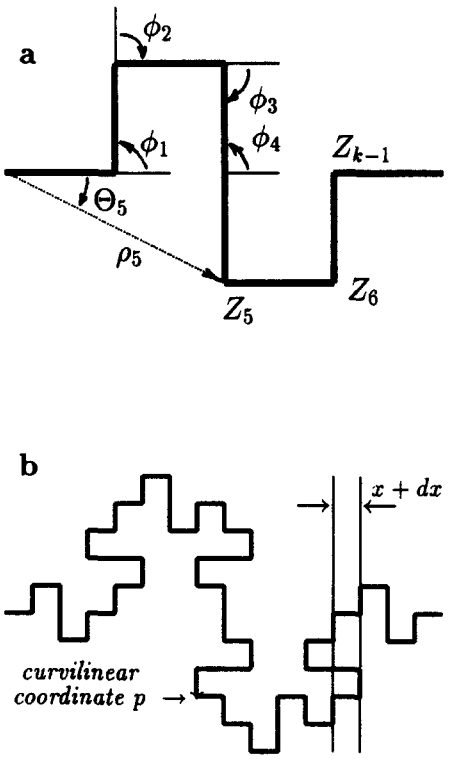

Fig. 14. (a) Building of a plane fractal Koch curve (see Fig. 3) from a generator, G_1, and (b) two cartesian coordinates of fractal curve, $x(p)$ and $y(p)$, in terms of the normalized curvilinear coordinate p. A curvilinear coordinate p is defined on the fractal curve $F = G_\infty$. Structural constants in Fig. 14(a) are defined in text.

length $1/n$. The coordinates of the k points K_ℓ of G_1 are given either in Cartesian or in polar coordinates (see Fig. 14(a)):

$$Z_\ell = x_\ell = iy_\ell = \frac{1}{n} \times \times \rho_\ell e^{i\theta_i}, \quad \ell \in (0, p). \tag{14}$$

If we number the segments from 0 to $p-1$, then another equivalent representation would be to give ourselves either the polar angle of the segment number ℓ, say ζ_ℓ, or the relative angle between segments $\ell - 1$ and ℓ, say ϕ_ℓ.

Below, for simplicity, we choose a coordinate system such that G_0 is identical to the segment [0,1]. In this system, the length of the individual segments is $1/n$, and the similarity (fractal) dimension, D_S, is given by relation eq. (4) according to which

$$D_S = \frac{\ln k}{\ln n}. \tag{15}$$

Furthermore, three conditions hold between the "structural constants":

$$Z_{\ell+1} - Z_\ell = \frac{1}{n} \times \exp(i\zeta_\ell), \quad \zeta_\ell = \sum_{j=0}^{\ell} \phi_j, \quad \text{and} \quad \sum_{i=0}^{k-1} e^{i\zeta_\ell} = n. \tag{16}$$

A curve G_2 is obtained by substituting each segment of G_1 by G_2 itself, scaled at its length $1/n$, as illustrated in Figs 1, 2 and 4. The resulting curve of an infinite sequences of these steps (substitution of each segment of G_m by $n^{-m}G_1$ giving G_{m+1}) is the fractal Koch curve $F_K \equiv G_\infty$.

As is readily seen from Fig. 14(a), the Koch curve (Fig. 3) can be parametrized by a real number $p \in [1,1]$ developed in the counting base k in the form

$$p = 0 \cdot p_1 p_2 \cdots p_j \cdots = \sum_j p_j n^{-j}, \tag{17}$$

where each p_j taking integer value from 0 to $p-1$. The fractal limit F will apparently be completely defined when the complex coordinate $Z(p)$ of the point on F parametrized by a normalized curvilinear coordinate p is known. For a Koch curve, $Z(p)$ can be easily obtained, thanks to the above building process of F. The hierarchy of figures G_1 reproduces the hierarchical structure of the fractal. Therefore, the fractal equation may be written in the form

$$Z(p) = Z_{p_1} + \frac{1}{n} e^{i\zeta p_1} \cdot \left[Z_{p_2} + \frac{1}{n} e^{i\zeta p_2} \cdot [Z_{p_3} + \ldots] \right] \tag{18}$$

so that we have

$$Z(p) = n \sum_{j=1}^{\infty} \rho_{p_j} n^{-j} \exp\left(i\Theta_{p_j}\right), \tag{19}$$

where

$$\Theta_{p_j} = \zeta_{p_1} + \zeta_{p_2} + \ldots + \zeta_{p_{j-1}} + \theta_{p_j}. \tag{20}$$

This is an "external" description of the fractal curve, in which for each value of the curvilinear coordinate p, the two coordinates $x(p)$ and $y(p)$ in the plane may be calculated as $Z(p) = x(p) + iy(p)$. In terms of p, $x(p)$ and $y(p)$ are fractal functions, for which successive approximations $x_q(p)$ and $y_q(p)$ may be built. Thought to each value of p corresponds only one value of x and y (while the reverse is false), their fractal character is revealed by the divergence of their slope when $q \to \infty$. Their fractal dimension is the same as that of the original fractal curve. This is illustrated in Fig. 14(b) for the Koch curve of Fig. 3.

The structure of eq. (18) is remarkable, since it evidences the part played by k on the fractal and n in the plane:

$$\left(p = \sum p_j k^{-j}\right) \leftrightarrow \left[Z(p) = \sum C_j(p) \cdot n^{-j}\right].$$

An "intrinsic" building of the fractal curve may also be made [149, 180]. Placing ourselves on G_q we only need to know the change of direction from each elementary segment of length n^{-q} to the following one. On the fractal generator G_1, these angles have been named ϕ_m. In this way, the problem is to find the function $\phi(p)$.

The points of G_q which are common with the fractal Koch curve F (those relating the segments) are characterized by rational parameters p written with q figures in the counting base k, $p = 0 \cdot p_1 \cdot p_2 \ldots p_q$. Let us designate by p_s the last non-null figure of p, i.e.

$$p = \frac{p_1}{k} + \frac{p_2}{k^2} + \ldots + \frac{p_s}{k^s}, \tag{21}$$

where $s \in {}^*\mathbf{N}$.

From the obvious condition of self-avoidance

$$\phi_0 = \zeta_0 - \zeta_{k-1} \tag{22}$$

it immediately follows that the relative angle between segment number $(p \times k^q - 1)$ and segment $(p \times k^q)$ on G_q is determined by the relation

$$\phi(p) = \phi_{p_s}. \tag{23}$$

This relation completely defines the fractal in a very simple way, uniquely from the $(k-1)$ structural angles ϕ_m and, independently, from any particular coordinate system in plane (x, y).

It should be noticed that G_s is not a fractal in the nonstandard sense (since the fragmentation is *-limited up to s), but its standard part is identical to the fractal, i.e. $F = St\{G_s\}$. This means that we define an *-curvilinear coordinate from its expansion in the base k:

$$^*p = 0 \cdot p_1 \ldots p_j \ldots p_s = \sum_{j=1}^{j=s} p_j n^{-j} \tag{24}$$

and that the equation of G_s is given by eq. (17) now summed from 1 to s, $Z(p)$ being its standard part.

One of the main interest of the introduction of the curve G_s is that it not only contains and sums up all the properties of each of the approximations G_j, but also of their fractal limit F. Hence the study of G_s allows us to study the properties of F, thanks to the standardization axiom [179]. Moreover a sense may now be given to the length of the fractal curve. The length of G_s is a number of $^*\mathscr{R}_\infty$:

$$L_s = L_0\left(\frac{k}{n}\right)^s = L_0 \times n^{s(D-1)} \tag{25}$$

and the (non-renormalized) curvilinear coordinate on G_s is

$$P = {}^*p \cdot L_s = n^{-s}\{p_s + p_{s-1}k + \ldots + p_1 k^{s-1}\}. \tag{26}$$

This verifies that G_s is built up with elementary segments of length n^{-s}. So, by using an infinitely great magnification power, G_s can be drawn exactly, while this was not the case for F. In this way the fractal is no more a limit concept.

Between 0 and p, it is made of $(p \times k^s)$ segments of length n^{-s}. The surface of G_s can be also defined as

$$S_s = L_0\left(\frac{k}{n^2}\right)^s = n^{-s(2-D)}, \tag{27}$$

which is an infinitesimal number when $D < 2$.

When taking the standard part of L_s or S_s, one finds again that the length is undefined (infinite) and the surface is null for $D < 2$. The surface is finite for plane filling curves (such as the Peano curve in Fig. 2) for which $D = 2$.

Thus, the nondifferentiability of fractal may be visualized by the fact that any standard point of the fractal may be considered as structured: when viewed with an infinite magnifier, it contains all the values of the slopes owned by the complete fractal. At the same time fractal may be defined by ϵ-differentiability. It consistsof setting that any part of the fractal magnified by n^s is to be differentiable. Indeed, there is an infinite number of curves F_ζ, the standard part of which will be the same fractal F; an ϵ-differentiable one may be *a priori* chosen. This is in fact equivalent, from the practical viewpoint, to imposing that each approximation G_j be differentiable, which is always a possible choice. Two consequences for physical modeling is not negligible. This means that the nondifferentiable fractal may be built as the limit of a family of differentiable curves, for which the usual integro-differential formalism may then be kept.

These concepts may be generalized by the case of the fractal curve in a space of three or more dimensions and for the case of statistically self-similar and self-affine surfaces. Nottale [180] has used these generalizations for the construction of fractal space–time, but the NSA approach may be applied to some other problems, for example to some problems of crack mechanics [43, 130].

2.4. *The concept of self-affinity and self-affine functions*

Above, we considered pattern scaling properties which are associated with similarity transformations, by means of which a rectangle is reproduced as a rectangle, a triangle with certain angles is reproduced as a triangle with the same angles and so on. The only thing which is changed is the scale of the image. One principal direction for an extension of the notion of fractals is the constructions associated with affine transformations. For example, the generator image may be reduced by a factor of $\lambda_1 = 1/2$ in the horizontal direction and by a factor $\lambda_2 = 1/3$ in the

vertical one. The effect of such transformation is to destroy similarity: a square is reduced to a rectangle; a triangle with certain angles is reduced to a triangle with different angles; etc. When an object is invariant under a transformation with different length scales in different directions it is a self-affine fractal.

It should be emphasized that most experimental studies indicate that fracture surfaces and crack propagation paths are self-affine rather than self-similar (see refs [42–47, 60, 66, 86, 89, 90, 102, 107, 121, 126–128, 130, 132, 137, 139, 144, 163, 181] and references therein). In the application of fractal models to real crack faces the concepts of self-similar and self-affine fractals must be carefully distinguished [41–49].

In order to discuss the difference between self-similar and self-affine fractals, let us consider a bounded set F in a Euclidean d-space. The position of each point in F is described by a vector $\mathbf{X} = (x_1, x_2, \ldots, x_d)$. An affine transformation of real scaling ratios $\lambda_i (0 < \lambda_i < 1,\ i = 1,2,\ldots,d)$ takes each element of F with position $\mathbf{X}$ into an element of the set $\lambda(F)$ with position $\mathbf{R} = (\lambda_1 x_1, \lambda_2 x_2, \ldots, \lambda_d x_d)$.† The set F is self-affine if it is the union of N distinct subsets congruent to $\lambda(F)$.‡ Set F is statistically self-affine if its subsets are statistically congruent to $\lambda(F)$.

For example, a statistically self-affine surface is invariant under an affine transformation, $x' \to \lambda_x x$, $y' \to \lambda_y y$, $z' \to \lambda_z z$. Requiring that such transformations be combined implies a group structure. As a consequence λ_y and λ_z have to be homogeneous functions of, say, λ_x; both scale as

$$\lambda_y \propto \lambda_x^{\nu_y}, \quad \lambda_z \propto \lambda_x^{\nu_z}, \tag{28}$$

but the exponents ν_y and ν_z are in general different [64]. If so, then $\lambda_z \propto \lambda_y^H$, where the Hurst exponent eq. (7), H, also called the roughness exponent [61, 62, 130], is given by the relationship

$$H = \frac{\nu_z}{\nu_y}. \tag{29}$$

Notice that in the case of self-similar surface we have

$$\nu_y = \nu_z = \frac{1}{D_S}, \text{ so that } \quad \frac{\nu_z}{\nu_y} \equiv 1. \tag{30}$$

This means that the Hurst exponent eq. (29) is useless when discussing both self-affine and self-similar fractals in the same context. For self-similar surface the roughness exponent is defined as $H = \nu_y \equiv \nu_z$. [130]. In the special case of an isotropic surface with mean plane parallel to the coordinate plane (x, y), we have $\nu_y \equiv 1$, so that $H = \nu_z$. The last relation is also valid for any self-affine profile on a two-dimensional plane. As an example of a self-affine curve in plane we can refer to the graph of the Mandelbrot–Weierstrass function [182, 183], which may be represented in the following particular form

$$z(x) = \sum_{k=0}^{\infty} \lambda^{-Hk} \left[1 - \cos\left(\lambda^k x\right)\right], \tag{31}$$

where $\lambda > 1$ and $0 < H < 1$.

The graph of function eq. (31) possesses self-affine scaling eq. (6). This implies that the whole function $z(x)$ can be reconstructed (in statistical sense!) from its value in the range $x_0 \le x < \lambda x_0$. For example, $z(x)$ in the ranges $\lambda x_0 \le x < \lambda^2 x_0$ and $\lambda^{-1} x_0 \le x < x_0$ are magnified and diminished versions, respectively, of $z(x)$ in the range $x_0 \le x < \lambda x_0$.

The nondifferentiability of this function can be formally expressed in the terms of Hölder inequality.

$$\lim_{\Delta x \to 0} [z(x + \Delta x) - z(x)] \le C(\Delta x)^H,$$

where C is a constant [150].

†When all the scaling ratios λ_i are equal we have a similarity transformation.
‡By congruent we mean identical under translations and/or rotations.

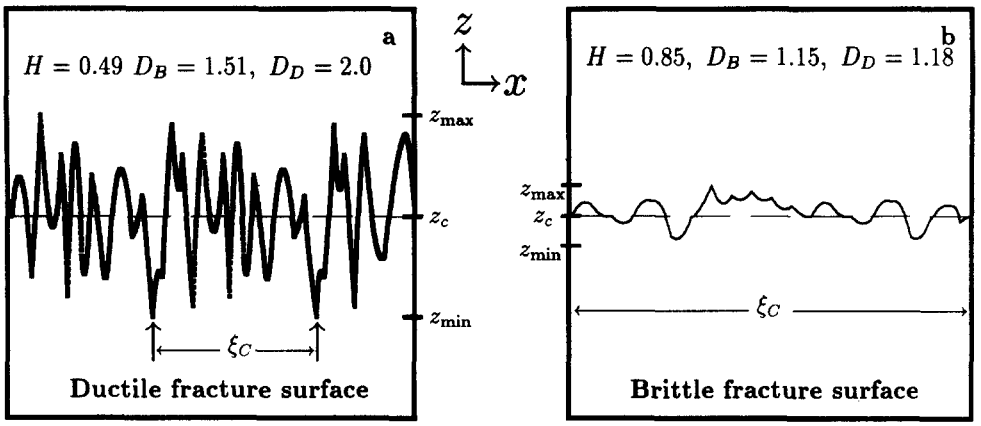

Fig. 15. The self-affine image of (a) a ductile and (b) brittle fracture modeled by the Weierstrass–Mandelbrot function (31).

Physically, the Weierstrass–Mandelbrot function eq. (31) represents the Gaussian roughness with mean zero, $\langle(z(0)\rangle = 0$ and the stationary randomness of increments, that implies

$$\langle z(x + \Delta x) - z(x)\rangle = 0. \tag{32}$$

In this way, the graphs of eq. (31) are often used as models of rough crack faces, as, for example, it is shown in Fig. 15(a,b). The statistical properties of a self-affine function are characterized by the delta-variance, $\delta(\Delta x)$, and the standard deviation

$$\langle|z(x)|^2\rangle = \sum_{i=1}^{N}(z_i - z_c)^2, \quad \text{where} \quad z_c = \frac{1}{N}\sum_{i=1}^{N} z_i; \tag{33}$$

here (z_i,x_i) are the coordinate of the ith measured point on the graph of $z(x)$.

Both the delta-variance and standard deviation obey self-affine scaling. For example, for the Mandelbrot–Weierstrass function in the form eq. (31) we obtain

$$\delta(\Delta x) = \langle|z(x) - z(x + \Delta x)|^2\rangle \simeq \frac{\Gamma(2(1 - H))\cos(\pi(2 - H))}{H(2H - 1)\ln \lambda}(\Delta x)^{2H} \tag{34}$$

and

$$\langle|z(x)|^2\rangle \simeq \frac{\Gamma(2(1 - H))\cos(\pi(2 - H))}{H(2H - 1)\ln \lambda}x^{2H}, \tag{35}$$

where $\Gamma(...)$ denotes the Γ-function.

Furthermore, the correlation function (covariance) of a self-affine fractal also scales in the same manner, namely

$$c(\Delta\mathbf{r}) = \langle z(\mathbf{r})z(bfr + \Delta\mathbf{r})\rangle \propto (\Delta\mathbf{r})^{2H} \tag{36}$$

where $\mathbf{r} = x$ for a self-affine curve in plane, or $\mathbf{r} = \{x,y\}$ for a self-affine surface with mean plane (x,y); the angular brackets denote averaging over the statistical ensemble of $z(\mathbf{r})$. For homogeneous patterns, the ensemble average is the same as the space average (over $\mathbf{r}$) for almost any realization of $z(\mathbf{r})$† (the ergodicity property), hence, $c(\Delta\mathbf{r})$ and $\delta(\Delta\mathbf{r})$ do not depend on $\mathbf{r}$.

We note that as $\Delta x \to \infty$ the delta-variance of a self-affine function in plane also approaches infinity $\delta(\Delta x) \to \infty$, but

$$\frac{\delta(\Delta x)}{(\Delta x)^2} \longrightarrow 0 \tag{37}$$

†For almost any means with probability one.

for $H < 1$, i.e. self-affine curves characterized by $H < 1$ are asymptotically linear (a self-affine surface is asymptotically flat). Hence, we can introduce the length ζ_C, such that in the scale $\Delta x \gg \zeta_C$ self-affine curve in plane can be treated as a smooth Euclidean curve, while in the local scale $\Delta x \ll \zeta_C$ the fractal properties of the curve should be taken into account. The existence of a well-defined correlation length ζ_C[64, 130] is the distinctive feature of self-affine fractals, which distinguishes them from (statistically) self-similar patterns, the fractal properties of which are limited only by physical factors[3, 130].

Because of this, any reasonable procedure of the fractal measurement should lead to the same fractal dimension D of a (statistically) self-similar pattern[3, 137], whereas a self-affine pattern is characterized by different fractal dimensions in the local ($\Delta x \ll \zeta_C$) and global ($\Delta x \gg \zeta_C$)limits[153–155].

Namely, the global fractal dimension of a self-affine fractal, D^G, equals its topological dimension [153], while in the limit $\Delta x \ll \zeta_C$ different scaling properties of the self-affine fractal are governed by different local fractal dimensions[64, 127, 130, 153–159].

Specifically, the length scaling of a self-affine curve in the scale $\Delta x \ll \zeta_C$ is governed by the local divider dimension of trail, also called the latent fractal dimension[158], which is equal to

$$D_D = \frac{1}{H}, \text{ if } H > \frac{1}{2}, \quad \text{or} \quad D_D = 2, \quad \text{if} \quad H \leq \frac{1}{2}. \tag{38}$$

At the same time, the metric properties of the same curve in the limit $\Delta x \ll \zeta_C$ are characterized by the local box-counting dimension $D_B = 2 - H$, while in the global limit $\Delta x \gg_C$ both the scaling and metric properties of self-affine curve are characterized by the global dimension, D^G, which equals the topological dimension of the curve, i.e.

$$D_B^G \equiv D_D^G \equiv D^G = 1, \tag{39}$$

and so, the self affine fractal may be treated as Euclidean object (differentiable curve, smooth surface, etc.), when it is analyzed in the global scale[69, 130].

There are some other fractional dimensions which are associated with other scaling properties of the self-affine fractal. These fractional dimensions govern different physical and chemical properties of the self affine fractal [1, 130]. The relationships between these different fractal dimensions and the roughness exponent, H, are listed in Table 12. Note that for a (statistically) self-similar fractal all these dimensions are equal.

We emphasize that different experimental techniques lead to estimation of different fractal dimensions which have quite different dependence from the Hurst exponent (Table 13). Notice that, whereas most of them increase as H decreases, the elliptical fractal dimension decreases as H decreases. This leads to the aforementioned contradictions between the experimental data

Table 12. Relationships between roughness (Hurst) exponent and various fractal dimensions for self-similar and self-affine fractals with topological dimension equal to $d-1$ embedded in d-dimensional Euclidean space (see refs [42, 153–155])

Dimension	Self-affine fractals		Self-similar fractals
	Local limit	Global limit	
Similarity, D_S	–	–	$(d-1)/H$
Hausdorff–Besicovitch, D_H	$d-H$	$d-1$	$(d-1)/H$
Box-counting, D_B	$d-H$	$d-1$	$(d-1)/H$
Divider, D_D (compass, rule)	*Latent fractal dimension*: $D_\ell = (d-1)/H$, if $H > (d-1)/d$; $D_\ell = d$, if $H \leq (d-1)/d$	$d-1$	$(d-1)/H$
Contour ($d = 2$), D_{cn} (single coastline)	$2/(1+H)$* $1 + (1-H)/(\nu+1)$†	$d-1$	$1/H$
Gap,‡ D_G	$\lg N/\lg b^+$	–	$(d-1)/H$
Mass, ★ D_M	$\log_{b'}(Nb''/b')$	$\log_{b''}(Nb'/b'')$	$(d-1)/H$

* Mean field approximation.

† ν is the correlation length exponent from percolation theory.

‡ N is the number of similar parts, $b^+ = (r_1 r_2, \ldots, r_d)^{1/d}$ is the effective base, r_i is the concern length of each part in i-direction (for self-similar fractal all r_i equals to r). ★ $b' = \max r_i$ and $b'' = \min r_i$ are the largest and smallest base of self-affine transformation (for self-similar transformation $b' \equiv b''$).

Table 13. Special values of the Rényi dimension, D_q, and corresponding values of $\tau(q)$, α, and $f(\alpha)$ for a multifractal measure $M = \{P_i\}$, supported by a set with fractal dimension $D_F = \dim_H M$, where $\dim_H M$ is the Hausdorff–Besicovitch (metric) dimension (see refs[17,152]).

q	Dimension D_q	$\tau(q)$	$\alpha = -d\tau/dq$	$f(\alpha) = q\cdot\alpha + \tau(q)$
0	Fractal dimension $D_B = D_0 = \dim_H M$	$\dim_H M$	α_0	$f_{max} = \dim_H M$
1	Information dimension $D_I = D_1$	0	$\alpha_1 = -I(r)/\ln r$	$f_I = \alpha_1 = I^*$
2	Correlation dimension $D_C = D_2$	$-D_C$	$-D_C - (dD_q/dq)_{q=2}$	$2\alpha_2 - D_C$
$+\infty$	Upper limit D_∞	$\sim -q\cdot\alpha_{min}$	$\to\alpha_{min} = -\ln P + \ln r$†	$f \to 0$
$-\infty$	Lower limit $D_{-\infty}$	$\sim -q\cdot\alpha_{max}$	$\to\alpha_{max} = -\ln P_- / \ln r$†	$f \to 0$

* The measure M has entropy $I = -\lim I(r)/\lim r = f_I$, which is the fractal dimension of the set of concentration for the measure M. (Here $I(r)$ is the entropy of partition of measure M over boxes of size r).
† Here P_+ and P_- are the largest and smallest probabilities in boxes of size r..

obtained by different authors in the studies of fracture surface topography (see refs [66, 74–80, 86, 102–105, 121, 130, 132, 133, 184–192]).

Furthermore, it is pertinent to note, that in a view of nondifferentiability of self-affine functions a standard formula for the increase in the true length of smooth curve

$$\Delta L_t = \int_{x_1}^{x_2} \left[1 + \left(\frac{dz}{dx}\right)^2\right]^{1/2} dx$$

is not valid for self-affine curves. The use of this formula (with one or other approximation for dz/dx, as, for example, in ref. [139]) leads to incorrect results. For example, in this way the authors of [139] have obtained relation $\Delta L_t \propto (\Delta L_x)^H$, where L_x is the curve projection length and $0 < H \leq 1$. According to this relation the true length of crack profile increases with increasing L_x more slowly that the true length of a smooth curve, $\Delta L_t^{smooth} \propto (\Delta L_x)$.† Actually, in the case of self-affine profile the true length increment relates to the projection length increment as $\Delta L_t \propto (\Delta L_x)^{D_D}$, where $1 \leq D_D \leq 2$ is the latent fractal dimension eq. (38).

Now, let us consider a special form [127] of the correlation function

$$C(x) = \frac{\langle -z(-x)z(x)\rangle}{\langle z^2(x)\rangle}. \tag{40}$$

It is easy to verify that for a self-affine fractal the correlation function eq. (40) does not depend on x (see ref. [127]).

For the Mandelbrot–Weierstrass function eq. (31) we have

$$C(x) = 2^{2H-1} - 1 = C^*, \tag{41}$$

where the sign of constant C^* is determined by the type of correlations which, in its turn, is governed by the value of H.

For $H = H^* = 1/2$ ($D_D = 2$) the graph of function eq. (31) represents the trajectory of a random walk with independent (uncorrelated) increments ($C^* = 0$). If $H > 1/2$ ($D_D < 2$) then $C^* > 0$ and self-affine function eq. (31) displays persistence, i.e. a trend (for example, a high or low value) at x is likely to be followed by a similar trend at $x + \Delta x$, whereas if $H < 1/2$ ($D_D = 2$), then $C^* < 0$ and function eq. (31) generates antipersistence, i.e. a trend at x is not likely to be followed by a similar trend at $x + \Delta x$ [127]. Thus, varying H allows us to model highly correlated or anticorrelated heterogeneities of crack face morphology.

It should be emphasized that two self-affine patterns with the same value of H are homeomorphic, so they cannot be distinguished in a statistical sense, even when the geometric images of these patterns are quite different [130]. This gives way to model real self-affine patterns by the graphs of deterministic self-affine functions.

†This result leads to incorrect conclusion that a more singular stress field is related to a more rough crack [139] (see also refs [42, 144]).

Notice that for a (statistically) self-similar fractal the correlation function eq. (40) always positive or equals zero,

$$C(x) = C^* = C\left(2^{2(d-1)/D-1} - 1\right) \geq 0, \tag{42}$$

so that (statistically) self-similar patterns are always highly correlated and cannot display anti-persistence.

2.5. *The concept of multifractals and multifractal analysis of random patterns*

A distinguishing feature of the patterns shown in Figs 1–3, 5–11, 13 and 15 is that they can be modeled by regular fractals and in this way are characterized by a unique value of the fractal dimension (Figs 1, 2 and 4–11) or the Hurst exponent (Figs 13 and 15). It is easy to see, that for patterns shown in Figs 1–3 and 5–11 all definitions listed in Tables 1, 3 and 7–10 lead to the same dimensional number, generally fractional, which coincides with the dimension of self-similarity D_S.

Unfortunately, we can use such simple representation only for some special cases. Generally, a failure pattern should be considered as multifractal which is not of the self-similar variety, but can be interpreted as an inextricable mixture of simple fractals, each one characterized by its own fractal dimension and the whole pattern described by an infinite family of relevant exponents α_q[127,130,150].†

Multifractal measure is related to the study of a distribution of physical or other quantities on a geometric support. The support may be an ordinary plane, the surface of sphere or a volume, or it could itself be a fractal. Statistical properties of a multifractal pattern can be completely described either by the spectrum of singularities $f(\alpha)$[127] or by an infinite number of the generalized dimensions

$$D_q = \lim_{r\to 0}\left\{\frac{I_q(r)}{\ln r}\right\}, \quad I_q(r) = -\frac{1}{q-1}\ln\left\{\sum_{i=1}^{N(r)} P_i^q(r)\right\}, \quad \sum_{i=1}^{N(r)} P_i(r) = 1, \tag{43}$$

also called Rényi dimensions[127]. Here, I_q is the generalized entropy of order $q(-\infty < q < \infty)$, and $P_i(r)$ is the probability that a point of the structure under consideration lies in the box (cell) number i of the covering network with box size r: $P_i = \int_{\text{box}i} d\mu$, μ is the probability measure.

Generally, D_q differs from the topological dimension d_T of a multifractal structure embedded in d-dimensional Euclidean space. Particularly, D_0 is equal to the metric dimension of a random structure evaluated by means of the box-counting algorithm, D_B, also called fractal dimension. The generalized dimension of order $q = 1$ is equal to the information dimension D_I, which is associated with information (Shannon) entropy $I_S = I_{q=1} = \sum_{i=1}^{N} P_i \ln P_i$. Generalized dimension D_2 is equal to the correlation integral exponent D_C, also called correlation dimension, which was introduced by Grassberg and Procaccia[193] as the exponent of a power-law correlation integral

$$C(r) = \lim_{N\to\infty} \frac{1}{N(N-1)} \sum_{i,j=1}^{N} \Theta(r - |\mathbf{r}_i - \mathbf{r}_j|) \propto r^{D_C}, \tag{44}$$

where $\theta(.)$ is the Heaviside function. Integral $C(r)$ counts the number of pairs of points (with coordinates $\mathbf{r}_i$ and $\mathbf{r}_j$) such that $r < |\mathbf{r}_i - \mathbf{r}_j|$. Note that, generalized Rényi dimensions satisfy the general inequality

$$D_{q'} \leq D_q, \text{ for } q' > q, \tag{45}$$

and the spectrum has the characteristic form shown in Fig. 16(a) [127]. The equality in eq. (45)

†The absolute disorder of a large system is in principle impossible by virtue of the Ramsey's theorem, rigorously proved in number theory (ref. [1]), according to which any sufficiently large quantity $N < R(N,n)$ of points (numbers, objects, congruent segments, etc.) will contain a highly ordered subsystems of $N_n < R(N,n)$ elements, where $R(N,n)$ are the Ramsey numbers. Moreover, it has been shown[1, 3, 38] that any random structure (or point set) consisting of a sufficiently large number of elements $N > B(N,n)$, where $B(N,n)$ is a certain set of numbers, can be represented as a multifractal consisting of a finite number, n, of the pre-fractals of i-generation ($i > n$).

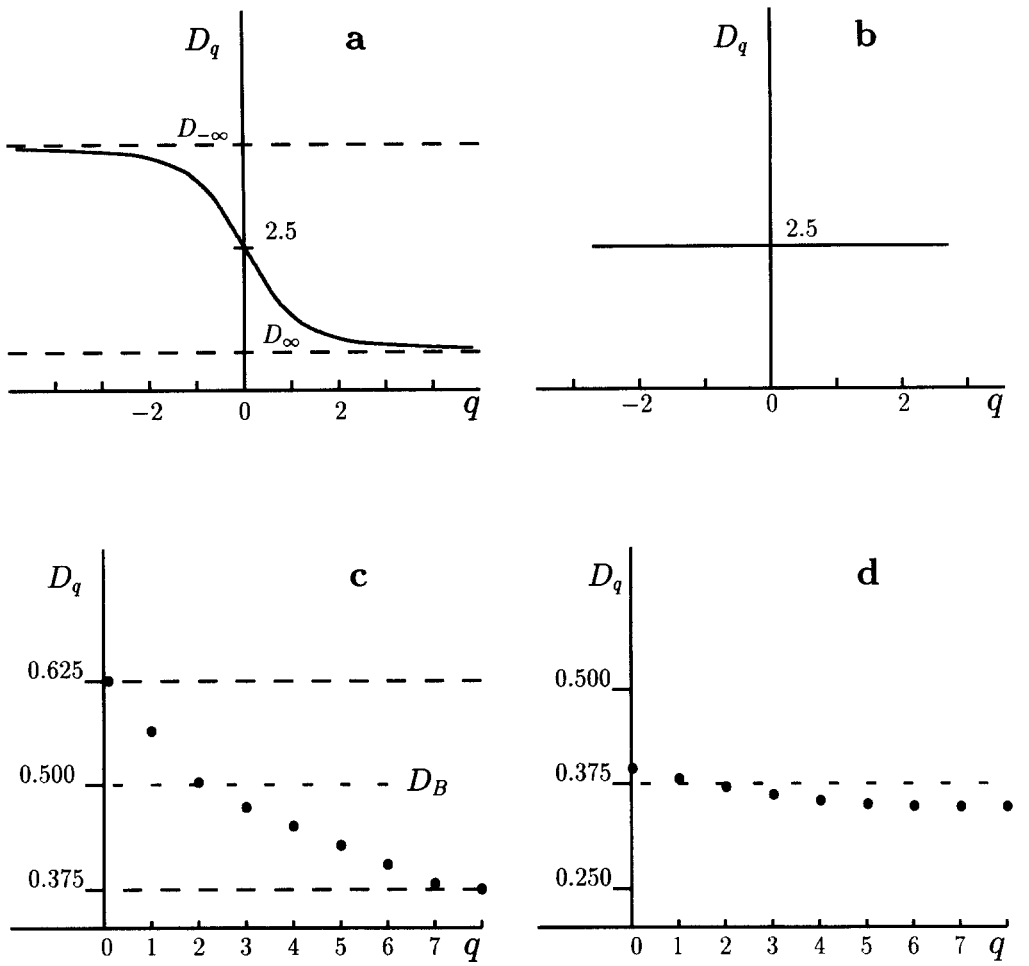

Fig. 16. The spectrum of fractal dimensions D_q as a function of the order q (a) for multifractal pattern with metric dimension equals 2.5; (b) for statistically self-similar monofractal with the same value of metric dimension; and experimental estimated in [101] spectrum of generalized dimensions for discontinuity spacing in a fractured rocks for two samples with (c) multifractal, and (d) monofractal size distribution of discontinuity spacing.

being obtained in the case of uniform sets (monofractals), i.e. such that the probability measure is constant, $P_i \equiv 1/N(r)$, and the generalized dimension D_q equals to the metric (fractal) dimension $D_F \leq d$ for all q (see Fig. 16(b)).

A statistical method for estimation of the correlation dimension of multifractal patterns was suggested in [194]. Box counting algorithms for the determination of generalized fractal dimensions spectrum were advanced in [195]. Two examples of the generalized dimensions spectrum for discontinuity spacing in a fractured rocks are given in Fig. 16(c,d).

The alternative characteristic of a multifractal pattern is the $f(\alpha)$ curve which is defined by

$$\alpha(x) = \lim_{\epsilon \to 0} \frac{\ln P(x)}{\ln \epsilon}, \tag{46}$$

where $P(x)$ is the integral of the probability measure $d\mu$ over a box with center in x. The function $f(\alpha)$ is then defined by the relation

$$N(\alpha^*, \Delta\alpha^*) \simeq \Delta\alpha^* \rho(\alpha^*) \epsilon^{f(\alpha^*)}, \quad \epsilon \to 0, \tag{47}$$

where $N(\alpha^*,\Delta\alpha^*)$ is the number of boxes with α between α^* and $\alpha^* + \Delta\alpha^*$, $\rho(\alpha^*)$ is the distribution probability of points with α between α^* and $\alpha^* + \Delta\alpha^*$, and $f(\alpha^*)$ may be regarded as the fractal dimension of these points.

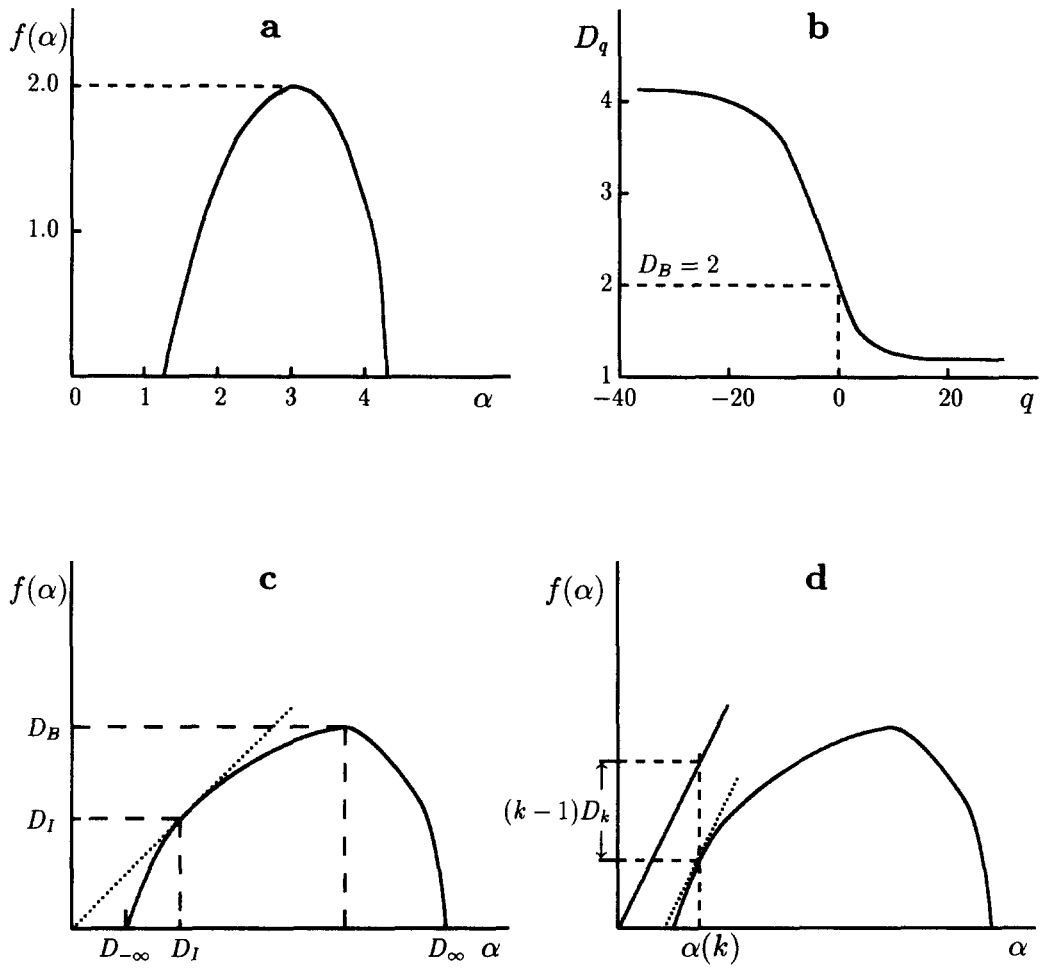

Fig. 17. (a,b) Multifractal characterization of the Pamir–Tien Shan seismic region and (c, d) graphical interpretation of the generalized dimension spectrum.

In the study of relation between the number of earthquakes and the size of the seismic area [4] the maps of the four seismic regions were divided into the nearly square cells of the area, ℓ^2, each, the minimum ℓ value being as small as 3 km. The frequencies of earthquakes in each cell for a selected period of time were used as sampling estimates of earthquake probability. In this way, the distribution function $f(\alpha)$ was obtained for each region (Fig. 17(a)).

The function $f(\alpha)$ relates to D_q by a Legendre transformation

$$f(\alpha(q)) = \tau(q) - q\alpha(q), \text{ where } \tau(q) = (q-1)D_q, \quad \alpha(q) = \frac{\mathrm{d}}{\mathrm{d}q}\tau(q), \tag{48}$$

where $\tau(q)$ is the sequence of mass exponents, $N(\epsilon, q) = \sum_i^N P_i^q \propto \epsilon^{-\tau(q)}$ [127]. A method to perform a direct evaluation of the spectrum of singularities $f(\alpha)$ of multifractal patterns was suggested in [196].† On the other hand, the generalized dimension spectrum, D_q, may be obtained from the spectral function $f(\alpha)$ by using the graphical method.

Figure 17(c,d) shows the geometric interpretation of the generalized dimensions and their relation with the spectrum of singularities $f(\alpha)$. According to the definition eq. (43) and eq. (48) at the point $q = 0$ we have $D_0 = f(\alpha_0)$, where the value α_0 is fixed by the condition $\mathrm{d}f/\mathrm{d}\alpha = 0$. This means that the fractal dimension $D_0 = D_B$ corresponds to the ordinate of the maximum of the spectral function $f(\alpha)$ (Fig. 17(c)).

Furthermore, it is easy to see that $\alpha(1) = f(\alpha(1))$ and $\mathrm{d}f/\mathrm{d}\alpha|_{\alpha = \alpha(1)} = 1$, so $D_1 = \alpha(1)$. Hence, in order to determine the dimension $D_1 = D_I$ from $f(\alpha)$ we must construct the tangent to

†We note some misprints in ref. [196], namely in eqs (5) and (8).

the plot of $f(\alpha)$, passing through the origin (Fig. 17(c)). Then the abscissa and ordinate of the point of tangency determine D_1.

In order to determine the quantities D_k graphically, let us rewrite eq. (48) for $q = k$ in the form

$$(k-1)D_k = k\alpha(k) - f(\alpha(k)), \quad k = \frac{df}{d\alpha}|_{\alpha=\alpha(k)}. \tag{49}$$

Now we can see that in order to determine D_k we must construct the straight line $f = k\alpha$, and then displace it parallel to itself until it is tangent to the dome of the spectral function $f(\alpha)$. According to the second relation of eq. (49) the point of tangency gives $\alpha(k)$, knowing which we determine from the first relation in eq. (49) the exponent D_k (Fig. 17(d)).

Finally, it is readily seen, that the limiting values $D_{-\infty}$ and D_{∞} can be determined from the equation $f(\alpha) = 0$, which has two solutions $\alpha_{\min} = D_{\infty}$ and $\alpha_{\max} = D_{-\infty}$ (Fig. 17(c)). Some useful relationships between special values of D_q, $\tau(q)$ and $f(\alpha)$ are given in Table 13. Figure 17(b) shows the generalized dimension spectrum for the Pamir–Tien Shan seismic region [5], which was obtained from the graph in Fig. 17(a).

2.6. *Morphology of crack faces in brittle and ductile fractured solids*

The quantitative description of rough fracture surfaces has been an important challenge for many years. Research into the field of quantitative fractography has progressed considerably during the past few years (refs [3, 62] and references therein). Numerous fractographic investigations have confirmed that under actual conditions, the crack face morphology in the microscale represents a complex mosaic of microstructural artifacts, the features of which are characteristics of the particular fracture mode and the overall material microstructure [3]. The size of these features varies over a wide range of length scales, from the atomic dimensions of dislocation slip steps to the macroscopic dimensions of grains. The understanding of this morphology requires the deconvolution of these characteristic dimensions, which together form the "building blocks" of the fracture surface. The characteristic failure dimensions are related to significant microstructural length which influence the specific local micromechanics of fracture[3].

Elevation information is needed in order to quantify the true magnitude of the features in the rough crack face. The essential key that unlocks these quantitative data is the true fracture surface area. The important parameters for characterizing the morphological properties of the crack patterns are: (1) fracture trace length; (2) fracture connectivity of a crack network (similar to the coordination number of a pore space); (3) fracture surface roughness (see, [3, 169]); (4) fracture density and spatial geometry are both important parameters in reservoir modeling (the areal fracture density is defined as the sum of fracture trace length per unit area and for an isotropic fracture network this is also the fracture area per unit volume); (5) fracture aperture (this is the crucial parameter that determines permeability). By means of these parameters, fracture processes may be categorized into some principal morphologies [3]: (1) microvoid coalescence; (2) intergranular microvoid coalescence; (3) intergranular fracture; (4) transgranular cleavage (rapid propagation of a crack along particular crystallographic plane); and (5) quasi-cleavage. Several, less common, processes have also been documented [147]. Each of these processes reflects a substantially different local failure criterion and dependence on microstructure and displays a definitive morphology with distinct characteristic dimensions. Various fractal models of crack face morphology were suggested in a number of works [1–5, 8–10, 16, 30–32, 45, 57, 64, 73–76, 82, 86, 87, 89–95, 103–106, 112–116, 138–143, 163, 167–169, 181, 197–205].

Looking at the crack morphology formation problem, one realizes that the self-affine geometry of crack faces results from the stochastic nature of crack growth. This issue can be illustrated by a crack advancement consisting of a sequence of local failures in front of the crack tip, which are random events, caused by the material local strength fluctuations (in inhomogeneous materials [181, 206, 207]), or existence of two or more alternating slip planes in a crystal lattice,† so that the crack trajectories behave randomly.

†As the cracks moved into the crystal, they often propagated in a zigzag manner by emitting dislocations on some alternating slip planes[208–211].

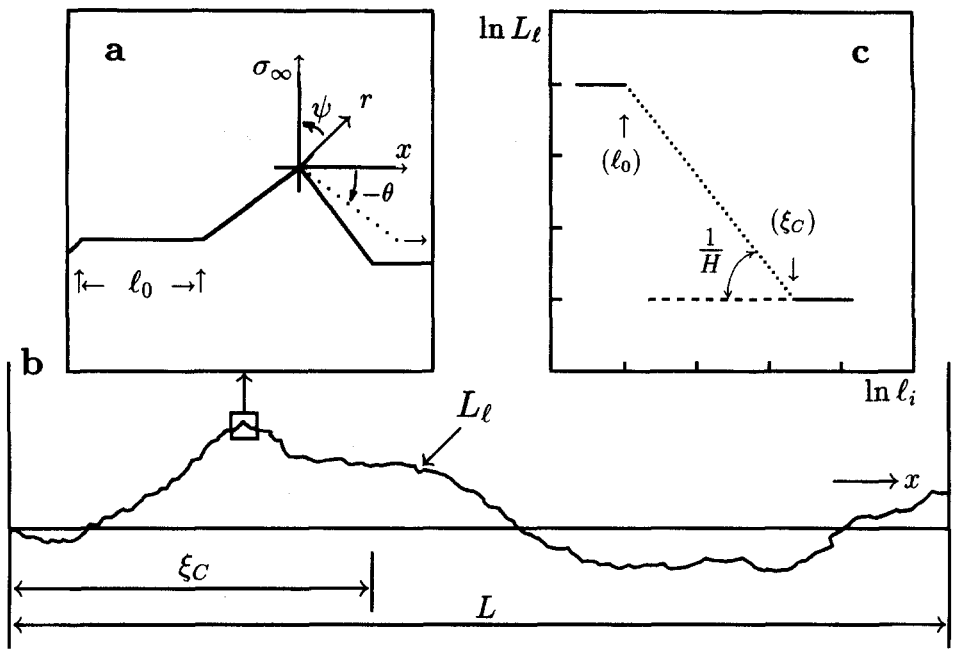

Fig. 18. (a, b) Self-affine crack propagation path and (c) the crack length vs yardstick length. L is the generally applied crack length assuming a planar form, $L(\ell_i)$ is the crack length measured with step (yardstick) length ℓ_i, $\ell_0 = \min_i \ell_i$ is the smallest roughness of crack faces determined by the microscopic cutoff. The nonstandard representation for a crack path and corresponding polar coordinate system are shown in Fig. 18(a).

Since we are particularly interested in the spatial geometry of crack faces, the first idea is to characterize the crack face morphology by the correlation function, eq. (36), or by a delta-variance, eq. (34). Fractographic investigations (see, for example, refs [3, 66]) show that for crack faces in real materials the delta-variance, eq. (34), possesses scaling behavior

$$\delta(\Delta r) \propto (\Delta r)^{2H}, \text{ when } \ell_0 \ll \Delta r \ll \xi_C \tag{50}$$

with $0 < H < 1$ and

$$\delta(\Delta r) = 2\langle |z(\mathbf{0})|^2 \rangle = r_{rmf}^2, \text{ when } \Delta r \gg \xi_C, \tag{51}$$

where parameter r_{rmf} is the rmf-saturated crack face roughness [3, 204]. Hence, real crack faces obey scaling properties only within the bounded interval of length scales

$$\ell_0 \ll L \ll \xi_C, \tag{52}$$

where $\ell_0 \sim 10^{-8}$–10^{-6} m [3, 113] is the microscopic cutoff (it would appear reasonable that this length coincides with the dislocation free zone size, which also has the order of 10^{-6} m for ductile materials [208–212] and of 10^{-8} m for brittle materials [10, 211]) and $\xi_C \sim 10^{-2}$–10^{-3} m [3, 66] is the self-affine correlation length.† Therefore, a real crack face has a finite length (area) and may be treated as a nonstandard curve (surface) whose standard part is a self-affine fractal (see Section 2.3).

In this way, one can build a curvilinear coordinate system along the crack face and, thus, the normal vector $\{n_j\}$ to the crack face can be defined (see Fig. 18(a)). Note that, on this consideration, the roughness (or Hurst) exponent H, which is the basic scaling parameter for a self-affine pattern, is nothing more than the characteristic exponent of the intermediate asymptotic regime (see [148]) and we can speak about crack face fractal properties only within the interval of self-affinity (52).

†As it was noted above, the crack faces morphology possesses self-affine geometry within a set of scale intervals. Here we will discuss only microscale roughness which possesses self-affine geometry within the interval (52).

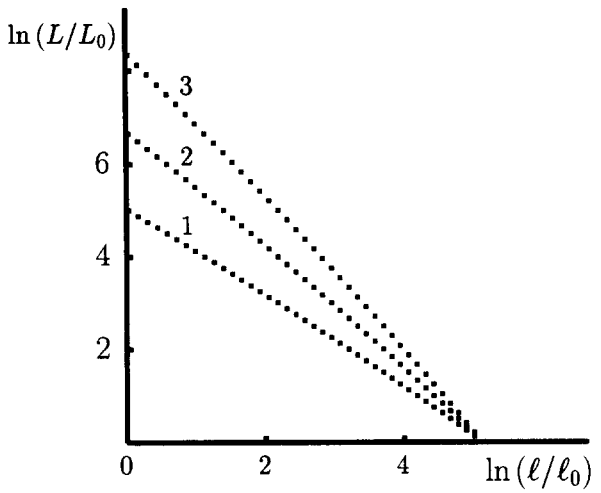

Fig. 19. Surface profile length L vs the divider length ℓ for the steel sample processed by a facegrinding machine to different classes of finishing (experimental data from[213]): (1) class 9; (2) class 10; and (3) class 14. The corresponding fractal values of roughness exponent are (1) $H = 0.56$; (2) $H = 0.67$; and (3) $H = 1$.

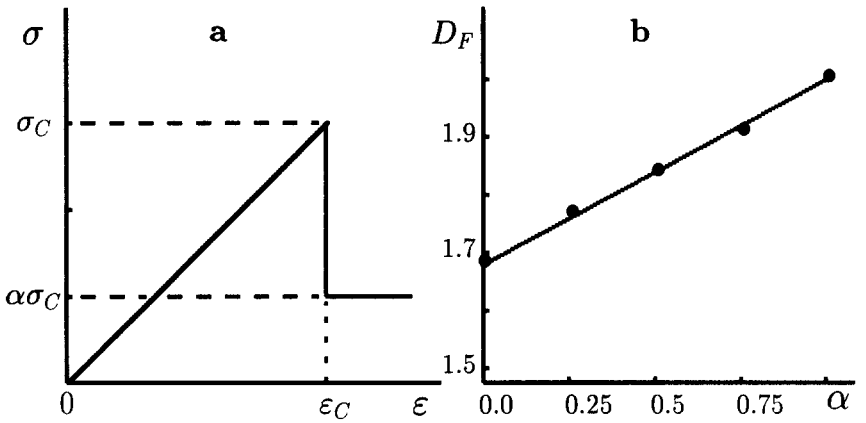

Fig. 20. (a) Force exerted by a given spring as a function of its deformation ϵ: ϵ_C gives the maximum deformation before failure and plastic behavior; and (b) the fractal dimension, D_F, dependence on the parameter α: points—results of computer simulations in [198], solid line—calculations by formula eq. -9pt >

Based on their data, the authors of ref. [132] conjectured that the crack faces roughness exponent H has a universal value close to 0.7. The authors of ref.[184] conjectured another universal value $H = 0.8$, the same for brittle and ductile fracture surfaces.† More recently, the authors of ref. [121] conjectured the existence of two universal roughness exponents, namely $H_1 \simeq 0.84$ and $H_2 \simeq 0.45$, which are associated with slow (H_2) and fast (H_1) crack propagation, respectively. However, a certain number of experimental data does not agree with the conjecture of universality for the fracture surface scaling exponent (see, for example, [3, 26, 60, 61, 66, 74–81, 102, 133, 192] and references therein).

Moreover, while in some simple, unrealistic models, such as those analyzed in ref.[214], the universal value of H was obtained. A number of theoretical models and computer simulations lead to the non-universal fractal dimension of crack faces, which usually depends on the parameters of the model being used [5, 16, 17, 64, 192, 197–203]. Three dramatic examples are illustrated by Fig. 20 and Tables 14–16. Figure 20(b) indicates that H is strongly dependent on the

†More early, it was suggested[189] (see also Fig. 14.1 in Ref.[127]) that the surface roughness of all objects ranging from supertanker hulls and concrete runways to hip joints and honed bearing raceways is characterized by the universal value $H = 1/2$. The data from Ref.[213] shown in Fig. 19 casts doubt on this conjecture.

Table 14. Fractal dimension clusters formed by dielectric breakdown for different values of occupancy probability density exponent η (see eqn (53)). Results of computer simulations on 2 d lattices from ref. [216] and calculations by empirical equation suggested in ref. [215]

The value of η	Corresponding model	Fractal dimension of clusters		
		$D_\eta = 2 - \eta/3$[215]	Data of simulations[216]	
			D_α	D_β
0	Eden cancer model	2	2	2
1/2	Dielectric breakdown (1)	$11/6 \simeq 1.83$	1.86 ± 0.02	1.92 ± 0.05
1	Diffusion-limited aggregation	$5/3 \simeq 1.67$	1.67 ± 0.05	1.71 ± 0.05
2	Dielectric breakdown (2)	$4/3 \simeq 1.33$	1.44 ± 0.02	1.39 ± 0.10
≥ 3	The probability distribution ceases to be normalizable, indicating the impossibility of sustaining a fractal structure under such an extreme growth rule			

parameter of the stress–strain diagram (see also Section 3.2). The data of Table 14 show that the fractal dimension of a failure pattern (formed in dielectric breakdown model) strongly depends on the exponent η of occupancy probability density

$$P(r) = \frac{|E(r)|^\eta}{\int_\Pi |E(r)|^\eta \mathrm{d}S}, \tag{53}$$

where $\vec{E} = -\vec{\nabla}\Phi$ is the electric field (the probability density is normalized over the cluster perimeter Π). Table 15 shows that the fractal dimension of clusters formed in aggregation processes strongly depends on the model used.

The authors of ref. [192] have studied the effect of disorder, material properties and anisotropy on surface roughness. They found that although the roughness exponent, H, is always found within a narrow range, its value systematically decreases as the exponent of disorder is increased. For anisotropic materials the scaling properties are found to be independent of the orientation. While values of the roughness exponent, H, are independent of the problem dimension, differences in the fracture morphology and in the breakdown characteristics are noted. The results of ref. [192] are reproduced in Table 16. These results indicate that the scaling properties of the fracture surface are not universal.

Finally, there are strong indications that H depends on material properties and mechanisms of fracture when experimental data is obtained by the same technique (see, for review, [66, 137]). In Tables 17 and 18 we have reproduced the experimental data from ref. [66]. While these data give no means of seeing a clear relation between H and mechanical properties studied, it is readily seen that the changes in the fractal properties of fracture surfaces, in steel 1045, coincide with those of mechanical properties. These observations cast doubts on the hypothesis of universality for the roughness exponent.

Table 15. Comparison of fractal dimension of clusters formed in aggregation processes calculated by using Flory's approximation[217] and Obukhov's relationships[218] with results of numerical experiments reported in refs[219,220]

d[1]	Trajectory of particles motion				Flory's approximation $D_F = (d + 2)/3$
	Random walk		Linear		
	D^{dif2}	D^{dif} Experimental data	D^{lin2}	D^{lin} Experimental data	
2	1.33	1.46 ± 0.04	1.33	1.55 ± 0.04	4/3 = 1.33
3	1.33	1.82 ± 0.10	1.60	1.91 ± 0.10	5/3 = 1.66
4	1.60	2.10 ± 0.15	2.00	2.25 ± 0.15	6/3 = 2.00
5	2.00	2.35 ± 0.15	2.40	$\geq 2.50 \pm 0.06$	7/3 = 2.33

†More early, it was suggested[189] (see also Fig. 14.1 in Ref. [127]) that the surface roughness of all objects ranging from supertanker hulls and concrete runways to hip joints and honed bearing raceways is characterized by the universal value $H = 1/2$. The data from Ref. [213] shown in Fig. 19 casts doubt on this conjecture.

Table 16. Values of the roughness exponent, H, derived for the various fracture samples[192]. In computer experiments the three-dimensional lattices of size $32 \times 32 \times 64$ and two-dimensional lattices of size 256×256 were used. All results are averaged over at least 20 runs

Breakdown distribution	$H(d = 3)$	$H(d = 2)$
Exponential	0.72 ± 0.05	0.76 ± 0.04
Levy field (meter)	–	0.83 ± 0.09
Levy field (kilometer)	–	0.78 ± 0.07
Power law ($n = 2$)	0.72 ± 0.06	0.68 ± 0.05
Power law ($n = 4$)	0.69 ± 0.04	0.61 ± 0.04
Power law ($n = 8$)	0.52 ± 0.07	0.55 ± 0.07
Power law ($n = 16$)	0.44 ± 0.10	0.53 ± 0.06

Furthermore, it was shown [35] (see also [1–3, 17, 42–44, 112, 221]) that the self-affine roughness of brittle fracture surfaces is characterized by the box-counting fractal dimensions, $D_B = d - H$, less than a certain critical value D_B^*, while the fractal dimensions of ductile fracture surfaces exceed this critical value, i.e. the ductile fracture surfaces are more rough than brittle ones (see Fig. 15).

To gain a greater insight into the nature of the difference between these two types of fracture surface morphology, let us analyze the correlation function eq. (40) for the crack profile on a two-dimensional plane (vertical cut of fracture surface). Within the interval of self-affinity eq. (52) $C(x)$ is independent of x and possesses the remarkable equality eq. (41). As was noted in Section 2.4, the type of correlation is determined by the value of H.

It would appear reasonable that the difference between crack face morphology, in the cases $H < 1/2$ and $H > 1/2$, is associated with the different types of correlations. Namely, brittle fracture surface always possesses persistence and, thus, it is characterized by $H < H^*$ (for a plane problem $H^* = 1/2$), whereas a ductile fracture surface possesses antipersistence and is characterized by $H > H^*$ $(D_D^* = 2)$. We note, that for the d-dimensional problem, the critical value H^* is determined by the condition $D_D = d$[43] (see eq. (38) and Table 12), so that

$$H^* = \frac{d-1}{d}. \tag{54}$$

If so, the critical value of box-counting dimension associated with the brittle to ductile transition, D_B^*, relates to H^* as $D_B^* = d - H^*$ and for two-dimensional problems $D_B^* = 1.5$, while for three-dimensional problems $D_B^* = 2.33$ ($H^* = 2/3$ and $D_B^* = 3$).

The model representations of ductile and brittle fracture surfaces are shown in Fig. 15(a,b), respectively. Note that a brittle fracture surface with fractal dimension D_B can be modeled by a (statistically) self-similar fractal with the same fractal dimension, whereas a ductile fracture surface (which possesses antipersistence) cannot be represented by a self-similar model because, as was noted above (see eq. (42)), self-similar fractals are highly correlated and cannot display antipersistence.

As will be shown below (see Section 4.1) the different character of the aforementioned correlations results from the different nature of brittle and ductile fracture and leads to differences

Table 17. Adsorbed energy and fractal properties of fracture surfaces in steel 1045 fractured in standard tests with strain rate 3.333×10^{-3} s^{-1} at different temperatures[66]

T, °C	E_a, J	$H^{(B)}$	$H^{(D)}$	H, eq. (59)
25	1.35	0.958	0.959	0.958
100	14.56	0.961	0.960	0.960
200	19.44	0.955	0.930	0.942
300	8.97	0.940	0.917	0.929
400	9.36	0.935	0.915	0.925
500	6.99	0.820	0.910	0.864
600	11.86	0.805	0.846	0.825
700	37.96	0.950	0.951	0.950
800	8.81	0.972	0.973	0.972
900	7.79	0.971	0.972	0.971
1000	0.972	29.96	0.970	0.971

Table 18. Adsorbed energy and fractal properties of fracture surfaces in steel 1045 fractured at 1000°C in the standard tests with different strain rates[66]

Property	Strain rate, s^{-1}		
	1.666×10^{-1}	3.333×10^{-3}	3.333×10^{-5}
E_a, J	30.253	29.960	5.320
D_D	1.041	1.030	1.171
$H^{(D)}$	0.961	0.970	0.853
D_B	1.041	1.028	1.140
$H^{(B)}$	0.956	0.972	0.960
H, eq. (59)	0.960	0.971	0.857

between the stress field behavior near the tip of a self-affine crack in the cases of brittle and ductile fracture.

Furthermore, we note that for a general case, the two-point correlation function eq. (33) is insufficient to completely characterize the crack face morphology. A more detailed description of crack face morphology requires that one uses the concept of multiaffinity which allows a much more complete representation of real crack patterns by using an infinite hierarchy of scaling exponents. This can be done by the consideration of the qth order height–height correlation function[123–125], defined as

$$G_q(x) = \frac{1}{N}\sum_{i=1}^{N}|z(x_i) - z(x_i + x)|^q, \tag{55}$$

where $N > > 1$ is the number of points over which the average is taken (only non-zero terms are considered). For real multiaffine crack faces, $G_q(x)$ exhibits a nontrivial multiscaling behavior

$$G_q(x) \propto x^{qH_q} \tag{56}$$

with H_q changing continuously with q for at least some region of the q values. It can be shown that a continuous spectrum of H_q values is not consistent with the equality eq. (41) which is only valid for standard self-affine patterns with a single exponent H; for multiaffine patterns

$$C(x) \propto C^* x^{-(H_2 - H_0)}, \tag{57}$$

so that correlations between increments vanish at large distances x.† Therefore, experimental measurements of H in the scale of the order of ξ_C will always give the values which are closed to $H^* = 1/2$ or $H^* = 2/3$. It seems to be the reason for the results which led to the aforementioned conjecture about the universal roughness exponent (universal value $H = 2/3$ was first suggested for the directed polymer polymer problem and was then used as a universal exponent for brittle fracture surfaces[128]).

From the experimental data reported, in refs[3,66], it follows that in the case of brittle fracture $(H_{-\infty} - H_{\infty})/H_0 < 1$, whereas for ductile fracture surfaces $(H_{-\infty} - H_{\infty})/H_0 \sim 1$. Hence, in the first case we can use the self-affine representation for real crack faces, while in the second case, the concept of multiaffinity should be used to model the real morphology of ductile fracture surfaces.

The test of crack face self-affinity was suggested in ref.[66]. For uniform self-affine patterns, such as the examples shown in Figs 12 and 15, the roughness exponent obtained from divider measurement, $H^{(D)} = (d-1)/D_D$ (see eq. (38)), equals the roughness exponent obtained by the box-counting method, $H^{(B)} = d - D_B$ (see Table 12). For real fracture surfaces $H^{(D)}$ usually differs from $H^{(B)}$ (see, for example, the experimental data in Tables 17 and 18). However, as was shown in[66], if

$$|H^{(B)} - H^{(D)}| < \frac{1}{D_D}\min\{H^{(B)}, H^{(D)}\}, \tag{58}$$

then the fracture surface can be treated as statistically self-affine and, so, can be characterized by the unique roughness (Hurst) exponent

†The different values of H for different scales of the same crack face were observed in experiments[3,113,121].

$$H = \sqrt{H^{(B)}H^{(D)}}. \tag{59}$$

Otherwise the surface (profile) must be considered as multiaffine. As is readily seen from Tables 17 and 18 for all surfaces studied in [66], the inequality eq. (58) is valid and they can be treated as statistically self-affine fractals.

It would appear reasonable that in the case of intergranular cleavage the fractal dimension of crack faces is governed by the statistical topography of grain boundaries and, thus, coincides with the fractal dimension, D_g, of grain boundaries. In the case of transgranular cleavage it should be reasonable to expect that the fractal dimension of crack faces, D_B, is less than D_g. A path integral representation for self-affine patterns to model a brittle crack paths has been suggested in [181] and developed in [163]. Using this representation, a more detailed specification for the brittle crack morphology may be made on the basis of the Rieman–Liuoville and Wigner–Valle spectra analysis [222] of the brittle crack profiles and surfaces. This analysis will be the subject of a forthcoming paper. It is important to note that the self-affine geometry of brittle crack faces leads to changes in the stress field distribution in the vicinity of the crack tip. Within the interval of self affinity, eq. (52), the value of the stress singularity exponent is governed by the crack roughness exponent, H [43–45].

On the other hand, when fracture is ductile, the crack morphology is governed by the kinetics of failure [1, 5] and is characterized by a wide spectrum of generalized dimensions D_q as shown in Fig. 16(a). In this case, the knowledge of the crack face metric dimension D_B is not sufficient to model crack face morphology, which is quite different for different types (mechanisms) of ductile fracture, whereas for any crack face with $D_B > D_B^*$ the stresses near the crack tip is constant within the interval eq. (52) [43]. Hence, for the classification of ductile fracture from a fractal point of view, we need a more detailed analysis based on percolation theory [1, 166–169] and generalized statistics [171, 172]. This topic will be the subject of a forthcoming paper.

Various aspects of fractal fracture mechanics were analyzed in a number of works (see, for example, [14–45] and reviews [1–5, 16, 17, 64, 130]). The most important implication of fractal concepts in fracture mechanics is that these concepts give a way for the prediction of fracture and fatigue phenomena in one scale using the corresponding data for another scale. However, the possibilities of this approach have not been used in their full measure. To do this, we need to understand the physics of fracture, on different scales, that gives a way for developing a statistical theory of fracture which should adapt classical fracture mechanics, as well as the dislocation theories of fracture in the nanoscale. Some efforts in this direction are suggested in the following sections.

3. THE PHYSICS OF FRACTURE

The irreversible deformation and fracture of solids are processes for which a macroscopic behavior is governed by the complex dislocation processes in the nanoscale. Hence, we can predict, and adequately describe, failure phenomena (without special experimental tests) only with a clear understanding of the nature and kinetics of real quantum dislocation processes in the deformed solid. The nature of the interrelation between processes of different scales constitute the central problem in fractal fracture mechanics [1–5]. With a profound understanding of this type, full scale, macroscopic behavior of materials could be predicted from minimal and fundamental characteristics of the material.

First of all, we note that there are three basic scales of fracture associated with characteristic length scales of a self-affine crack, namely, ℓ_0 and ξ_C. In fact, as was already noted above, the crack possesses self-affine geometry only within the interval eq. (52), whereas in the nano-, $L < \ell_0$, and macro-, $L \gg \xi_C$, scales it may be treated as a smooth cut, the metric dimension of which coincides with its topological dimension $d_T = d - 1$, where d is the dimension of the problem under consideration. Furthermore, it was found [208–211], that in the crack tip zone of the size $\ell_d \simeq \ell_0$ the stress field is ideally elastic. Hence, within this zone the concept of stress intensity factor can be used (see Fig. 21(a,b) and Fig. 22). A correct description of the material beha-

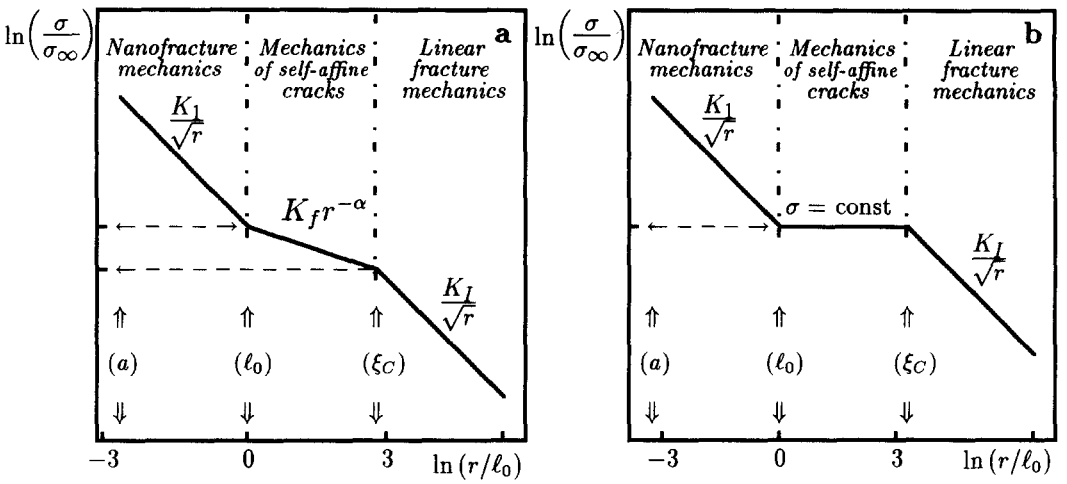

Fig. 21. Stress distribution in the front of a self-affine crack in a linearly elastic solid in the case: (a) brittle ($H > H^*$ $C^* > 0$), and (b) ductile ($H < H^*$, $C^* < 0$) fracture.

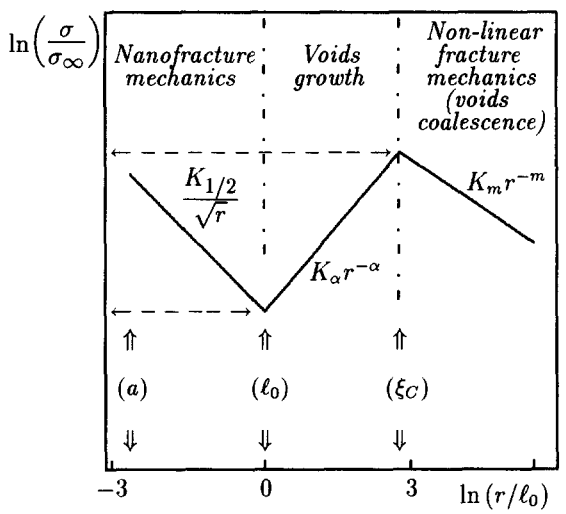

Fig. 22. Stress distribution in the front of a self-affine crack in a power-law hardening material. Note, that within the dislocation free zone (60) elasto-plastic materials possess, for example, linear elasticity and, so, stresses obey the inverse square root asymptotic form eq. (90), whereas at distances $r \gg \xi_C$ stresses possesses power-law behavior with power-law exponent defined by eq. (88). The stress field behavior within the interval eq. (52) is defined by eq. (87) with exponents β and m given by eq. (79)

vior and failure within this zone should include actual dislocation processes in the elastic field, in the vicinity of the crack tip[5,45,47,212]. Furthermore, the methods and predictions of classical fracture mechanics, based on the concepts of stress intensity factors and invariant integrals, are valid for macrocracks with length $L \gg \xi_C$ (see Fig. 21(a,b)), if we consider discrete crack increments $\Delta L \gg \xi_C$[43],† while the roughness of real crack faces leads to a change in stress field behavior within the interval of self-affinity eq. (52) and, thus, affects the macrofracture toughness[42,55].

In this way, in order to construct a completely general theory of fracture that transcends all length scales, we should understand the physics of processes associated with crack increments in three intervals: (1) $a \leq \Delta L \leq \ell_0$, where a is the interatomic spacing; (2) $\ell_0 < \Delta L \leq \xi_C$; and (3) $\xi_C < \Delta L \leq \ell_G$, as well as the nature and mechanisms of the interrelations between processes in the different scales (see Fig. 21(a,b) and Fig. 22).

†Notice that the suitability of classical fracture mechanics may be restricted by the upper limiting length ℓ_G if the crack possesses a self-affine property in the global scale $\ell_G < L < \xi_G$. For example, for some geophysics phenomena $\ell_G \sim 1$ *km* and $\xi_G \sim 10^3$ *km*[4].

3.1. *Physics of nanofracture*

The nanofracture of crystal materials has been the subject of numerous experimental investigations *in situ* for the past 15 years (see, for example, refs [208–211] and references therein), but the basic mechanisms of the phenomena are not fully understood at present. In fact, according to a well-accepted view [147], a plastic zone is always ahead of a crack tip in a ductile material. Furthermore, it is assumed that the size of this zone increases as the external stresses increase.

At the same time, electron microscope observations by Kobayashi and Ohr [209], Horton and Ohr [208], Ohr [210] and Novikov and Ermishkin [211], have shown that actually all dislocations drive out of the crack tip area, leaving behind a dislocation-free zone in the vicinity of the crack tip. The dislocations come to rest at the points where the repulsive force is balanced by the lattice friction. By these means the plastic deformations are always localized and occur at distances $r > \ell_d$ from the crack tip, where $\ell_d \sim 10^{-8} \div 10^{-6}$ m is the dislocation-free zone size [210–212]. Furthermore, we emphasize, that in the nanoscale, the concept of plastic deformations, as averaged on many dislocations, cannot even be used. Actually, the generation, nucleation, motion and interaction of dislocations and point defects in the elastic stress field, in nanoscale, create what we observe as inelastic deformations in fracturing on the micro- and macro-scales. Hence, the problems of dislocation generation and nucleation are of primary importance for a physical theory of fracture.

Once created, a dislocation-free zone restores the elasticity to the crack tip region [210]. Hence, within the bounded interval

$$a < r < \ell_d \tag{60}$$

in the vicinity of the crack tip ($a \sim 10^{-9}$ m is the interatomic spacing) stresses obey the classic inverse square root singularity (see Fig. 21(a,b) and 22). Therefore, it is possible to define the local stress intensity factors K_1 (K_2 and K_3 for nanocrack modes II and III, respectively). We use arabic indices for local stress intensity factors, instead of roman indices which are accepted in linear fracture mechanics. Note that the local stress intensity factors differ from the conventional stress intensity factors. For example

$$K_1 \simeq \sigma_{11}\sqrt{\pi \ell_d} \ll K_I \simeq \sigma_{11}\sqrt{\pi L_c},$$

where L_c is the macrocrack length ($L_c \gg \ell_d$) and σ_{11} is stress applied in infinity.

It should be emphasized that without the dislocation-free zone the local stress intensity factor approaches zero and the crack cannot propagate in the nanoscale, because there is not elastic energy release associated with the propagation [210].

Armstrong [223] and Kelly *et al.* [224] advanced the viewpoint of brittle vs ductile response as the competition between Griffith cleavage and plastic shear at a crack tip. Rice and Thomson [225] specifically modeled the shear process of the nucleation of a dislocation from a stressed crack tip. The Rice–Thomson's approach made use of elasticity solutions for a fully formed dislocation (i.e. a dislocation with slip equal to the Burgers vector **b** of some complete or partial lattice dislocation) and a core cut-off parameter had to be introduced to derive a nucleation criterion. Later, Rice [226] advocated the analysis of dislocation nucleation from a crack tip based on the Peierls concept as applied to a slip plane emanating from the tip. Cherepanov [227] suggested an alternative general approach to the problems of dislocation generations and fracturing, which was called nanofracture mechanics [5, 212]. According to this approach, the size of the dislocation free zone ℓ_0 and nanofracture toughness K_c may be determined from the equation of equilibrium for a virtual dislocation in the near crack tip stress field:

$$A\frac{K}{\sqrt{r}} = \tau_0 + B\frac{Gb}{r}, \tag{61}$$

where A and B are some numerical coefficients depending on the slope of slip plane (in the case of a mode III crack and a screw dislocation moving along the slip plane coinciding with the crack propagation, $A = 1/\sqrt{2\pi}$ and $B = 1/4\pi$ [227]), G is the shear modulus, b is the absolute value of the Burgers vector of the elementary dislocation and τ_0 is the Schmid stress of a crystal lattice. At the stage of equilibrium

Table 19. Ultimate tensile strength and various brittleness parameters for some crystal materials

Material	σ_C, GPa[10]	B_*,[12]	Re_{cr}[11]	η_1^{-1}[227]	η_R^{-1}[225]	η_2 eq. (65)
Ductile materials ($B_* \geq 1$[12], $Re_{cr} > 0.707$[11], $\eta_1^{-1} \gg 1$[227], $\eta_R^{-1} \geqslant 0.35$[225]):$\eta_1 < 1$, $\eta_2 < 1$						
Au	25.3	1.81	1.01	70	0.45	0.08
Al	18.5	1.44	1.14	$25 \div 50$	0.35	0.1
Ag	18.9	1.28	0.85	$50 \div 100$	0.39	0.09
Ti	24.6	1.26	1.10	40	?	0.1
Cu	29.0	1.18	0.93	$30 \div 50$	0.40	0.1
Quasi-ductile and quasi-brittle materials ($0.65 < B_* < 1$, $\eta_1^{-1} \sim \eta_R^{-1} \sim 1$): $\eta_1 < 1$, $\eta_2 > 1$.						
Fe	38.1	0.90	0.71	10	0.34	1.5
Ru	57.2	0.73	0.70	?	?	2.5
Mo	40.9	0.72	0.61	0.87	?	8
W	50.5	0.70	0.55	0.93	0.33	3
Al_2O_3	49.8	0.68	0.705	0.63	0.24	–
Brittle materials ($B_* < 0.65$, $Re_{cr} < 0.707$, $\eta_1^{-1} < 1$, $\eta_R^{-1} < 0.25$): $\eta_1 > 1$, $\eta_2 > 1$.						
B_4C	48.2	0.53	0.60	?	?	6
Si	13.9	0.46	0.52	0.77	0.23	5
Ge	10.7	0.42	0.53	?	0.18	10
SiC	37.1	0.41	0.32	0.59	?	20
Diamond	81.7	0.34	0.51	0.42	0.20	30

$$K = K_c = \frac{2B}{A}\sqrt{Gb\tau_0} \text{ and } r = B\frac{Gb}{\tau_0} \simeq \ell_d, \tag{62}$$

A crack-tip emits the first stable dislocation at $K = K_c$. Once generated, the dislocations moved out of the dislocation-free zone because of a repulsive force (the dislocations come to rest at a point $r = \ell_d$ where the repulsive force is balanced by the lattice friction). Because of this, the elastic dislocation-free zone is universally presented around the crack tip. This fact was confirmed by electron microscope observations[208–211], but is ignored in most models of fracture.

Just after an actual dislocation is born, the crack-tip advances a certain amount, which is specific for the given crystal lattice. On the other hand, the same crack tip can propagate in an ideally brittle (cleavage) way (without a dislocation emanation) when K achieves the critical value

$$K_c^B = 2\sqrt{G\gamma}, \tag{63}$$

where γ is the surface tension. This criterion immediately follows from the energy conservation law[228,229].

Which of these two opportunities occurs first when K increases? According to all the aforementioned models[212, 223–227], the quantitative parameter which governs the type of the material response is the ratio

$$\eta_1 = \frac{K_c}{K_c^B}. \tag{64}$$

If $\eta_1 > 1$, a crack-tip cannot serve as a source of dislocations and will propagate in a cleavage manner, whereas if $\eta_1 < 1$, some edge dislocations will be generated from the crack tip under loading. When $\eta_1 < 1$, but, $\eta_1 \sim 1$, the number of emerging dislocations is comparatively small and fracture is quasiductile or quasibrittle, while if $\eta_1 \ll 1$, the fracture is ductile (see Table 19).

To obtain a more rigorous criterion we note that a cleavage crack can only propagate if $\ell_C \leq \ell_d$, where $\ell_C = (\sigma_C/K_c^B)^2$ is the Griffith's critical crack length. Thus, we can introduce a new nano-brittleness criterion in the form

$$\eta_2 = \frac{\ell_C}{\ell_d} = \left(\frac{\sigma_c}{K_c^B}\right)^2 \times \frac{\tau_0}{BGb} = \frac{E_0\tau_0}{10\gamma Gb}, \tag{65}$$

where $\sigma_c \simeq \sqrt{n_b E_0/144}$[10] is the ultimate tensile threshold stress for solid crystal, n_b is the near-

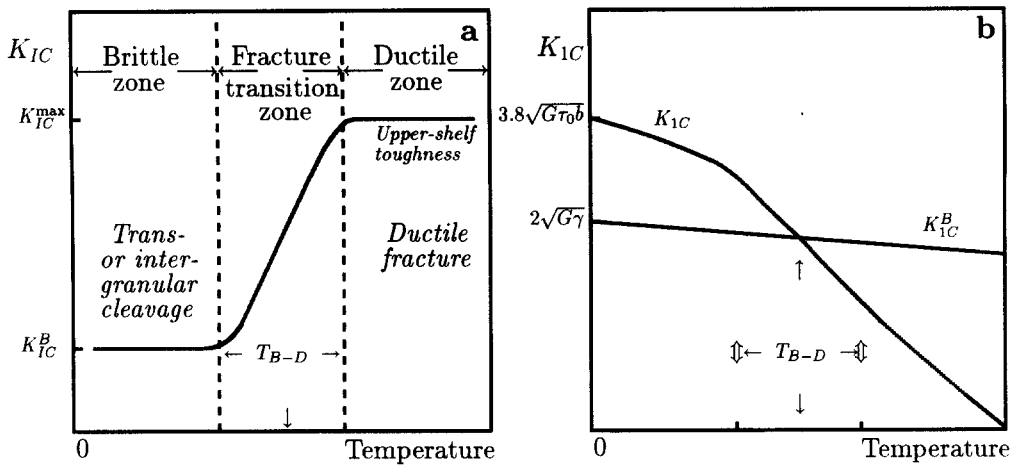

Fig. 23. (a) Schematic of the effect of temperature on macro-fracture toughness K_{IC} of metals that exhibit a brittle-to-ductile fracture transition [230], and (b) the temperature dependences of nano-fracture toughness in brittle and ductile regimes. The temperature dependences of K_{1c} and K_{1c}^{B} were calculated by using the model suggested in ref. [12].

est neighbor bonds number in the elementary cell, and E_0 is the sublimation energy of gram-atom of the solid [10].

Now, the fracture will be ideally ductile, if $\eta_1 < 1$ and $\eta_2 < 1$, it will be quasibrittle or quasiductile, if $\eta_1 < 1$, but $\eta_2 > 1$, and it will be truly brittle cleavage, if $\eta_1 > 1$ and $\eta_2 > 1$.

The criterion eq. (64) leads to valid predictions when the theoretical values for the nano-fracture toughness K_c and K_c^B are used† (see [5, 223–227]), whereas the macro-fracture toughness of ductile materials is usually well over the macro-fracture toughness of brittle materials. Moreover, for a material which possesses the brittle-to-ductile transition at a certain temperature T_{B-D}, $K_{1c}^{B}(T > T_{T-D}) > K_{1c}(T > T_{T-D})$ (see Fig. 23(b)), whereas when the macro-fracture toughness K_{IC} is measured by standard mechanical tests, the toughness in the ductile regime is always large than the brittle fracture toughness (see Fig. 23(a)). By this means the ratio

$$\eta_M = \frac{K_{IC}}{K_{IC}^{B}} \gg 1 \tag{66}$$

at any temperature. Hence, the nanofracture models cannot be directly applied to the problems of macrofracture and we need to analyze processes in the microscale.

3.2. *The nature of self-affine roughness of crack faces in brittle and ductile materials*

As was noted, in Sections 2.4 and 2.6, the fractal properties of brittle and ductile fracture surfaces are dramatically different. Namely, a brittle fracture surface possesses persistence, whereas a ductile fracture surface possesses antipersistence. This difference resulted from the different kinetics of brittle and ductile fracture [1, 5]. Moreover, the reasons for self-affine geometry of crack faces in brittle and ductile materials are most likely to be different.

The self-affine geometry of intergranular cleavage cracks arises from the stochastic nature of crack growth [181]. This issue can be illustrated by crack advancement consisting of a sequence of local failures in front of the crack. These failures are random events caused by the material local strength fluctuations [206, 207], so that the crack trajectories behave randomly. We note that this process is similar to directed percolation in the random network (of grain boundaries) and, thus, the crack trajectory should exhibit some self-affine geometry. Obviously, in this case the fractal (box-counting) dimension of crack faces should be larger or equal to the fractal dimensions of grain boundaries and the microscopic cutoff size of self-affinity, ℓ_0, is determined by the grain size [47, 48].

†Notwithstanding the dramatic difference between absolute values for nanofracture toughness predicted by different models, all models lead to the same predictions about the nature of fracture for a given material (see Table 19).

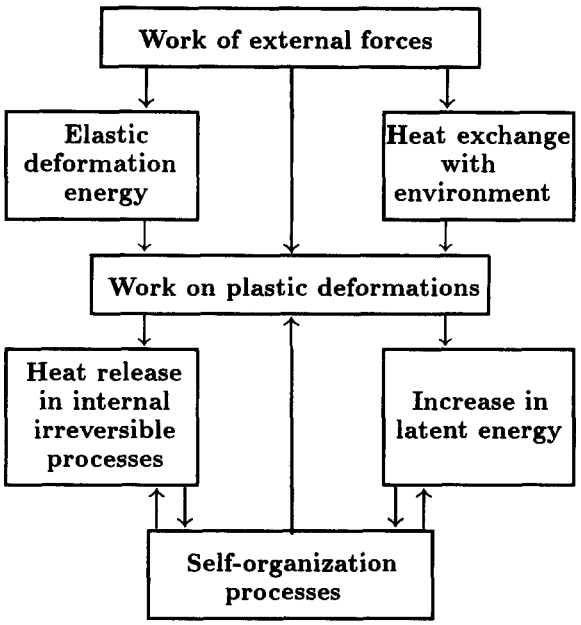

Fig. 24. Schematic representation of thermodynamic description for plastic deformations in the dislocation (disclination) dissipative zone in the crack front.

In the case of transgranular cleavage, self-affine crack growth can be directly modeled on the basis of the principle of maximum energy dissipation rate suggested in[231]. Computer simulations[41] have shown that the crack path formed in an elastic medium by elementary crack advancements of the equal length ℓ_C possesses self-affine scaling within a wide range of length scales $\ell_C < L < \zeta_C$, where ζ_C is the "mathematical" self-affine correlation length which was defined in Section 2.4.

A fractal crack growth in an elastic network was simulated in[198] on the basis of model stress–strain diagram shown in Fig. 20(a). Computer simulations[198] have shown that cracks formed in such a network, possess self-similarity within a wide range of length scales. The fractal dimension of a crack formed in this model strongly depends on the parameter α (see Fig. 20(b)). We note that the data of computer simulations can be adjusted by simple empirical relation

$$D_F = \frac{5+\alpha}{3}. \tag{67}$$

Some other models of this type were considered in refs[5,17].

The phenomena of ductile fracture are more complex. In fact, in the microscale these phenomena are governed by the irreversible, far from equilibrium processes of self-organization of the dislocation and disclination dissipative structures[1,3]. Hence, the morphology of a ductile fracture surface is governed by the topography of the dissipative structure which is formed near the crack tip (see, for example, Figs 7–9).

One can notice that dissipative structures formed far from equilibrium always possess fractal properties, which are governed by the competition between processes of entropy production and energy redistribution[14]. In a deformed solid the self-organization of fractal dissipative structures yields an optimal (for specific loading) level of dissipation of energy of an external action[1].

For a complete description of the ductile fracture in the microscale we then need to use the thermodynamic[232,233] (or synergetic[1,3,6]) approach. In this way, the conventional concept that the crack tip is headed by a plastic zone should be replaced by the concept of the dislo-

cation (disclination) dissipative structures near the crack tip. Schematic representation of the thermodynamic description for plastic deformations in the dissipative zone† is given in Fig. 24.

It seems to be reasonable, that in the case of ductile fracture the the lower limit ℓ_0 of the interval of crack face self-affinity eq. (52) coincides with the dislocation-free zone size, i.e. $\ell_0 = \ell_d$. More detailed analysis of these topics will be the subject of a forthcoming work.

3.3. *Physics of macrofracture and scale effects*

It is well-accepted that inhomogeneous in microscale materials can be treated as homogeneous elastic medium when the larger scale phenomena are analyzed [147, 134, 235]. However, over the last few years, it was recognized that some basic concepts of linear elastic fracture mechanics (LEFM) are not valid, even when material response is exceptionally brittle in nature [55, 236–238].

A dramatic example is the size dependence of the "measured fracture toughness", which was observed in the standard mechanical tests for various materials (see refs [236, 237] and references therein), whereas LEFM is based on the assumption that fracture toughness, K_{IC}, is the physical constant of a given material. Moreover, essential for the success of LEFM as a truly predictive theory is that the stress intensity factor really controls fracture. Hence the issue of whether or not fracture toughness is size independent goes right to the very basis of LEFM.

Moreover, it is a pity that we traditionally classify materials as being ductile or brittle based upon tests in the laboratory, for there is a scale effect in the fracture mechanics which produces unexpected transitions in behavior. That is, components and structures made from brittle materials can behave in a ductile fashion and those made from ductile materials can behave in a brittle fashion. The transition from ductile behavior in the small to brittle behavior in the large has figured prominently in catastrophic engineering failures [234].

Furthermore, the relations between the structural parameters of a material and its strength are changed dramatically under dynamic loads when, in contrast to quasi-static loading, the influence of defect nucleation an propagation is not decisive in the deformation and fracture of the solid [239–251].

The conventional approach to fracture, based on the model of isotropic an elastic or elasto-plastic continuum, does not provide adequate tools for analysis of these effects. As will be shown in the next section, the aforementioned phenomena can be advantageously explained within a framework of self-affine crack mechanics. Furthermore, the length scale interval of LEFM validity will be also determined.

4. MECHANICS OF SELF-AFFINE CRACKS

Unfortunately, it is not even possible to formulate the crack propagation problem with non-differentiable self-affine profiles (surfaces) using the conventional methods of continuum mechanics. Actually, the boundary conditions on the crack face are formulated for normal and tangential stress or displacement components. To determine these components, the unit vector normal to the crack face must be known and this is expressed in terms of the spatial derivatives of the face forms. For non-differentiable self-affine crack faces, it is impossible to introduce the normal vector because the spatial derivatives are undefined. Consequently, we cannot formulate the boundary conditions on the self-affine (non-differentiable) crack face in the conventional form. Hence, to deal with this problem it is necessary to use an adequate approach which gives a way to benefit the fractal properties of cracks.

In Section 2.6, we have already noted that the boundary conditions can be formulated by using the nonstandard representation of real crack face, the standard part of which is self-affine fractal. On the other hand, as will be shown below, the problems with self-affine cracks may be advantageously analyzed within a framework of the renormalization group approach.

Below, the problems with self-affine cracks are analyzed within a framework of the renormalization group theory. The crack tip stress field behavior associated with self-affine cracks in linear elastic and power-law hardening materials are evaluated. The fractal represen-

†Notice, that from the physical point of view, the concept of inhomogeneous (multifractal) dislocation dissipative structure is more acceptable than the concept of homogeneous plastic zone, because plastic deformations are always localized.

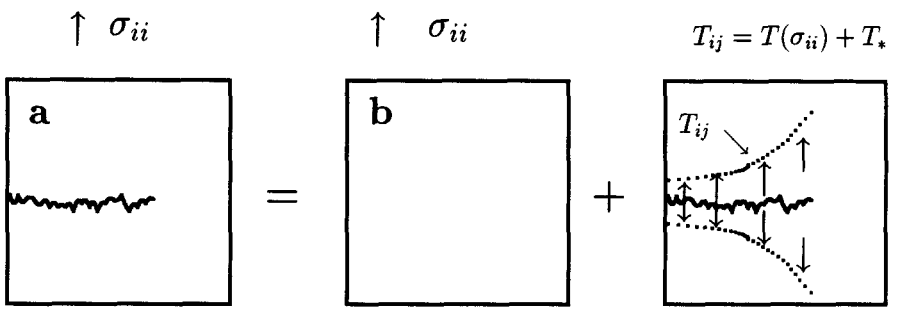

Fig. 25. Reduction of the problem (a) with self-affine crack and longitudinal tensile stress σ_{ii}; to the problem (b) with self-affine crack loaded by unknown traction T_{ij}.

tation of the real crack morphology provides a strict approach for deriving relations between nano- and macrofracture parameters. Then the concept of equivalent traction is formulated to account for the mechanics of self-affine cracks. This concept is used to construct path-independent integrals for some problems with self-affine crack. It is shown that a self-affine roughness can affect crack mechanics in a dramatic way. Moreover, some fracture phenomena can be adequately described only when the self-affine geometry of crack faces is taken into account. Three examples of the dramatic role of crack fractality in crack mechanics are analyzed in Sections 4.7, 4.8 and 4.9.

4.1. *The asymptotic stress fields in the vicinity of self-affine crack in a linear elastic solid*

In an effort to examine a stress field distribution associated with a self-affine crack, let us consider a plane problem with a traction-free self-affine crack with mean plane perpendicular to the direction on tensile stress $\sigma_{yy} = \sigma_{yy}^{\infty}$ applied at infinity as shown in Fig. 25(a). This picture relates to the tensile mode (Mode I) of loading for the problem with a straight cut. At the same time, we note that while in the problem with linear crack (cut), the crack tip is the unique singular point for the elastic fields, in the case of a self-affine crack singular points occur along the self-affine crack face at all scales (see Section 2.4). Furthermore, for the problem with rough crack, the resultant stress field is generally a superposition of three basic modes of loading. However, for the plane problem considered below (see Fig. 25(a)), this field is a linear superposition of only two modes, namely, the tensile (Mode I) and in-plane shear (Mode II)modes.

The general solution of the equilibrium equations

$$\frac{\partial \sigma_{rr}}{\partial r} + \frac{1}{r}\frac{\partial \sigma_{r\theta}}{\partial \theta} + \frac{\sigma_{rr} - \sigma_{\theta\theta}}{r} = 0, \quad \frac{\partial \sigma_{\theta r}}{\partial r} + \frac{1}{r}\frac{\partial \sigma_{\theta\theta}}{\partial \theta} + 2\frac{\sigma_{\theta r}}{r} = 0 \tag{68}$$

in the polar coordinates ($r = \sqrt{x^2 + z^2}$, $\theta = \arccos(z/\sqrt{x^2 + z^2})$) for an isotropic linearly elastic solid with self-affine crack has the form

$$\sigma_{ij} = K_{\alpha} r^{-\alpha} \phi_{ij}(\theta, \nu, D_{\mathrm{D}}), \tag{69}$$

where r is a distance from the crack tip ($i,j = r,\theta$); ν is the Poisson's ratio, D_{D} is the latent fractal dimension of crack face (see Table 12) and K_{α} is the stress intensity coefficient associated with the power-law exponent α. The latter, as well as dimensionless functions $\phi_{ij}(\theta,\nu,D_{\mathrm{D}})$, may be determined from the boundary conditions.

For a straight crack (cut) in the linear elastic solid we have a notable inverse square root ($\alpha = 0.5$) asymptotic form

$$\sigma_{ij} = \frac{K_{1/2}}{\sqrt{r}} \phi_{ij}(\theta, \nu), \tag{70}$$

where $K_{1/2}$ is a complex stress intensity factor which can be represented as a function of K_{I}, K_{II} and the crack form[228]. For a straight crack (cut) perpendicular to the direction of applied tensile stress σ_{yy}^{∞} we have $K_{1/2} = K_{\mathrm{I}}$.

Furthermore, according to the Sain Venant's principle, for any problem with smooth (differentiable) crack profile, $z(r)$, the asymptotic form eq. (70) restores at distances $r > r_{\mathrm{rmf}}$, where r_{rmf} is the rmf-saturated roughness of crack face (see eq. (51)). The validity of Sain

Venant's principle for the problems with rough, but differentiable crack in an elastic continuum can be proved rigorously (see, for example, ref. [228]). Notice that this proving requires the differentiability of crack faces and cannot be applied to problems with self-affine cracks. Furthermore, as will be shown below, in the problem with self-affine crack, the standard asymptotic form eq. (70) restores only at distances $r \gg \xi_C \gg r_{rmf}$.

The scaling properties of self-similar and self-affine patterns give rise to the advantage of using the dimensional analysis for the problems with fractal cracks.

Buckingham's Π-theorem [148] states that the dependence of a physical quantity on a set of dimensionful parameters may be expressed as the dependence of a dimensionless quantity Π on dimensionless combinations Π_0, Π_1,..., Π_n of the governing parameters:

$$\Pi = F(\Pi_0, \Pi_1, \ldots, \Pi_n). \tag{71}$$

This elementary result is the root of dimensional analysis and, as is well-known, has an extraordinary range of applications [148, 252, 253]. However, while in many cases, Buckingham's Π-theorem is sufficient for derivation of self-similar solutions, there is a large category of situations where simple dimensional analysis fails: the function F in eq. (71) is not well-defined in the limit $\Pi_0 \to 0$ [148, 252]. Instead, the following limit is well-defined:

$$\lim_{\Pi_0 \to 0} \frac{\Pi}{\Pi_0^{-\beta}} = \lim_{\Pi_0 \to 0} \Pi_0^{-\beta} F\left(\Pi_0, \frac{\Pi_1}{\Pi_0^{-\beta_1}}, \ldots, \frac{\Pi_n}{\Pi_0^{-\beta_n}}\right) \tag{72}$$

with the exponents $\beta, \beta_1, \ldots, \beta_n$ being real numbers, not determined by dimensional analysis, but determined, in principle, by the differential equation obeyed by function F. On the other hand, these exponents are nothing more than the anomalous dimensions of field theory [253] and they can be computed using the renormalization group technique [254].

From the renormalization group theory view, the crucial question to ask is: which parameters of the problem are observable under given conditions and which are not?

Among the physical quantities in the original formulation of the problem with self-affine crack the quantities σ_{yy}^{∞}, r, θ and $D_D = 1/H$ are obviously directly observable. The stresses σ_{ij} are concentrated "in every point of the non-differentiable self-affine crack face" [43] in the original formulation of the problem and over a distance ℓ in its regularized version. So, the original formulation is a degenerate limit of the regularized problem, but supposedly corresponds to the description of what we are able to observe in the experiments. In this way the stress tensor σ_{ij} has some ambiguity due to gauge invariance [255], but it is also essentially observable.

The renormalized stress intensity coefficient $K_{\alpha,\ell}$ will, in principle, depend upon the regularization ℓ. This means that as the degenerate limit $\ell \to 0$ is taken, there is nothing that guarantees that $K_{\alpha,\ell}$ and K_α will be the same and, in general, they will not be. Hence, $K_{\alpha,\ell}$ and ℓ are bare parameters of the problem, which are not accessible to our chosen level of description.

The usual hypothesis of phenomenology is that there is a closed functional relation among directly observable and phenomenological quantities and this should be true irrespective of the microscopic details. In particular, this should be true in the limit $\ell \to 0$.

In this way, the observable K_α is related to the bare $K_{\alpha,\ell}$ by the relation $K_\alpha = \eta K_{\alpha,\ell}$, where the renormalization constant η is dimensionless, but must depend upon ℓ, because $K_{\alpha,\ell}$ depends upon ℓ and K_α does not. Dimensional analysis then requires that there is another length in the problem, which we denote ξ, introduced in order to ensure that η is dimensionless. This is the length that sets the scale, in the language of statistical field theory [256] and is arbitrary. Thus, we have

$$\sigma_{ij} = \frac{\eta(\ell/\xi) K_{\alpha,\ell}}{\sqrt{r}} \Psi_{ij}\left(\frac{r}{\ell}, \theta, \nu, D_D\right) \tag{73}$$

with Ψ_{ij} being some functions to be determined. We can write this as

$$\sigma_{ij} = \frac{\eta(\ell/\xi) K_{\alpha,\ell}}{\sqrt{r}} \Phi_{ij}\left(\frac{r}{\xi}, \theta, \nu, D_D\right), \tag{74}$$

where Φ_{ij} are another functions to be determined.

In order to establish the functional form of σ_{ij}, one may draw on the Gell–Mann–Low argument [256]. Since ξ is not presented in the original specification of the problem, it should not be present in the solution of the elastic problem. Hence, we arrive at the renormalization group equation†

$$\xi \frac{\partial \sigma_{ij}}{\partial \xi} = 0 \tag{75}$$

and thus

$$R \frac{\partial \Phi_{ij}}{\partial R} - \beta \Phi_{ij} = 0, \text{ where } R = \frac{r}{\xi}, \text{ and } \beta = + \frac{\partial \ln \eta}{\partial \ln \xi}. \tag{76}$$

Solving this linear partial differential equation, we get

$$\sigma_{ij} = \frac{K_\alpha}{\sqrt{r}} \left(\frac{r}{\xi} \right)^\beta \Phi_{ij}(\theta, \nu, D_D). \tag{77}$$

Thus, we have derived the crack tip stress distribution in the same form that was postulated for a self-similar crack in ref. [5] and for self-affine crack in ref. [42].

In a spirit of renormalization group theory, the exponent β can be treated as a single valued function of the anomalous dimension $\epsilon = D_D - 1$,‡ such that

$$\beta = 0, \text{ if } \epsilon = 0, \text{ and } \beta = \frac{1}{2}, \text{ if } \epsilon = 1. \tag{78}$$

The simplest form of the function $\beta(\epsilon)$ which possesses property eq. (78) is

$$\beta = \frac{\epsilon}{2} = \frac{D_D - 1}{2}, \tag{79}$$

so that stress distribution exponent α in eq. (69) is equal to

$$\alpha = \frac{2 - D_D}{2}. \tag{80}$$

This relation coincides with the corresponding formula for the problem with self-similar crack (see eq. (60) in ref. [5]), since for self-similar fractals $D_D = D_B = D$. Furthermore, in the case of self-affine crack geometry, we can rewrite eq. (80) in the form

$$\alpha = \frac{2H - 1}{2H}, \text{ if } H > H^* = \frac{1}{2}, \text{ or } \alpha = 0, \text{ if } H < H^*, \tag{81}$$

which coincides with relations obtained in [42] on the basis of energy balance arguments (the critical roughness exponent, H^*, is defined by eq. (54)), but differs from those derived in ref. [142]. This difference results from the incorrect definition for fractal dimension governed the true crack area scaling which was used in [142].

Furthermore, it is pertinent to note, that eq. (81) differs dramatically from the formula obtained in [139] on the basis of incorrect geometric manipulations (see Sections 2.4 and 3.2 and refs [42, 144]).

The authors of [143] suggested a quite interesting model of self-similar crack§ dynamics. However, in the work [143] was assumed that crack tip field obey the classical asymptotic form eq. (70). Actually, as it was shown above, stress behavior in the vicinity of fractal crack (self-similar crack can be treated as a particular form of self-affine crack for which

†All the partial derivatives below are taken with bare parameters keep constant.
‡This statement can be proved rigorously within a framework suggested in [257].
§Note that a brittle crack face can be modeled by a self-similar fractal, because in the case of $H > H^*$ self-affine fractal displays persistence (see eq. (42) and Section 2.6).

$D_D = D_B = D_S = D$) differs from those for smooth crack. Hence, the model of ref. [143] must be corrected in this way.

Now we note that in the contrast to self-affine function eq. (31) which possesses scaling properties for all x, real crack faces possess self-affine scaling only within the interval eq. (52). As it was already noted in Sections 2.6, 3.1 and 3.2, crack advances $\Delta\ell = \ell_0$ (within the dislocation-free zone of the size $\ell_0 \sim 10^{-8} \div 10^{-6}$ m) are linear, therefore, in the nanoscale $r < \ell_0$ real crack face is characterized by $D_D = 1$ and so, the crack tip stress displays behavior eq. (70) within the dislocation free zone, as it is shown in Fig. 21(a,b). Furthermore, since in the scale eq. (51) self-affine crack is characterized by the integer global fractal dimension eq. (39), at distances $r > > \xi_C$ from the crack tip stresses also obey classical asymptotic eq. (70), but with different stress intensity factor $K_{1/2,\xi_C}$ (see Fig. 21(a,b)).

Using the scaling properties of self-affine functions and stress distribution eq. (77), it is easy to show (see also Fig. 21(a,b)) the that stress intensity factor in the macroscale, $K_{1/2,\xi_C}$, is related to the stress intensity factor in the dislocation free zone, $K_{1/2}$, as

$$K_{1/2,\xi_C} = K_{1/2}\left(\frac{\xi_C}{\ell_0}\right)^{\beta}. \tag{82}$$

Furthermore, note that in the problem under consideration $K_{1/2,\xi_C} = K_I$ (see Fig. 25(a)).

4.2. *The relation between nano- and macrofracture toughness*

If we assume that the fracture occurs when $K_{1/2}$ reaches the nanofracture threshold, K_{1c}, at the same time as $K_{1/2,\xi_C} = K_I$ reaches the macrofracture toughness K_{IC}, then from eq. (77) follows that in the case of brittle fracture

$$K_{IC} = K_c^B\left(\frac{\xi_C}{\ell_C}\right)^{\beta}, \tag{83}$$

where the exponent β is defined by eq. (79), the nanofracture toughness, K_c^B, is given by eq. (63) and ℓ_C is the Griffith's critical length (see eq. (65)).

In the case of ductile fracture ($H < H^*$), the macrofracture toughness K_{IC} relates to nanofracture toughness eq. (62) as

$$K_{IC} = K_c\sqrt{\frac{\xi_C}{\ell_0}}, \tag{84}$$

where ℓ_0 is the dislocation-free zone size eq. (62).

Note, that relations eqs (83) and (84) coincide with formulas derived in[42] by other means and agree with experimental observations[80].

Furthermore, relations eqs (83) and (84) give a way to explain the difference in the ratio of brittle to ductile fracture toughness in nano- eq. (64) and macro- eq. (66) scales (see also Fig. 23). In fact, the ratio

$$\eta_M = \sqrt{\eta_2}\left(\frac{\xi_C}{\ell_C}\right)^{\beta} \gg 1, \tag{85}$$

since $\beta = 1/2 - n > 0$ and $\xi_C \gg l_C$ while according to eq. (65) $\eta_2 \sim 1$ ($0.1 < \eta_2 < 10$).

4.3. *The asymptotic stress fields in the vicinity of self-affine crack in a power-law hardening material*

The renormalization group approach, suggested above, can be directly applied to problems with self-affine cracks in nonlinear elastic and power-law hardening materials. The constitutive equations of these materials may be represented in the unified form

$$\sigma_{ij} = C\varepsilon_{ij}^n + F_{ij}(\varepsilon_{kl}^n), \tag{86}$$

where ϵ_{ij} is the components of strain tensor, $F_{ij}(\epsilon_{kl}^n)$ is a linear function of its arguments[1]. The power law exponent $n > 1$ for a nonlinear elastic material, and $n < 1$ for a power-law hardening plastic material.

By making use of the well-known (see, for example ref.[228]) stress asymptotic form in the vicinity of the linear cut in the incompressible material possessing constitutive eq. (86), after an almost literal repetition of the derivation of eq. (77), we obtain stress distribution in the vicinity of the self-affine crack in the nonlinear elastic or power-law hardening incompressible material in the following form

$$\sigma_{ij} = \frac{K_{m-\beta}}{r^m}\left(\frac{r}{\xi}\right)^{\beta}\Phi_{ij}(\theta, \nu, D_D), \tag{87}$$

where exponent β is defined by eq. (79) and

$$m = \frac{n}{n+1}. \tag{88}$$

It is easy to see that stresses in the vicinity of the crack tip in a nonlinear elastic material ($n > 1$) are always more singular than those in a linearly elastic solid, since $m > 0.5$. Specifically, in nonlinear elastic materials even a very rough cracks with $D_D = 2$ produce stress concentration within the interval eq. (52).

The stress field behavior in a power-law hardening solid with self-affine crack is more surprising. Namely, if

$$n < \frac{D_D - 1}{3 - D_D}, \tag{89}$$

then stresses increase in a direction away from the crack tip within the interval eq. (52) as shown in Fig. 22. In this case stress distribution has a maximum at distance ξ_C from the crack tip, since stresses obey classical asymptotic form $\sigma_{ij} \sim r^{-m}$[228] for $r \gg \xi_C$. Furthermore, stresses in the zone spaced at ξ_C away from the crack tip can be larger than stresses at the crack tip. This type of stress distribution was observed by Ermishkin in experiments reviewed in ref.[211].

Obviously, in the latter case, the fracture criterion will be achieved at distance ξ_C from the crack tip and, before then, at the crack tip. Because of this, nanocracks (voids) will be borne at distances $\sim\xi_C$ away from the crack tip and the crack will grow by a notable mechanism of void coalescence (see, for example refs.[147]).

A suggested approach may be directly applied to problems with self-similar and self-affine cracks in materials with random (multifractal) microstructure. The latter may be linearly or nonlinearly elastic[9], visco-elastic[28] or of the type considered in refs[18–20].

4.4. *The concept of equivalent traction for the problems with self-affine crack*

Looking back at the problem with self-affine crack in a linear elastic solid (see Fig. 25), we note that the boundary conditions on the traction-free edges can be formulated if we model the crack profile by a nonstandard curve the standard part is a self-affine fractal, as is shown in Fig. 18. In this case, the crack tip stresses associated with nanocracks of length $\ell_s = \ell_0$ (see Section 2.3) can be represented in the following form

$$\sigma_{xx} = \frac{K_I}{\sqrt{2\pi r}}\left[\cos\frac{\theta}{2}\left(1 - \sin\frac{\theta}{2}\sin\frac{3\theta}{2}\right) - k\sin\frac{\theta}{2}\left(2 + \cos\frac{\theta}{2}\cos\frac{3\theta}{2}\right)\right],$$

$$\sigma_{yy} = \frac{K_I}{\sqrt{2\pi r}}\left[\cos\frac{\theta}{2}\left(1 + \sin\frac{\theta}{2}\sin\frac{3\theta}{2}\right) + k\cos\frac{\theta}{2}\sin\frac{\theta}{2}\cos\frac{3\theta}{2}\right],$$

$$\sigma_{zz} = \nu(\sigma_{xx} + \sigma_{yy}), \quad k = \frac{K_2}{K_I} \propto \sin\left(\frac{\pi}{2} - \psi\right), \tag{90}$$

where ν is the Poisson's ratio, K_I and K_2 are the stress intensity factors associated with nanocrack modes I and II, respectively; ψ is the angle between the stress applied at infinity and the linear nanocrack face, and θ is the the angle between the (nano) crack face and the direction of observation (see Fig. 18(a)).

Furthermore, if the principle of superposition for contributions from all parts (nanocracks) is valid, the problem under consideration can be replaced by an equivalent one: self-affine crack faces are loaded by a traction T_{ij} and stresses vanish at infinity as shown in Fig. 25(b).

Traction T_{ij} consists of the regular σ-induced traction $T(\sigma_{ii})$ and the unknown additional traction T_{ij}^{*} due to the contribution from all singular points along the crack faces. The latter (singular) term of the stress field near the self-affine crack can be represented as a sum of the contributions eq. (90) from all linear parts (nanocracks) along the crack edges (within the interval of self-affinity eq. (52)). By virtue of the fact that $\ell_s \ll \xi_C$ this sum can be replaced by the integral

$$\sigma_{ij} \propto \phi(\theta, \nu, D_D) \int_{-\xi_s}^{X} \frac{n(-x)}{|x|\sqrt{|x|}} \Theta(-x)\mathrm{d}x \propto K_{\alpha,\ell_s} X^{-\alpha}, \quad \alpha = \frac{1}{2} - \eta \tag{91}$$

where $\xi_s = \xi_C/\ell_s$, $X = r/\ell_s$, r is the distance from the crack tip and x is a dimensionless variable; $n(-x) \propto x^{\eta}$ is the number of singular points within the interval $(-x,0)$ and $\Theta(...)$ is the Heaviside unit function: $\Theta(-x) = 1$ for $x \leq 0$ and $\Theta = 0$ for $x > 0$; $\phi_{ij}(\theta,\nu,D_D)$ is the dimensionless function of θ, ν and D_D. The explicit expression for $\phi(\theta,\nu,D_D)$ depends on the specific crack geometry and may be also derived by the integration of the angular terms in eq. (90) over the nanocrack orientation distribution. The coefficient K_{α,ℓ_s} is defined in Section 4.1. Note that eq. (91) coincides with eq. (77) obtained above on the basis of the renormalization group arguments.

For the problem with a regular (smooth) crack (that is the special case of the problem under consideration) we simply have $H \equiv 1$ and $\eta = 0$, so that the singular term of an elastic field obeys the standard inverse square root asymptotic form eq. (70), while for the graph of an independent random (Wiener) process (which was used in [181] as a model of crack trajectory) $H = 1/2$ and $\eta = 1/2$, so that there is no stress field (power law) singularity, because $\alpha = 0$ ($\sigma_{ij} \propto \ln X$).

Generally, we can expect that η is a monotonically increasing function of the roughness (Hurst) exponent H, which varies from 0 to 1 [163], so that always $\eta > 0$ and $0 \leq \alpha \leq 1/2$ ($\alpha < 0$ must be excluded from the solution as physically unfeasible [228]). Hence, in the problem with a self-affine crack the asymptotic stress field near the crack tip always should be less singular than the classical asymptotic form eq. (70) for regular cracks. At the same time, at distances $r < l_C$ (i.e. within the dislocation free zone) and $r \gg \xi_C$ (i.e. when the self-affine crack can be treated as a smooth cut) the asymptotic stress field obeys the inverse square root behavior in the form eqs (70)(90) and (70), respectively (see Fig. 21).

Experimental studies have revealed that a crack propagates in an elastic solid due to the initiation of new nanocracks at its tip [181]. This initiation results in a release of elastic energy ΔU_E which provides energy for further crack development. The well-known path-independent (invariant) J integral of fracture mechanics has been related to potential-energy-release rates associated with moving or extending cracks in linear elastic solids [228].

Considering a small circular contour Γ of radius R, encompassing the crack tip (see Fig. 26 *a*), we can write the J integral as

$$J = \int_{\Gamma} \left(W_{n_i} - \sigma_{ij} n_j u_{i1}\right)\mathrm{d}s, \tag{92}$$

where s is the arc length along Γ, σ_{ij} is the stress tensor, u_i is the displacement vector, $\{n_j\}$ is the normal vector† and the strain-energy density W is a single-valued function of the strains u_{ij}.

It is well-known that this integral is path-independent for any smooth crack in an elastic solid [228, 229]. At the same time, it is easy to understand that in the case of a self-affine crack this integral is not invariant, because the number of singular points enclosed by different contours is different (see Fig. 26(b)).

Substituting eq. (91) into eq. (92) shows that within the interval eq. (52) the conventional J-integral scales as

†For the problem with a self-affine crack $\{n_j\}$ can be defined within a framework of non-standard analysis (see Section 2.3); notice that for the purpose of the present work we need to know only the change in $\{n_j\}$ along the crack trajectory.

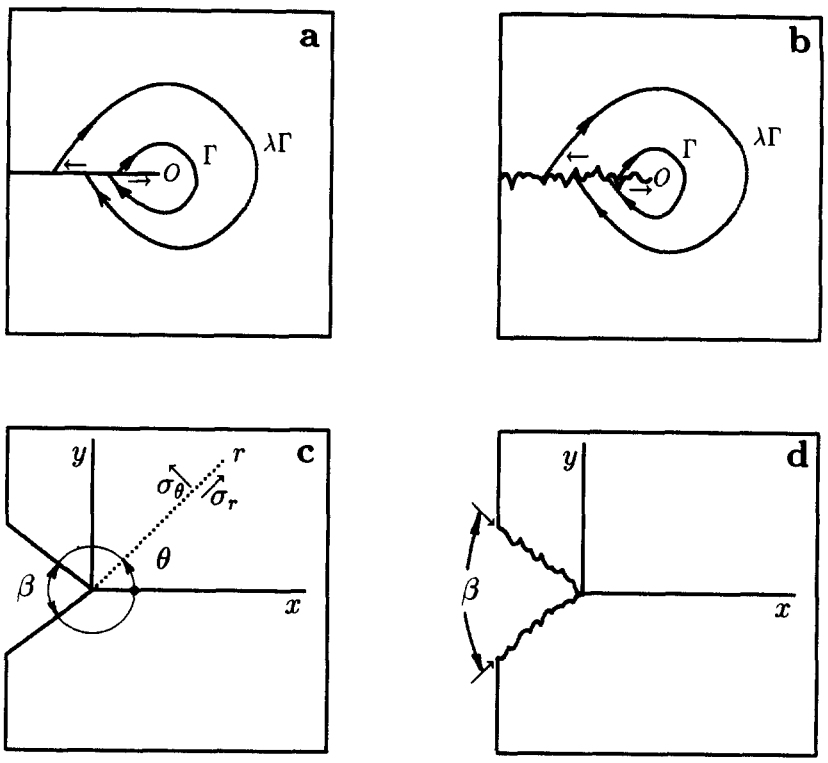

Fig. 26. Paths of J integration for (a) cracks with smooth edges, $J(\Gamma) = J(\lambda\Gamma)$; (b) with self-affine edges, $J(\Gamma) < J(\lambda\Gamma)$, but $J_f(\Gamma) = J_f(\lambda\Gamma)$; and polar stresses at a wedge-like notches (c) with smooth and (d) self-affine edges.

$$J(\lambda\Gamma) = \lambda^{1-2\alpha} J(\Gamma). \tag{93}$$

On the other hand, suppose that $\Delta U_E = J(\Delta L_x)^{d-1}$ is the energy flux at the crack tip as the true crack length (area), S_L, increases. Obviously, $\Delta U_E \propto \Delta S_L$. In the case of a self-affine crack $\Delta S_L \propto (\Delta L_x)^{D_D}$, where ΔL_x is the crack projection length and D_D is the latent fractal dimension (see Table 12) of the crack face. So, the conventional J-integral eq. (92) obeys the scaling

$$J(\lambda\Gamma) = \lambda^{D_D-(d-1)} J(\Gamma). \tag{94}$$

It immediately follows from eqs (93), (94) and (38) that if fracture is brittle, i.e. $H > H^*$, then the stress field in the vicinity of self-affine crack obey the scaling behavior eq. (91) with exponent α defined by eq. (81), whereas in the case of ductile fracture, when $H \leq H^*$ (very rough crack), stresses does not depend on r within the interval eq. (52), so that

$$\sigma_{ij}(\ell_0) = \sigma_{ij}(r) = \sigma_{ij}(\xi_C). \tag{95}$$

Thus, we have obtained the same results that those in Section 4.1, but by other means.

4.5. *Path-independent integrals for a problem with self-affine crack*

In a certain sense, a decrease of the stress singularity exponent α owing to an increase in the crack roughness is similar to a decrease of the exponents of stress field singularity in the vicinity of a wedge-like notch on account of the increase in its angle (see Fig. 26(c) and ref. [228]). Therefore, the stress intensity factor K_α and invariant integral for a self-affine crack, J_f, can also be estimated using the weight function method[258].

For a wedge-like notch with angle β (see Fig. 26(c)) the invariant integral J_β can be defined by introducing the weight function F_β obeying the scaling behavior $F_\beta = s^{-\varphi} f(\theta)$[228] and reads

$$J_\beta = \int_\Gamma \left(Wn_1 - \sigma_{ij} n_j u_{i1}\right) F_\beta\left(s^{-\varphi}, \theta\right) \mathrm{d}s, \tag{96}$$

where θ is the angular coordinate, and $\varphi = \varphi(\beta)$ is a function of notch angle.

It is important that in the case of self-affine crack the scaling behavior eq. (91) occurs only within a bounded interval eq. (52), so we can apply to the weight function F_f a scaling (incomplete self-similarity) representation (see ref.[148]):

$$F_f = s^{-\phi} f(\theta), \quad \phi = 2\eta = 1 - 2\alpha, \tag{97}$$

where α is defined by eq. (81). Now, it is easy to verify that the integral

$$J_f = \int_\Gamma \left(Wn_1 - \sigma_{ij} n_j u_{i1}\right) F_f \mathrm{d}s \tag{98}$$

with σ_{ij} and F_f given by eqs (91) and (97), respectively, does not depend on the chosen contour Γ.

This gives a reason to introduce a new micro-fracture criterion

$$J_f = J_f^C, \tag{99}$$

where the critical value J_f^C may be expressed in terms of the concept of "crack diffusion coefficient" first introduced in[181] and later generalized in[163].

4.6. *The energy release scaling*

The elastic energy release associated with self-affine crack growth may be estimated as

$$\Delta U_E \propto \int_{V_{\Delta L}} u_e(r) \mathrm{d}^d r, \tag{100}$$

where $u_e(r) \simeq \langle \sigma^2(r) \rangle / 2E$ is the mean density of the elastic energy in the unloading zone $V_{\Delta L}$ near the crack tip and E is the Young modulus[259]. After averaging the stresses eq. (91) along $\mathbf{r}$ in the unloading zone $V_{\Delta L}(\ell_0 < \Delta L_x < \xi_C)$, we find $\langle \sigma^2(r) \rangle \propto r^{-2\alpha}$, and after substitution $\langle \sigma^2 \rangle$ into eq. (100) we obtain $\Delta U_E \propto (\Delta L_x / \ell_0)^{d-2\alpha}$. So, the energy release rate $G = \Delta U_E / \Delta L_x$ scales with the increment of self-affine crack length in the direction of crack growth ΔL_x (within the interval $\ell_0 < \Delta L_x < \xi_C$) as

$$G = G^* \left(\frac{\Delta L_x}{\ell_C} \right)^\phi, \quad \phi = \frac{(d-1)(1-H)}{H}, \tag{101}$$

if fracture is brittle ($H > H^*$), or as

$$G = G^* \left(\frac{\Delta L_x}{\ell_0} \right), \tag{102}$$

if fracture is ductile ($H \leq H^*$),† while at larger scales the effective energy release rate is constant, $G = J_C$, where J_C is the critical value of the conventional J-integral eq. (92). It is precisely this macroscopic value of energy release rate J_C that is estimated in standard mechanical tests[147, 258].

The results obtained by eq. (100) are in good agreement with experimental data which were reported and analyzed in[111], as indicated by Fig. 27. Furthermore, we note that, according to relation eq. (101) we can use the Griffith's solution for brittle materials[260] in the macroscale, $\Delta L_x \gg \xi_C$, with the surface tension, γ, replaced by the effective surface energy density

$$\gamma_{\text{eff.}} = \gamma \times \left(\frac{\xi_C}{\ell_C} \right)^\phi, \tag{103}$$

where the second relation in eq. (101) may be rewritten in the form $\phi = D_D - (d-1)$ from

†In the mechanics of straight cracks $G \equiv J_C \equiv$ const![228,259].

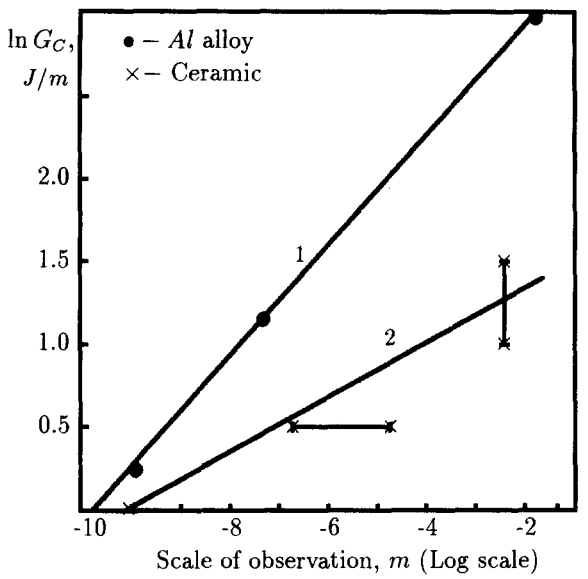

Fig. 27. Size dependence of energy release in (1) fractured aluminum alloy, and (2) alumina ceramic. Points-data of experimental observations, which were collected in Ref. [111]; solid lines-calculations by eq. (101) with $H = 0.85$ for Al alloy and $H = 0.92$ for alumina ceramic[17,33].

which immediately follows that the increase in the γ_{eff} arises from the increase in the true area (length) of crack faces. Note that, for self-similar cracks with $D_D = D_B$, relation eq. (103) coincides with the relation suggested in[109] for the effective surface energy density of monofractal cracks.

4.7. *The size dependence of "effective fracture toughness"*

Current practice for measuring fracture toughness applies predominantly bending loads to cracks in test pieces, e.g. three-point-bend, compact, disk-shaped compact and arc-shaped specimens. Further, test pieces are quite geometrically similar, with cracks penetrating about half the widths of specimens and being about equal in extent to their thicknesses (see ASTM standard E399[235]). Therefore, loading type and geometric proportions can be expected to have no affect on the measured fracture toughness K_C, which according to the classical concept should be size independent, i.e.

$$K_C(\lambda L) = K_C(L), \tag{104}$$

where L is the characteristic sample size.

Actually, however, analysis of this topic [236] shows that the experimental values of K_C obtained for the same material in different experiments vary by more than a factor of two from the lowest apparently valid values to the highest.

More recently, it was shown [237] that this difference in the fracture toughness data arises from the size dependence of the fracture toughness, because the absolute size of the test piece is not completely dictated by ASTM standards. On the basis of this analysis, the authors of[237] have concluded that the strength intensity factor cannot be used as a parameter which controls fracture.

It is easy to understand, that the aforementioned size dependence of K_C shown in Fig. 28 results from the fact that within the interval eq. (52) the concept of stress intensity factor as the coefficient in the inverse square root stress asymptotic eq. (70) cannot even be introduced, because the stress fields obey the asymptotic form eq. (91) in the case of brittle fracture, or is independent of r (within the interval eq. (52)), if fracture is ductile. So that, the toughness measurements on specimens with characteristic absolute size L which is comparable with ξ_C lead to invalid results. From eqs (70), (77) and (90) immediately follows that if $\ell_0 < L \leq \xi_C$ the "effective toughness" obtained by standard mechanical tests will possess power law behavior

$$K_C(\lambda L) = \lambda^{\beta} K_C(L) \tag{105}$$

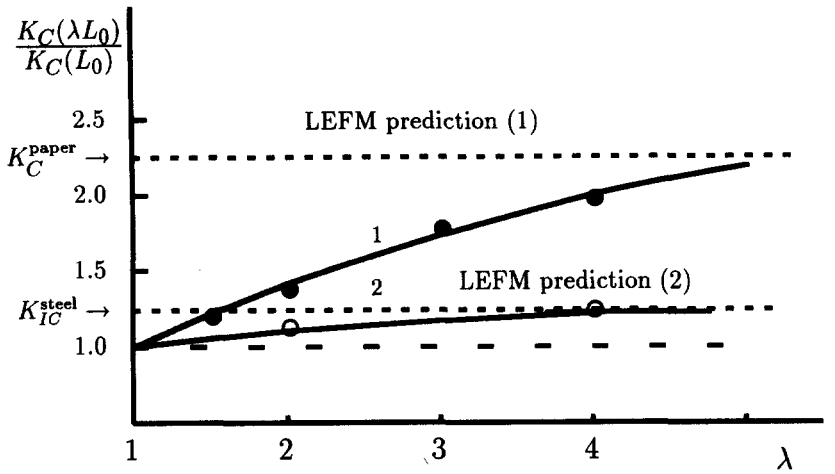

Fig. 28. Size dependence of the effective fracture toughness K_C for (1) xerox paper, and (2) *AI3I* steel at −196°C. Points—experimental data from [237]; solid lines—calculations by eq. (105) with $H = 0.67$ for paper [128] and $H = 0.88$ for steel [3]; dotted line—classical prediction of linear fracture mechanics, eq. (104). K_{IC} is the plane-strain and K_C is the plane-stress macrofracture toughness.

with β defined by eq. (79) if fracture is brittle, or universal scaling

$$K_C(\lambda L) = \sqrt{\lambda} K_C(L) \tag{106}$$

for the case of ductile fracture.

As is evident from the graphs in Fig. 28, the calculations by eq. (105) are in excellent agreement with experimental data reported in [237]. It should be emphasized, that for test pieces of size $L \gg \xi_C$, the measured toughness should be size independent. Hence, the ASTM standards should be amended to include the specification of the absolute specimen size. Such specification may be formulated on the basis of special research of this problem, which includes fractographic investigations combined with standard mechanical tests.

4.8. *Unloading from the free self-affine boundaries of an elastic solid under load*

Now, let us consider a wedge-like notch with self-affine edges (see Fig. 26(d)). Under the assumption that the weight function can be represented as the product of the F_β and F_f functions we derive the asymptotic stress field, which is produced by such a wedge-like notch, in the following form

$$\sigma_{ij} \simeq K_{nf} X^{-\alpha_n} \Phi_{ij}(\theta, \nu), \quad \alpha_n = \lambda + \frac{d-1}{2H} - \frac{d+1}{2}, \quad \ell_0 < r < \xi_C \tag{107}$$

where λ is defined by the conventional equation [228]:

$$\sin 2\lambda(\pi - \beta) = \pm\lambda \sin 2(\pi - \beta). \tag{108}$$

It is easy to see that stresses cease to be singular if $\beta \leq \beta^*$, where the critical value for the notch angle β^* is defined by the equation

$$\lambda(\beta^*) = \frac{(d+1)H - (d-1)}{2H}. \tag{109}$$

Moreover, from eqs (107)–(109) it follows that a self-affine roughness leads to unloading of an elastic material near the free boundary, $\beta = \pi/2$, i.e.

$$\sigma_{ij} \propto \left(\frac{r}{\ell_0}\right)^m, \quad 0 < m = (d-1)\frac{1-H}{2H}, \quad r < \xi_C, \tag{110}$$

if $H > H^*$, or

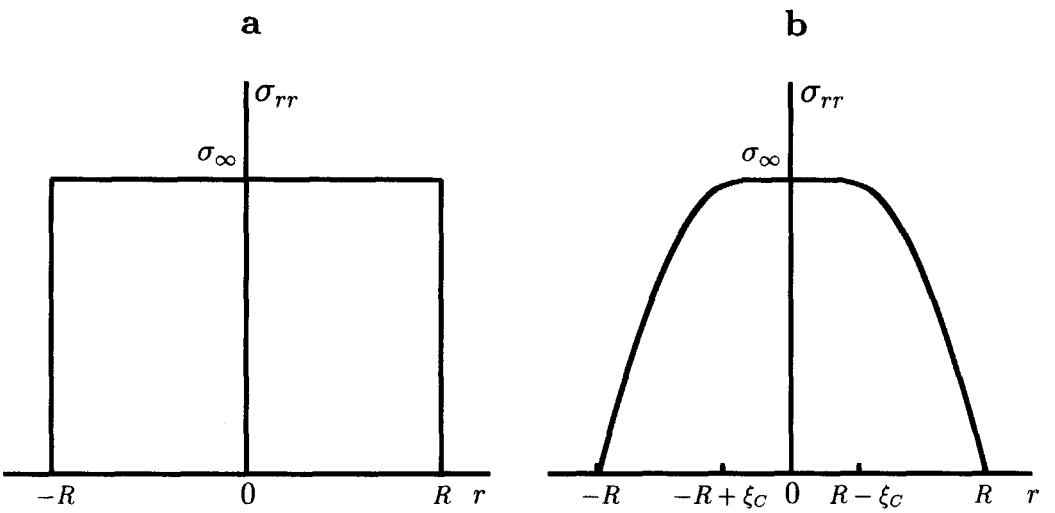

Fig. 29. Stress distribution in an elastic cylinder of radius R under longitudinal tensile load σ_∞ in the case of (a) smooth and (b) self-affine boundary surface.

$$\sigma_{ij} \propto \sqrt{\frac{r}{\ell_0}}, \quad r<\xi_C \tag{111}$$

if $H \leq H^*$. Therefore, the stress distribution in the specimen with a self-affine boundary surface has the form shown in Fig. 29(b), instead of the stress distribution in the specimen with a smooth boundary surface, which is shown in Fig. 29(a).

4.9. *Self-affine crack growth in the direction of uniaxial compression*

Experimental data provide evidence that under uniaxial compression, an elastic material can undergo a brittle fracture associated with crack propagation in the direction of compression [261–263]. In this case an elastically deformed solid separated into two or more vertical columns. At first glance, this ordinary phenomenon disagrees with the basic concepts of classical fracture mechanics.† In fact, this type of fracture could not be explained by using the conventional fracture criteria for a straight crack in a homogeneous continua. A crack orientated in the direction of uniaxial compression does not interact with a uniform stress field (there is no dependence of the energy release rate on a uniform stress applied parallel to the crack), so that a stress concentration does not arise at the crack edge, i.e. $K_{1/2} = 0$.

Now, let us cut a sample which has a uniform stress field, into two parts along a cylindrical surface with the axis oriented in the direction of compression. The stressed state in each half remains the same, as before and the sum of the energies is equal to the energy of the whole sample. Thus, if the crack propagation is rectilinear, the energy necessary to form new (fracture) surfaces is not released. Therefore, new approaches have to be developed to deal with it.

The compressive description and quantitative estimation of fragmentation for brittle materials caused by uniaxial compression is a challenging topic that mechanic researchers have faced for some time. Various suggestions have been published to resolve this paradox. For example, Obert [263] developed a fracture model that is based upon compression of a stack of blocks (grains). Compression in this case gives rise to lateral bursting forces that break transverse bonds. Guz [264] suggested a new criterion for tensile fracture (along a crack), based on the concept of a local surface loss of stability. It proposes that the quantitative fracture criterion is not the stress intensity coefficient but the value of the critical load corresponding to the local crack stability loss, as estimated by using the three-dimensional, linearized, elastic stability theory. However, in their experiments Pisarenko *et al.* [265] determined that the shape of the crack at its edge corresponds to a non-zero stress intensity factor, $K_{1/2} > 0$.

†For this reason this phenomenon is not considered in many textbooks of fracture mechanics (see, for example, ref. [259]).

Various methods have been proposed on the basis of allowance for possible inhomogeneities in the structure of the material and/or in the stress field [266, 267]. In fact, the columnar fracture may be caused by the initial inhomogeneties in solids, however, experiments [265] provide that at least in some cases it is inadequate to appeal to initial defects.

It was noted [23, 268] that a macroscopically rectilinear crack propagation along the line of compression is also possible without the influence of initial inhomogeneties. For this to occur, the macroscopically rectilinear crack at the "micro level" must propagate along a curvilinear trajectory, oscillating about a straight line. In the previous section it was shown that a self-affine geometry of the macroscopically linear boundaries leads to unloading from them. Hence, if a self-affine crack propagates along the compression lines, the elastic energy can be released due to unloading from the crack faces.

In the case of self-affine geometry of the crack faces it is easy to show (see Sections 4.5 and 4.6) that the energy release scales as

$$\Delta U_{\mathrm{E}} \propto \frac{p^2 \ell_0^d}{[(d-1)-2\alpha_{\|}]}\left(\frac{\Delta L}{\ell_0}\right)^{(d-1)+[(d-1)-2\alpha_{\|}]H}, \tag{112}$$

where $\alpha_{\|}$ is the stress asymptotic exponent for the problem with a self-affine crack with a mean plane parallel to the direction of uniaxial compression $\sigma_{11} = p$.

From (eqs (12) and (103) we obtain an expression for the asymptotic stress fields near ($\ell_0 < r < \xi_{\mathrm{C}}$) the tip of a self-affine crack in the following form

$$\sigma_{ij}(r) \propto p\sqrt{D_{\mathrm{D}} - (d-1)}\left(\frac{r}{\ell_0}\right)^{-\alpha_{\|}}, \quad \alpha_{\|} = \frac{(d-1)(H^2+H-1)}{2H^2}. \tag{113}$$

The crack can grow in the direction of compression only when stresses have a singularity at the crack tip, i.e. if $\alpha_{\|} > 0$; so that a self-affine crack can grow in the direction of uniaxial compression if

$$1 > H > H_* = \frac{\sqrt{5}-1}{2} = \Phi^*. \tag{114}$$

It is interesting to note, that in this case the critical value for the roughness (Hurst) exponent H_* coincides with the golden mean Φ^* for both two and tree dimensional problems. Note, that for two-dimensional problem $H_* > H^* = 1/2$, while for three-dimensional problems $H_* < H^* = 2/3$.

5. CONCLUSIONS

Full scale material behavior and failure can only be predicted if the fractal properties of failure patterns are taken into account. Adequate modeling of crack face topography gives a way to describe fracture phenomena in one scale using the corresponding data for another scale. Moreover, some phenomena associated with macro-crack propagation can be understand only on the basis of fractal models for crack roughness. It is important that mechanics of self-affine cracks allow a sufficiently rigorous mathematical formulation that meet requirements adopted in classical solid mechanics. Moreover, the conventional linear fracture mechanics may be treated as a special case of self-affine crack mechanics and may be used only in length scales larger than the correlation length of crack patterns. In this way, it is shown that the ASTM standards for test pieces for fracture toughness measurements must be completed by the specification of absolute specimen size, which should be larger than the self-affine correlation length for the fracture surface roughness.

Acknowledgements—This work was partially supported by SNI (Sistema Nacional de Investigadores) Mexico. The authors are grateful to G. Cherepanov, E. Ermishkin and V. Ivanova for useful discussions. The courtesy and support of the staff and faculty of the Materials Research Center at the Monterrey University of Technology, and especially the Chairperson Armando Bravo, are gratefully acknowledged.

REFERENCES

1. Balankin, A. S., *Synergetics of Deformed Solid*, Department of Defense USSR Press, Moscow, 1991 (in Russian).
2. Cherepanov, G. P., Balankin, A. S. and Ivanova, V. S., Fractals and fracture. In *Fracture: A Topical Encyclopedia of Current Knowledge Dedicated to Alan Arnold Griffith*, ed. G.P. Cherepanov. Krieger, Melbourne, 1997.
3. Ivanova, V. S., Balankin, A. S., Bunin, I. J. and Oksogoev, A. A., *Synergetics and Fractals in Materials Science*. Nauka, Moscow, 1994 (in Russian); English version will be published by Gordon and Beach in 1997.
4. Sadovskii, M. A. and Pisarenko, V. F., *Seismic Process in Bloc Medium*. Nauka, Moscow, 1991 (in Russian).
5. Cherepanov, G. P., Balankin, A. S. and Ivanova, V. S., Fractal fracture mechanics—a review. *Engineering Fracture Mechanics*, 1995, **51,** 997–1033.
6. Balankin, A. S., Quantum-statistical approach to the synergetics of deformed media. *Soviet Technical Physics Letters*, 1991, **17,** 531–533.
7. Balankin, A. S., Izotov, A. and Lazarev, V., Synergetics and fractal thermomechanics of inorganic materials I: thermomechanics of multifractals. *Inorganic Materials*, 1993, **29,** 375–381.
8. Izotov, A. D., Balankin, A. S. and Lazarev, V. D., Synergetics and fractal thermomechanics of inorganic materials, II: fractal geometry of fracture in solids. *Inorganic Materials*, 1993, **29,** 883–893.
9. Lazarev, V. D., Balankin, A. S. and Izotov, A. D., Synergetics and fractal thermomechanics of inorganic materials, III: fractal thermomechanics of fracture in solids. *Inorganic Materials*, 1993, **29,** 1027–1045.
10. Lazarev, V. B., Balankin, A. S., Izotov, A. D. and Kozhushko, A. A., *Structure Stability and Dynamical Strength of Inorganic Materials*. Nauka, Moscow, 1993 (in Russian).
11. Balankin, A. S., Quantum-statistical approach to dynamic problems of solid mechanics. *Revista Mexicana de Física*, 1995, **41,** 147–180.
12. Balankin, A. S. and Izotov, A. D., Ultimate strength and brittleness of crystal solids. *Revista Mexicana de Física*, 1995, **41,** 783–790.
13. Balankin, A. S., Synergetics and the mechanics of a deformed solid. *Soviet Technical Physics Letters*, 1990, **15,** 878–881.
14. Balankin, A. S., Extremal technologies of material treatments. *News of Science and Technic, Ser.: New Materials and Technologies of Their Creation and Treatment*, N5. Academy of Science USSR Press, Moscow, 1991, pp. 1–66 (in Russian).
15. Ivanova, V. S., Balankin, A. S., Ermishkin, V., Kovneristyi, Y. and Tamayo, P., The fractal geometry of amorphous structures and the synergetics of vitrification of metallic alloys. *Soviet Physics Doklady*, 1993, **37,** 222–224.
16. Meakin, P., Models for materials failure and deformation. *Science*, 1991, **252,** 226–234.
17. Balankin, A. S. and Tamayo, P., Fractal solid mechanics. *Revista Mexicana de Física*, 1994, **40,** 506–532.
18. Balankin, A. S., The concept of multifractal elasticity. *Physics Letters A*, 1996, **210,** 51–59.
19. Balankin, A. S., Elastic behavior of materials with multifractal structures. *Physics Review B*, 1996, **53,** 5438–5443.
20. Balankin, A. S., The theory of multifractal elasticity: basic laws and constitutive equations. *Revista Mexicana de Física*, 1996, **42,** 307–317.
21. Balankin, A. S., Fractal dynamics of deformed media. *Soviet Technical Physics Letters*, 1991, **17,** 229–231.
22. Balankin, A. S. and Ivanova, V. S., Micro-, meso- and macrokinetics of self-similar crack growth. *Soviet Technical Physics Letters*, 1991, **17,** 12–14.
23. Balankin, A. S., Elastic properties of fractals, transverse deformation effect, and dynamic of free solid fracture. *Doklady Academy of Science, USSR*, 1991, **319,** 1098–1101.
24. Balankin, A. S., Fractal dynamics of fracture. *Soviet Technical Physics Letters*, 1991, **17,** 391–393.
25. Balankin, A. S. and Bugrimov, A. L., Fractal dimensions of cracks formed during brittle fracture of model lattices and solids. *Soviet Technical Physics Letters*, 1991, **17,** 630–632.
26. Balankin, A. S. and Yanevich, G. N., Ergodynamics of impact cratering and principles of simulation of an impact. *Soviet Technical Physics Letters*, 1991, **17,** 236–238.
27. Balankin, A. S., Theory of elasticity and entropic high-elasticity of fractals. *Soviet Technical Physics Letters*, 1991, **17,** 632–634.
28. Balankin, A. S. and Bugrimov, A. L., A fractal theory of polymer plasticity. *Polymer Science*, 1992, **34,** 246–248.
29. Balankin, A. S. and Bugrimov, A. L., Fractal theory of elasticity and rubber elasticity of polymers. *Polymer Science*, 1992, **34,** 889–891.
30. Balankin, A. S., Fractal dynamics of solids. *News of the Academy of Science Russia, Series: Metals*, 1992, **N2,** 41–51 (in Russian).
31. Balankin, A. S., Fractal mechanics of deformed media and the topology of fracture in solids. *Doklady Academy of Science, USSR*, 1992, **322,** 869–874 (in Russian).
32. Balankin, A. S. and Bugrimov, A. L., Fractals in mechanics of deformed body. *Abstracts of the XXVIII International Congress Theoretical and Applied Mechanics*, Haifa, Israel, 22–28 August 1992, IUTAM, Hifa, 1992, p. 17.
33. Balankin, A. S. and Tamayo, P., Fractal geometry and multifractal analysis in the science of materials. *Proceedings of the International Congress IBEROMET—2*, Vol. 2, Mexico, 8–14 November 1992, Harry Mazal, Mexico, 1992, pp. 570–583.
34. Balankin, A. S., Elastic properties of fractals and dynamics of brittle fracture of solids. *Soviet Physics of Solid State*, 1992, **34,** 658–665.
35. Balankin, A. S., Ivanova, V. S. and Breusov, V. P., Collective effects in the kinetics of metal fracture and spontaneous change in the fractal dimensionality of dissipative structure during the ductile to brittle transition. *Soviet Physics Doklady*, 1992, **37,** 105–108.
36. Balankin, A. S., Ivanova, V. S., Kolesnikov, A. A. and Saviskaya, E. E., Fractal kinetics of self-organization of dissipative structures in the process of mechanical alloying in attritors. *Soviet Technical Physics Letters*, 1992, **17,** 504–505.
37. Balankin, A. S., Theory of elasticity of fractals and model of nonlinear elasticity, high elasticity and fracture of materials with multifractal structure. *Soviet Physics Doklady*, 1993, **37,** 379–382.
38. Balankin, A. S., Bugrimov, A. L., Kozlov, G. V. and Mikitaev, A. K., The fractal structure and physicochemical properties of amorphous glass polymers. *Doklady Academy of Science, Russia*, 1992, **326,** 463–466 (in Russian).

39. Balankin, A. S., Thermodynamics and mechanics of materials with multifractal microstructure. *Abstracts of the CAM 94, Physics Meeting*, 26–30 September 1994, Cancun, Mexico, 1994, p. 74.
40. Balankin, A. S. and Bravo, A., New approach to percolation theory and its application for fluid percolation problems. *Abstracts of the CAM 94, Physics Meeting*, 26–30 September 1994, Cancun, Mexico, 1994, p. 32.
41. Balankin, A. S., Mechanics of self-affine cracks. *Abstracts of the XXXVIII Congreso National de Física*, 20–24 October, Zacatecas, Mexico, 1995, p. 120.
42. Balankin, A. S., Mechanics of self-affine cracks. *Revista Mexicana de Física*, 1995, **41,** 473–479.
43. Balankin, A. S., Mechanics of self-affine cracks: the concept of equivalent traction, path integrals and energy release rate. *Revista Mexicana de Física*, 1996, **42,** 147–157.
44. Balankin, A. S. and Bravo, A., Diseño de nuevos y avanzados materiales empleando una nueva teoria de mecanica multifractal del solido. *Transferencia*, 1997, **38,** 18–20 (in Spanish).
45. Balankin, A. S., Cherepanov, G. P. and Garcia, V. J., Mechanics of self-affine cracks: the physics and mechanics of manofracture. *Revista Mexicana de Física*, 1997 (in press).
46. Balankin, A. S. and Susarey, O., Statistical topography of the set of admissible crack paths in a brittle solid. *International Journal of Fracture*, 1996, **81,** R27–R32.
47. Balankin, A. S. and Cherepanov, G. P., Mechanics of self-affine cracks: interface crack growth. *Revista Mexicana de Física*, 1997 (in press).
48. Balankin, A. S. and Bravo, A., Fractal concepts for solid mechanics. In *Proceedings of the I IUTAM Symposium on Micromechanics of Plasticity and Damage of Multiphase Materials*, 29 August to 1 September 1995, Paris, France, ed. A. Pineau and A. Zaoui. Kluver, Paris, 1996, pp. 339–346.
49. Balankin, A. S. and Bravo, A., Diseño de nuevos y avanzados materiales empleando una nueva teoría de mecánica multifractal del sólido. *Proc. XXVI Reunión de Investigación y Desarrollo Tecnológico del Sistema*, Vol. 2, ITESM, Monterrey, 1996, pp. 341–350.
50. Balankin, A. S. and Bravo, A., Effect of the deformation-produced anisotropy on elastic response of cracked solids. *Proc. International Materials Research Congress*, Cancun, 1–4 September 1996, Mexico, Academia Mexicana de Materiales, 1996, p. 37.
51. Balankin, A. S., Nonlinear mechanics of self-affine cracks. *Proceedings of the XXXIX Congress Nacional de Física*, 14–18 October 1996, Oxaca, México, UNAM, 1996.
52. Balankin, A. S., Models of self-affine cracks in brittle and ductile solids. *Philosophical Magazine Letters*, 1996, **74,** 415–422.
53. Balankin, A. S., Mechanics of self-affine cracks in embrittled paper sheets. *Proceedings of the International Materials Research Congress*, 1–5 September 1996, Cancun, Mexico, Peer S.A. de C.V., Mexico, 1996.
54. Balankin, A. S., Physicsics of nanofracture and mechanics of self-affine cracks. *Pre-print of the presentation of the 1st European Mechanics of Materials Conference, EUROMECH-MECAMAT '96: Local Approach to Fracture*, 9–11 September 1996, Fontainebleau, France. Kluver, Paris, 1996.
55. Balankin, A. S., The effect of fracture surface morphology on the crack mechanics in a brittle material. *International Journal of Fracture*, 1996, **76**(4), R63–R70.
56. Kleiser, T. and Bocek, M., The fractal nature of slip in crystals. *Zeitschrift Metallika*, 1986, **77,** 582–587.
57. Morgenstern, O., Sokolov, I. M. and Blumen, A., Statistical model for surface fracture. *Europhysics Letters*, 1993, **22,** 487–492.
58. Poliakov, A. B., Herrmann, H. J., Podladchikov, Y. Y. and Roux, S., Fractal plastic shear bands. *Fractals*, 1994, **2,** 567–581.
59. Carpinteri, A., Fractal nature of material microstructure and size effects on apparent mechanical properties. *Mechanics Materials*, 1994, **18,** 89–101.
60. Xie, H. and Sanderson, D. J., Fractal kinematics of crack propagation in geomaterials. *Engineering Fracture Mechanics*, 1995, **50,** 529–536.
61. Underwood, E. E. and Banerji, K., Fractals in fractography. *Materials Science and Engineering*, 1986, **80,** 1–14.
62. Underwood, E. E. and Banerji, K. K., Fractal analysis of fracture surfaces. In *Metals Handbook*, Vol. 12. Fractography, ASM, New York, 1992, pp. 211–215.
63. Ivanova, V. S. and Shanyavsky, A. A., *Quantitative Fractography*. Metallurgya, Cheliabinsk, 1988, (in Russian).
64. Meakin, P., The growth of rough surfaces and interfaces. *Physics Report*, 1993, **235,** 189–289.
65. Nowicki, B.. *Wear*, 1985, **102,** 161–182.
66. Balankin, A. S. and Sandoval, F., Self-affine properties of fracture surfaces. *Revista Mexicana de Física*, 1997, **43,** 483–502.
67. Ziman, J. M., *Models of Disorder*. Cambridge University, New York, 1979.
68. Adler, R. J., *The Geometry of Random Fields*. Wiley, New York, 1981.
69. Mandelbrot, B. B., *The Fractal Geometry of Nature*. Freeman, New York, 1984.
70. Mandelbrot, B. B., Passoja, D. E. and Paullay, A. J., Fractal character of fracture surfaces in metals. *Nature*, 1984, **308,** 721–722.
71. Allégre, C. J., LeMouel, J. L. and Provost, A., Scaling rules in rock fracture and possible implications for earthquake prediction. *Nature*, 1982, **297,** 47–49.
72. Matsushita, M., Fractal viewpoint of fracture and accretion. *Journal of the Physics Society of Japan*, 1985, **54,** 857–860.
73. Turcotte, D. L., Fractals and fragmentation. *Journal of Geophysics Research*, 1986, **91,** 1926–1931.
74. Pande, C. S., Smith, S. and Richards, L. E., Fractal characteristics of fractured surfaces. *Journal of Material Science Letters*, 1987, **6,** 295–297.
75. Brown, S. R., A note on the description of surface roughness using fractal dimension. *Geophysics Research*, 1987, **92,** 331–344.
76. Wang, J. S. Y., Narasimhan, T. N. and Scholz, C. H., Aperture correlations of a fractal fracture. *Journal of Geophysics Research*, 1988, **93,** 2216–2224.
77. Mecholsky, J. J., Passoja, D. E. and Feinberg-Ringel, K. S., Quantitative analysis of brittle fracture surface using fractal geometry. *Journal of the American Ceramics Society*, 1989, **72,** 60–75.
78. Richards, L. E. and Dempsey, B. D., Fractal characterization of fractured surfaces. *Scripta Metallica*, 1988, **22,** 687–689.

79. Mecholsky, J. J. and Mackin, T. J., Fractal analysis of fracture in Ocala chert. *Journal of Material Science Letters*, 1988, **7**, 1145–1147.
80. Wang, Z. G., Chen, D. L., Jiang, X. X., Ai, S. H. and Shih, C. H., Relationships between fractal dimension and fatigue threshold value in dual-phase steels. *Scripta Metallica*, 1988, **22**, 827–832.
81. Mu, Z. Q. and Lung, C. W., Studies on the fractal dimension and fracture toughness of steel. *Journal Physics D: Applied Physics*, 1988, **21**, 848–851.
82. Pointe, P. R., A method to characterize fracture density and connectivity through fractal geometry. *International Journal of Rock Mechanics, Mineral Science & Geomechanics Abstracts*, 1988, **25**, 421–429.
83. Norton, D. and Sorenson, S., Variations in geometric measures of topographic surface underlain by fractured granitic plutons. *Pure and Applied Geophysics*, 1989, **131**, 77–97.
84. Hirata, T., Fractal dimension of fault systems in Japan, fractal structure in rock fracture geometry at various scales. *Pure and Applied Geophysics*, 1989, **131**, 157–170.
85. *Statistical Models for the fracture of Disordered Media*, ed. H. J. Hermann and S. Rox. North Holland, Amsterdam, 1990.
86. Rough, S., Schmittbuhl, J., Vilotte, J. P. and Hansen, A., Some physical properties of self-affine rough surfaces. *Europhysics Letters*, 1993, **23**, 277–282.
87. Hornborgen, E., Fractals in microstructure of metals. *International Material Review*, 1984, **34**, 277–296.
88. Lu, S. Z. and Hellawel, A., An application of fractal geometry to complex microstructures: numerical characterization of graphite in cast irons. *Acta Metallica Material*, 1994, **42**, 4035–4047.
89. Dobrescu, G., Rusu, M. and Vass, M., Computer simulations of fractal surfaces: application in adsorption. *Fractals*, 1993, **1**, 430–438.
90. Schmittbuhl, J., Roux, S. and Berthaud, Y., Development of roughness in crack propagation. *Europhysics Letters*, 1994, **28**, 585–590.
91. Silberschmidt, V. V., On the multifractal character of load distribution near the cracks. *Europhysics Letters*, 1993, **23**, 593–598.
92. Caldarelli, G., Castellano, C. and Vespignani, A., Fractal and topological properties of directed fractures. *Physics Review E*, 1994, **49**, 2673–2679.
93. Williford, R. E., Multifractal fracture. *Scripta Metallica*, 1988, **22**, 1749–1754.
94. Anderson, T. L., Application of fractal geometry to damage development and brittle fracture in materials. *Scripta Metallica*, 1989, **23**, 97–102.
95. Heping, X., The fractal effect of irregularity of crack branching on the fracture toughness of brittle materials. *International Journal of Fracture*, 1989, **41**, 267–274.
96. Krivobodrov, V. S., Diffusion equation for crack growth in solids. *Philosophical Magazine Letters*, 1990, **61**, 1–4.
97. Lu, Ch. and Xie, H., A physical limit of Weibull modulus in rock fracture. *International Journal of Fracture*, 1995, **72**, R55–R58.
98. Fidlin, A. Y., Calculation of the fractal crack surface properties in the analysis of the brittle fraction in mining rock. *Soviet Physics Doklady*, 1992, **37**, 473–474.
99. Nagahama, H. and Yoshii, K., Fractal dimension and fracture of brittle rocks. *International Journal of Rock Mechanics, Mineral Science & Geomechanics, Abstracts*, 1993, **30**, 173–175.
100. Carpinteri, A., Scaling laws and renormalization groups for strength and toughness of disordered materials. *International Journal of Solids and Structures*, 1994, **31**, 291–302.
101. Boadu, F. K. and Long, L. T., The fractal character of fracture spacing and RQD. *International Journal of Rock Mechanics, Mineral Science & Geomechanics, Abstracts*, 1994, **32**, 127–134.
102. Dossou, F. and Gauvin, R., The correlation between the fractal dimension of fractured surfaces and mechanical properties of $6061/Al_2O_3/10–20\%_p$. *Fractals*, 1994, **2**, 249–252.
103. Ochiai, M., Ozao, R., Yamazaki, Y. and Holz, A., Self-similarity law of particle size distribution and energy law in size reduction of solids. *Physica*, 1992, **A 191**, 295–300.
104. Zhang, S. and Lung, C., Fractal dimension and fracture toughness. *Journal of Physics D: Applied Physics*, 1989, **22**, 790–793.
105. Lung, C. W. and Zhang, S. Z., Fractal dimension of the fractured surface of materials. *Physica*, 1989, **D 38**, 242–245.
106. Power, W. L. and Tullis, T. E., Euclidean and fractal models for the description of rock surface roughness. *Journal of Geophysics Research*, 1991, **96**, 424–451.
107. McAnulty, P., Meisel, L. V. and Cote, P. J., Hyperbolic distributions and fractal character of fracture surfaces. *Physics Review*, 1992, **A 46**, 3523–3526.
108. Khvorov, M. M. and Nigmatulin, R. R.. *Soviet Physics of Solid State*, 1990, **38**, 1334–2332.
109. Pokropivnyi, V. V. and Skorohod, V. V., Fractal correction to the tensile strength and fracture toughness of brittle solids taking into account the atomic roughness of the breaking surface. *Physics of Solid State*, 1995, **37**, 664–665.
110. Palmer, A. C. and Sanderson, T. J. O., Fractal crushing of ice and brittle solids. *Proceedings of the Royal Society of London*, 1991, **A 433**, 469–477.
111. Rosenfield, A. R., Fractal mechanics. *Scripta Metallica*, 1987, **21**, 1359–1361.
112. Williford, R. E., Fractal fatigue. *Scripta Metallica Material*, 1990, **24**, 455–460.
113. Dauskardt, R. H., Haubensak, F. and Ritchie, R. O., On the interpretation of the fractal character of fracture surfaces. *Acta Metallica Material*, 1990, **38**, 143–159.
114. Brown, S. R. and Scholz, C. H., Broad band width study of the topography of natural rock surfaces. *Journal of Geophysics Research*, 1985, **90**, 12575–12582.
115. Avnir, D., Farin, D. and Pfeifer, P., Surface geometric irregularity of particulate materials: the fractal approach. *Journal Colloid and Interface Science*, 1985, **103**, 112–123.
116. Cox, B. L. and Wang, J. S. Y., Fractal analyses of anisotropic fracture surfaces. *Fractals*, 1993, **1**, 547–559.
117. Beghdadi, A., Andraud, C., Lafait, J., Peiro, J. and Perreau, M., Entropic and multi-fractal analysis of disordered morphologies. *Fractals*, 1993, **1**, 671–679.
118. Pande, C. S., Richards, L. E., Louat, N., Dempsey, B. D. and Schwoeble, A. J., Fractal characterization of fractured surfaces. *Acta Metallica*, 1987, **35**, 1633–1637.

119. Malygin, G. A., Kinetic mechanism of the formation of defectless channels upon plastic deformation of irradiated and quenched crystals. *Soviet Physics Solid State*, 1991, **33,** 1069–1076.
120. Imre, A., Pajkossy, T. and Nyikos, L., Electrochemical determination of the fractal dimension of fractured surfaces. *Acta Metallica Material*, 1992, **40,** 1819–1826.
121. Bouchaud, E. and Navéos, S., From quasi-static to rapid fracture. *Journal Physics I France*, 1995, **5,** 547–554.
122. Greis, N. P. and Greenside, H. S., Implication of a power-law power-spectrum for self-affinity. *Physics Review*, 1991, **A 44,** 2324–2334.
123. Barabási, A. L. and Vicsek, T., Multifractality of self-affine fractals. *Physics Review*, 1991, **A 44,** 2730–2733.
124. Barabási, A. L., Szépfalusy, P. and Vicsek, T., Multifractal spectra of multi-affine functions. *Physica*, 1991, **A 178,** 17–28.
125. Barabási, A. L., Bourbonnais, R., Jensen, M., Kertész, J., Vicsek, T. and Zhang, Y. Ch., Multifractality of growing surfaces. *Physics Review*, 1992, **A 45,** R6951–R6954.
126. Isichenko, M. B. and Kalda, J., Statistical topography. I: fractal dimension of coastlines and number-area rule for islands. *Journal of Nonlinear Science*, 1991, **1,** 255–263.
127. Feder, J., *Fractals*. Plenum Press, New York, 1988.
128. Kertész, J., Horváth, V. K. and Weber, F., Self-affine rupture lines in paper sheets. *Fractals*, 1993, **1,** 67–74.
129. Bouchaud, E., Lapasset, G., Planés, J. and Naveos, S., Statistics of branched fracture surfaces. *Physics Review*, 1993, **B 48,** 2917–2928.
130. Balankin, A. S., Fractal mathematics for physicists: 1. Basic concepts, physical notions and mathematical tools. *Revista Mexicana de Física*, 1997 (in press).
131. Huang, Z. H., Tian, J. F. and Wang, Z. G., A study of the slit island analysis as a method for measuring fractal dimension of fractured surface. *Scripta Metallica Material*, 1990, **24,** 967–972.
132. Måløy, K. J., Hansen, A., Hinrichsen, E. L. and Rough, S., Experimental measurements of the roughness of brittle cracks. *Physics Review Letters*, 1992, **68,** 213–215.
133. Cox, B. L. and Wang, J. S., Fractal surfaces: measurement and applications in the earth sciences. *Fractals*, 1993, **1,** 87–115.
134. Neimark, A., A new approach to the determination of the surface fractal dimension of porous solids. *Physica*, 1992, **A 191,** 258–262.
135. Kyriacos, S., Buczkowski, S., Nekka, F. and Cartilier, L., A modified box-counting method. *Fractals*, 1994, **2,** 321–324.
136. Nikora, V. I., Nikora, O. I., Noever, D. A. and Smart, G. M., New method of structural functions for analysis fractal scaling properties of natural processes. *Journal of Physics A: Mathematics General*, 1994, **27,** L403–L409.
137. Balankin, A. S., Fractal Mathematics for physicists: 2. Experimental methods of fractal measurement. *Revista Mexicana de Física*, 1997 (in preparation).
138. Jiang, X. G., Chu, W. Y. and Hsiao, C. M., Relationship between J_{IC} and fractal value of fracture surface of ductile materials. *Acta Metallica Material*, 1994, **42,** 105–108.
139. Bouchaud, E. and Bouchaud, J. P., Fracture surfaces: apparent roughness, relevant length scales and fracture toughness. *Physics Review*, 1994, **B 50,** 17752–17755.
140. Ley, W. and Chen, B., Fractal characterization of some fracture phenomena. *Engineering Fracture Mechanics*, 1995, **50,** 149–155.
141. Juang, X. G., Chu, W. Y. and Xiao, J. M., Fractal analysis of orientation effect on K_{IC} and K_{Isec}. *Engineering Fracture Mechanics*, 1995, **51,** 805–808.
142. Mosolov, A., Mechanics of fractal cracks in brittle solids. *Europhysics Letters*, 1993, **24,** 637–678.
143. Xie, H. and Sanderson, D. J., Fractal effects of crack propagation on dynamic stress intensity factors and crack velocities. *International Journal of Fracture*, 1995, **74,** 29–42.
144. Balankin, A. S., Bravo, A., Galicia, M. A. and Susarey, O., Mecánica de las grietas auto-afines en hojas de papel fragilizado. *Proc. XXVII Reunion de Investigacion y Desarrollo Tecnologico del Sistema*, Vol. 2, ITESM, Monterrey, 1997, pp. 163–171.
145. *Fractals: Non-Integral Dimensions and Applications*, ed. G. Cherbit. Wiley, New York, 1987.
146. Empiricus, S., *Against the Physicists*, trans. W.G. Bury. Harvard University Press, Harvard, 1936.
147. Hertzberg, R. W., *Deformation and Fracture Mechanics of Engineering Materials*. Wiley, New York, 1989.
148. Barenblatt, G. I., *Similarity, Self-Similarity and Intermediate Asymptotics*. Consultant Bureau, New York, 1979.
149. Nottale, L. and Schneider, J., Fractals and nonstandard analysis. *Journal of Mathematics and Physics*, 1984, **25,** 1296–1300.
150. Falkoner, K., *Fractal Geometry: Mathematical Foundations and Applications*. Wiley, New York, 1990.
151. Streitenberg, P., Förster, D., Kolbe, G. and Veit, P., The fractal geometry of grain boundaries in deformed and recovered zinc. *Scripta Metallica Material*, 1995, **33,** 541–546.
152. Feder, J., *Physica*, 1989, **D 38,** 104–111.
153. Mandelbrot, B. B., Self-affine fractal sets, I: the basic fractal dimensions. In *Fractals in Physics*, ed. L. Pietronero and E. Tosatti. Elsevier, New York, 1986, pp. 3–16.
154. Mandelbrot, B. B., Self-affine fractal sets, II: length and surface dimensions. In *Fractals in Physics*, ed. L. Pietronero and E. Tosatti. Elsevier, New York, 1986, pp. 17–20.
155. Mandelbrot, B. B., Self-affine fractal sets, III: Hausdorff dimension anomalies and their implications. In *Fractals in Physics*, ed. L. Pietronero and E. Tosatti. Elsevier, New York, 1986, pp. 21–28.
156. *Fractals in Science*, ed. A. Bunde and Sh. Havlin. Springer, New York, 1994.
157. Matsushita, M. and Ouchi, S., On the self-affinity of various curves. *Physica*, 1989, **D 38,** 246–251.
158. Voss, R. F., Random fractals: characterization and measurement. In *Scaling Phenomena in Disordered Systems*, ed. R. Punn and A. Skjeltorp. Plenum, New York, 1985, pp. 1–11.
159. Matsushita, M., Ouchi, S. and Honda, K., On the fractal structure and statistics of contour lines on a self-affine surface. *Journal of the Physics Society of Japan*, 1991, **60,** 2109–2112.
160. Moreira, J. G., Silva, J. K. L. and Kamphorst, S. O., On the fractal dimension of self-affine profiles. *Journal of Physics A: Mathematics General*, 1994, **27,** 8079–8089.
161. Schmittbuhl, J. and Vilotte, J. P., Reliability of self-affine measurements. *Physics Review*, 1995, **E 51,** 131–147.
162. Stauffer, D. and Stanley, H. E., *From Newton to Mandelbrot*. Springer, New York, 1989.

163. Kunin, B. and Gorelik, M., On representation of fracture profiles by fractional integrals of a Wiener process. *Journal of Applied Physics*, 1991, **70,** 7651–7653.
164. Lorenz, E. N., Deterministic non-periodic flow. *Journal of Atmosphere Science*, 1983, **20,** 130–141.
165. Carleson, L. and Gamelin, T. W., *Complex Dynamics*. Springer, New York, 1994.
166. Feynman, R. P. and Hibbs, A. R., *Quantum Mechanics and Path Integrals*. McGraw-Hill, New York, 1965.
167. Newton, I., *Philosophie Naturalis Principia Matematica*. Joseph Steater, London, 1687.
168. Schmutz, M., The Hausdorff dimension as an intrinsic metric property of fractals. *Europhysics Letters*, 1986, **2,** 897–899.
169. Kappraff, J., *Connections: the Geometric Bridge between Art and Science*. McGraw-Hill, New York, 1991.
170. Zeldovich, Ya. B. and Sokolov, D. D., Fractals, similarity, intermediate asymptotics. *Soviet Physics Uspehy*, 1985, **28,** 608–616.
171. Balankin, A. S., Self-organization and dissipative structures in deformed body. *Soviet Technology Physics Letters*, 1990, **16,** 248–251.
172. Chelidze, T. L., *Methods of Percolation Theory in the Theory of Geomaterials*. Nauka, Moscow, 1987 (in Russian).
173. Isichenko, M. B., Percolation, statistical topography and transport in random media. *Review of Modern Physics*, 1992, **64,** 961–1043.
174. Sahimi, M., Flow phenomena in rocks. *Review of Modern Physics*, 1993, **65,** 1393–1534.
175. Yong, Z. and Hanson, M. T., Topological measure of brittle fragmentation. *International Journal of Solids and Structures*, 1994, **31,** 391–415.
176. Tsallis, C., Possible generalization of Boltzmann–Gibbs statistics. *Journal of State Physics*, 1988, **52,** 479–487.
177. Tsallis, C., Comment on Thermodynamic stability conditions for the Tsallis and Rényi entropies by J. D. Ramshaw. *Physics Letters*, 1995, **A 206,** 389–391.
178. Robinson, A., *Non-Standard Analysis*. North-Holland, Amsterdam, 1965.
179. Nelson, E.. *Bulletin of the American Mathematics Society*, 1977, **83,** 1165.
180. Nottale, L., Fractals and the quantum theory of space-time. *International Journal of Modern Physics*, 1989, **A 4,** 5047–5117.
181. Chudnovsky, A. and Kunin, B., A probabilistic model of brittle crack formation. *Journal of Applied Physics*, 1987, **62,** 4124–4129.
182. Berry, M. V. and Lewis, Z. V., On the Weierstrass–Mandelbrot fractal function. *Proceedings of the Royal Society of London*, 1980, **A 370,** 459–484.
183. Ausloos, M. and Berman, D. H., A multivariate Weierstrass–Mandelbrot function. *Proceedings of the Royal Society of London*, 1985, **A 400,** 331–350.
184. Bouchaud, E., Lapasset, G. and Planés, J.. *Europhysics Letters*, 1990, **13,** 73–75.
185. Milman, V. Y., Blumenfeld, R., Stelmashenko, N. A. and Ball, R. C., Comment to ref. [184]. *Physics Review Letters*, 1993, **71,** 204.
186. Hansen, A., Hinrichsen, E. L., Måløy, K. J. and Roux, S., Reply to ref. [68]. *Physics Review Letters*, 1993, **71,** 205.
187. Hansen, A. and Hinrichsen, E. L., Roughness of crack interfaces. *Physics Review Letters*, 1991, **66,** 2476–2478.
188. Bouchaud, J. P., Bouchaud, E., Lapasset, G. and Planes, J., Models of fractal cracks. *Physics Review Letters*, 1993, **71,** 2240–2243.
189. Sayles, R. S. and Thomas, T. R., Surface topography as a nonstationary random process. *Nature*, 1978, **271,** 431–434.
190. Bouchaud, E., Complex microstructures analysis: fracture surfaces as an example. *Solid State Phenomena*, 1994, **35-36,** 353–368.
191. Plouraboué, F., Roux, S., Schmittbuhl, J. and Vilotte, J. P., Geometry of contact between self-affine surfaces. *Fractals*, 1995, **3,** 113–122.
192. Zhang, X., Knackstedt, M. A., Chan, D. Y. C. and Paterson, L., On the universality of fracture surface roughness. *Europhysics Letters*, 1996, **34,** 121–126.
193. Grassberg, P. and Procaccia, I., Measuring the strangeness of strange attractors. *Physica*, 1983, **D 9,** 189–195.
194. Pisarenko, D. V. and Pisarenko, V. F., Statistical estimation of the correlation dimension. *Physics Letters*, 1995, **A 197,** 31–39.
195. Meisel, L. V., Johnson, M. and Cote, P. J., Box-counting multifractal analysis. *Physics Review*, 1992, **A 45,** 6989–6996.
196. Yamaguti, M. and Prado, C. P. C., A direct calculation of the spectrum of singularities $f(\alpha)$ of multifractals. *Physics Letters*, 1995, **A 206,** 318–322.
197. Louis, E. and Guinea, F., The fractal nature of fracture. *Europhysics Letters*, 1987, **3,** 871–877.
198. López-Sancho, M. P., Guinea, F. and Louis, E., Crack growth in a plastic medium. *Journal of Physics A: Mathematics General*, 1988, **21,** L1079–L1083.
199. Louis, E. and Guinea, F., Fracture as a growth process. *Physica*, 1989, **D 38,** 235–241.
200. Herrmann, H. J., Fractal deterministic cracks. *Physica*, 1989, **D 38,** 192–197.
201. Meakin, P., Li, G., Sander, L. M., Louis, E. and Guinea, F.. *Journal of Physics A: Mathematics General*, 1989, **22,** 1393–1403.
202. Sánches, A., Guinea, F., Louis, E. and Hakim, V., On the fractal character of the η model. *Physica*, 1992, **A 191,** 123–127.
203. Kertéz, J., Fractal fracture. *Physica*, 1992, **A 191,** 208–212.
204. Palasantzas, G., Self-affine fractals and the limit $H \to 0$. *Physics Review*, 1994, **E 49,** 1740–1742.
205. Bai, Y., Lu, C., Ke, F. and Xia, M., Evolution induced catastrophe. *Physics Letters*, 1994, **A 185,** 196–200.
206. Jeulin, D., Random functions and fracture statistics models. In *Geostat Tróia '92*, Vol. 1, ed. A. Soares. Kluver, Dordrecht, 1993, pp. 225–236.
207. Jeulin, D., Damage simulation in heterogeneous materials from geodesic propagation. *Engineering Computations*, 1993, **10,** 81–91.
208. Horton, J. A. and Ohr, S. M., TEM observations of dislocation emission at crack tips in aluminum. *Journal of Material Science*, 1982, **17,** 3140–3148.

209. Kobayashi, S. and Ohr, S. M., Dislocation arrangement in the plastic zone of propagating cracks in nickel. *Journal of Material Science*, 1984, **19,** 2273–2277.
210. Ohr, S. M., An electron microscope study of crack tip deformation and its impact on the dislocation theory of fracture. *Material Science Engineering*, 1985, **72,** 1–35.
211. Novikov, I. I. and Ermishkin, V. A., *Fracture Micromechanisms in Metals*. Nauka, Moscow, 1991 (in Russian).
212. Cherepanov, G. P., Nanofracture mechanics approach to dislocation generation and fracturing. *Applied Mechanics Review*, 1994, **47,** 326–330.
213. Demkin, N. B., *The Actual Contact Area of Solid Surfaces*. Moscow, 1962 (in Russian).
214. Nakano, A., Kalia, R. K. and Vashisha, P.. *Physics Review Letters*, 1994, **73,** 2336–2338.
215. Turcevich, L. and Scher, H., In *Fractal in Physics*, ed. L. Pietronero and E. Tosatti. North-Holland, New York, 1986.
216. Meakin, P., In *On Growth and Form. A Modern View*, ed. H.E. Stanley and N. Ostrowski. Nijhoff, Dordrecht, 1985.
217. Flory, P., *Principles of Polymer Chemistry*. Cornel University Press, Itaca, 1969.
218. Obukhov, S.. *Soviet Physics JETP*, 1984, **87,** 2024–2029.
219. Kolb, M., Botel, R. and Jullen, R.. *Physics Review Letters*, 1983, **51,** 1122–1125.
220. Meakin, P.. *Physics Review*, 1984, **A 29,** 997–1101.
221. Balankin, A. S., The effect of self-affine roughness on crack mechanics in elastic solids. *International Journal of Fracture*, 1996, **79,** R63–R68.
222. Sithi, V. M. and Lim, S. C., On the spectra of Riemann–Liouville fractional Brownian motion. *Journal of Physics A: Mathematics General*, 1995, **28,** 2995–3003.
223. Amstrong, R. W.. *Material Science Engineering*, 1966, **1,** 251–260.
224. Kelly, A. and Macmillan, N. H., *Strong Solids*. Clarendon, Oxford, 1986.
225. Rice, J. R. and Thomson, R., Ductile versus brittle behavior of crystals. *Philosophical Magazine*, 1974, **29,** 73–97.
226. Rice, J. R., Dislocation nucleation from a crack tip: an analysis based on the Peierls concept. *Journal of Mechanics, Physics and Solids*, 1992, **40,** 239–271.
227. Cherepanov, G. P., Quantum fracture mechanics. *Strength of Materials*, 1990, **N 2,** 155–163.
228. Cherepanov, G. P., *Mechanics of Brittle Fracture*. McGraw-Hill, New York, 1979.
229. Rice, J. R., A path independent integral and the approximate analysis of strain concentration by notches and cracks. *Journal of Applied Mechanics*, 1968, **35,** 379–386.
230. Rosenfield, A. R., Ductile-to-brittle fracture. In *Metals Handbook*, Vol. 11. Failure, ASM, New York, 1992, pp. 66–71.
231. Slepyan, L. I., Principle of maximum energy dissipation rate in crack dynamics. *Mechanics, Physics and Solids*, 1993, **41,** 1019–1033.
232. Sih, G. C., Thermomechanics of solids: nonequilibrium and irreversibility. *Theories of Applied Fracture Mechanics*, 1988, **9,** 175–198.
233. Balankin, A. S. and Foundations of fracture mechanics, I., Thermodynamics of fracture and energy balance approach. *Revista Mexicana de Física*, 1997 (in preparation).
234. Atkins, A. G., Scale effects in engineering failures. *Engineering Failure Analysis*, 1994, **1,** 201–214.
235. *Annual Book of ASTM Standards*. ASTM, New York, 1987.
236. Hoysan, S. F. and Sinclair, G. B.. *International Journal of Fracture Mechanics*, 1993, **60,** R43–R49.
237. Sinclair, G. B., Kondo, M. and Pieri, R. V., The size dependence of fracture toughness for two embrittled materials. *International Journal of Fracture Mechanics*, 1995, **72,** R3–R10.
238. Cherepanov, G. P., Super-deep penetration. *Engineering Fracture Mechanics*, 1994, **47,** 691–713.
239. Balankin, A. S., Penetration of a plastic object into obstacles made of brittle material. *Soviet Technical Physics Letters*, 1988, **14,** 534–536.
240. Balankin, A. S., Physics of the high-speed impact of solid objects with porous media. *Soviet Physics Technical Physics*, 1988, **33,** 1451–1452.
241. Balankin, A. S., Kinetic (fluctuational) nature of the hydrodynamic regime of high-velocity deformation of solids. *Soviet Technical Physics Letters*, 1988, **14,** 539–540.
242. Balankin, A. S., Lubomudrov, A. A., Sevryukov, I. T. and Yanevich, G. N., Physical aspects of cumulation effect. *Soviet Technical Physics Letters*, 1988, **14,** 537–538.
243. Balankin, A. S., Laser modeling of high velocity impact. *Soviet Physics Technical Physics*, 1988, **33,** 1107–1108.
244. Balankin, A. S., Lubomudrov, A. A. and Sevryukov, I. T., Scale effects in the kinetics of impact fracture and explosion of solids and the problem of modeling highly nonequilibrium processes. *Soviet Physics Technical Physics*, 1989, **34,** 1431–1433.
245. Balankin, A. S., Physics of penetration of a cumulative jets into porous media. *Physics of Burning and Explosion*, 1989, **N 4,** 130–140(in Russian).
246. Balankin, A. S., Lubomudrov, A. A. and Sevryukov, I. T., *Kinetic Theory of Armor Piercing Using V-Shaped Charges*. Department of Defense USSR Press, Moscow, 1989 (in Russian).
247. Balankin, A. S., Lubomudrov, A. A. and Sevryukov, I. T., *The Physics of High Velocity Impact*. Department of Defense USSR Press, Moscow, 1990 (in Russian).
248. Balankin, A. S. and Yanevich, G. N., Physical meaning and structure of the strength component of the resistance to high-velocity penetration of thin and compact objects into semi-infinite media and the macrokinetics of penetration. *Soviet Physics Technical Physics*, 1992, **37,** 625–629.
249. Balankin, A. S., Levin, S. V. and Yanevich, G. N., Predicting the shock strength of target made of a brittle material. *Soviet Physics Technical Physics*, 1992, **37,** 339–341.
250. Kozhushko, A., Balankin, A. S., Izotov, A. and Lazarev, V., Hydrodynamic model concepts in the problem of the dynamic strength of materials of various physicochemical nature, I: inviscid incompressible flow model and the effect of the compressibility of solids. *Inorganic Materials*, 1993, **29,** 1043–1056.
251. Kozhushko, A., Balankin, A. S., Izotov, A. and Lazarev, V., Hydrodynamic model concepts in the problem of the dynamic strength of materials of various physicochemical nature. II: Effect of the strength characteristics of media. *Inorganic Materials*, 1993, **29,** 1057–1074.

252. Barenblatt, G. I. and Botvina, L. R., Self-oscillatory modes of fatigue fracture and the formation of self-similar structures at the fracture surface. *Proceedings of the Royal Society of London*, 1992, **A 442**, 489–494.
253. Goldenfeld, N. and Oono, Y., Renormalization group theory for two problems in linear continuum mechanics. *Physica*, 1991, **A 177**, 213–219.
254. *Renormalization: From Lorentz to Landau (and Beyond)*, ed. L.M. Brown. Springer, New York, 1993.
255. Martin, O., Parodi, O. and Pershan, P. S.. *Physics Review*, 1972, **A 6**, 2401–2406.
256. Amit, D. J., *Field Theory, the Renormalization Group and Critical Phenomena*. McGraw-Hill, New York, 1978.
257. Aronson, D. G. and Vazquez, J. L., Anomalous exponents in nonlinear diffusion. *Journal of Nonlinear Science*, 1995, **5**, 29–56.
258. Tada, H., *The Stress Analysis of Cracks Handbook*. Del Research Corporation, New York, 1986.
259. Anderson, T. L., *Fracture Mechanics: Fundamentals and Applications*. CRC Press, London, 1995.
260. Griffith, A. A.. *Philosophical Transactions of the Royal Society of London*, 1920, **A 221**, 163–198.
261. *Fracture, An Advanced Treatise*, ed. H. Liebowitz. Academic Press, New York, 1968.
262. Walsh, J. B., The effects of cracks on the uniaxial elastic compression of rocks. *Journal of Geophysics Research*, 1965, **70**, 399–411.
263. Obert, L., In *Fracture*, Vol. 1. Mir, Moscow, 1976, pp. 59–87 (in Russian).
264. Guz', A. N., *Brittle Fracture Mechanics for Materials with Initial Stresses*. Naukova Dumka, Kiev, 1983 (in Russian).
265. Pisarenko, G. S., Naumenko, V. P., Mitchenko, O. V. and Volkov, G. S., Experimental determination of the value of K_I in compression. *Strength of Materials*, 1984, **N 11**, 1497–1504.
266. Ashby, M. F. and Hallam, S. D., The failure of brittle solids containing small cracks under compressive stress states. *Acta Metallica*, 1989, **34**, 497–510.
267. Dyskin, A. V. and Salganik, R. L., Models of dilatancy of brittle materials under compression. *Mechanics of Solids*, 1987, **6**, 165–173.
268. Lavrov, N. A. and Slepyan, L. I., Brittle fracture of elastic bodies under compression. *Soviet Physics Doklady*, 1991, **36**, 344–346.
269. Dubuc, B., Quiniou, J. F. and Roques-Carmes, C., Evaluating the fractal dimensions of profiles. *Physics Review*, 1989, **A 39**, 1500–1512.
270. Dubuc, B., Zucker, S. W., Tricot, C., Quiniou, J. F. and Wehbi, D., Evaluating the fractal dimension of surfaces. *Proceedings of the Royal Society of London*, 1989, **A 425**, 113–127.
271. Hansen, A., Engóy, T. and Måløy, K. J., Measuring Hurst exponents with the first return method. *Fractals*, 1994, **2**, 527–533.

(*Received* 2 *January* 1996)

APPENDIX A

Experimental methods of fractal measurement of fracture surfaces

In order to investigate the fractal properties of a rough fracture surface, it is necessary to determine its area as a function of measurement length. Several techniques have been developed for these measurements (see, for review, refs [133, 137] and references therein). In principle, stereophotogrametry should more or less provide an adequate topographic description of rough surfaces. Provided the computer used has enough memory, this very rich information can be analyzed to measure the fractal dimension of the surface. A technique which provides a similar information, although in a very different length scale domain is the scanning tunneling electron microscopy [3]. In practice, however, more commonly the one- or bidimensional cuts of fracture surface are studied by using the fractographic methods [3, 61–64].

Fractographic methods used to obtain fractal information from rough fracture surfaces, involve either obtaining surface profiles from metallographic sections cut perpendicular to the surface plane (vertical section method), or from sequentially prepared sections parallel to the surface plane (slit island method), or from spectral analysis of roughness of surface (spectral methods) [133, 137]. Usually, an additional hypotheses is needed in order to achieve relation between fractal properties of surface and its cuts.

The main purpose of these fractographic investigations is to determine the fractal dimension of fracture surface and the limits within which the surface exhibits fractal properties. Of course, for a dimension to have any significance, repeating an experiment must lead to the same value. One of the most critical problems of fractal measurement and applications is the ability to recognize and correctly measure the fractal dimension of self-affine fracture surfaces. The horizontal contours of a fracture surface may be statistically self-similar, but the vertical profiles are commonly self-affine [130, 137]. Hence, the horizontal and vertical cuts of a fracture surface have quite different scaling properties which must be estimated by means of different measurements.

For statistically self-similar horizontal contours any reasonable procedure of fractal measurement should lead to the same value of fractal dimension [3]. The question is how this fractal dimension relates to the fractal properties of self-affine (or, generally, multiaffine) fracture surface. It seems that horizontal sections cannot give sufficient information for fractal characterization of the fracture surface.

On the other hand, as it was already noted in Sections 2.4 and 2.6, for self-affine vertical profiles, there are many different fractal dimensions, some local and global. The latter always equals the topological dimension of profile, while the local dimensions may be expressed as functions of the roughness exponent, H (see Table 12).

Methods for measuring self-affine roughness exponent can be schematically cast into two groups. One find the classical methods, developing for analyzing self-similar fractals: box-counting, divider, perimeter–area relation, power spectrum scaling, which provide the different fractal dimensions for a self-affine surface [66, 135, 160, 269, 270]. Several other methods sometimes used in practice of fractal measurement. Namely, the chord-length measurements [137, 169], variogram method [130, 137], and correlation function measurement [169] are commonly used. On the one hand, several

methods have been designed to specifically determine the self-affine exponents: a variable band-width method [161] and return probability method [271].

Various experimental techniques are used for fractal analysis of fracture surfaces. Among them, the scattering techniques (small-angle neutron scattering [127], optical diffraction experiments [3, 63, 127] and secondary-electron emission measurement [127]), fractographic studies [61–63], adsorption–desorption studies (adsorption probes method [127] and thermodynamic method [134]), deposition experiments [190], electro- and heat-chemical methods [120, 190], nuclear magnetic resonance pore-size distribution measurement [169] and some indirect methods, such as skin effect measurement and charge relaxation measurement [137], etc. For detailed review of experimental methods see ref. [137] and references therein.

(*Received* 2 *January* 1996)